ORGANIC COATINGS TO PROTECT FERROUS STRUCTURES

A Dissertation
Submitted to the Graduate Faculty
of the
North Dakota State University
of Agriculture and Applied Science

By
Yaping Huang

In Partial Fulfillment
for the Degree of
DOCTOR OF PHILOSOPHY

Major Department:
Coatings and Polymeric Materials

October 2013

Fargo, North Dakota

North Dakota State University
Graduate School

Title

ORGANIC COATINGS TO PROTECT FERROUS STRUCTURES

By

YAPING HUANG

The Supervisory Committee certifies that this ***disquisition*** complies with North Dakota State University's regulations and meets the accepted standards for the degree of

DOCTOR OF PHILOSOPHY

SUPERVISORY COMMITTEE:

Prof. Gordon Bierwagen
Chair

Prof. Andriy Voronov

Dr. Dante Battocchi

Prof. Annie Tangpong

Approved:

Nov. 1, 2013 — Date

Prof. Dean Webster — Department Chair

ABSTRACT

Corrosion induces damages that can result in enormous costs and safety issues. Steels are the most commonly used metallic structural materials but they can corrode rapidly when exposed to corrosive environments and need to be protected. The thesis research focuses on two aspects of steel protection. The first aspect is using barrier protection mechanism to protect steel pipeline structures in the presence of Super-Critical CO_2. The second aspect is improving cathodic protection of steels by metal rich coatings in ground vehicles, bridges, water tanks, and other structures.

In part one, coatings for protection of steel pipeline used for carbon transportation in the form of supercritical carbon dioxide were examined. Pipeline coatings serve to protect pipelines by maintaining their integrity and to increase their service time. Different pipeline coatings with the exposure to $SCCO_2$ have been examined, and these results will be presented here. Different parameters, such as the thickness of coatings, the exposure temperature and pressure, and the exposure time as they affect pipeline coating were investigated and will be described.

In the second part of this thesis research, the addition of magnesium particles to the standard zinc particles as metal rich primer was examined for the improvement of current zinc rich coatings to serve as protection for metal substrates in Army ground vehicles. Optimization of primer formulation, such as ratio of Mg and Zn, was investigated. The test primers were exposed in accelerated weathering tests, including ASTM B117 salt spray method and Prohesion^{TM} cycle test as part of this research. The results have been compared with the behavior of the current commercial zinc rich primers to identify the improvements in the protection of the steel with mixed metal systems.

For both investigations, electrochemical impedance spectroscopy was mainly used to examine coating performance. Other tests, including color measurement, thickness measurement, X-ray diffraction measurements, and pH measurements, were used to examine the corrosion behavior of steel structures under different corrosive environments. Results showed that coating systems can protect ferrous structures in ways of barrier protection and cathodic protection and can be improved by the application of modern methods and equipment.

ACKNOWLEDGEMENTS

First and foremost, I would like to acknowledge my academic advisor, Professor Gordon Bierwagen. He helped me not only to build a strong knowledge background on corrosion, and to guide me in the thesis research, but also to teach me to be a qualified research investigator, and to make suggestions on the way to succeed. I am also thankful to Prof. Andriy Voronov, Prof. Annie Tangpong and Dr. Dante Battocchi for their efforts to improve my thesis work as my committee members and mentors.

I would like to acknowledge Dr. Nick Wilson, Mr. Mark Hatzenbeller, Mr. Nick Richter, Dr. Jinhai Wang, Dr. Duhua Wang, Ms. Hong Xu, Ms. Junren Lin, Ms. Bobbi Merten, Mr. Vinod Upadhyay, and Mr. Andrew Huovinen for their help and the discussions in my thesis work. I would also like to acknowledge Dr. Angel Ugrinov, Ms. Heidi Docktor, and Mr. Jim Barr for their help in the instrument operations.

I would like to acknowledge Prof. Dean Webster, Prof. Stuart Croll, Prof. Victoria Gelling, and Prof. Dennis Tallman for their wonderful lectures, which were applied to my thesis research. I also appreciate the staff in Coatings and Polymeric Materials, Ms. Carol Johnson, Ms. Katherine Backen-Andersen, and Ms. Jacinda Wollan for the administrative work.

My colleagues Niteen Jadhav, Erin Pavlacky, TJ Nelson, Ivan Hevus, Hanzhen Bao, Eric Sapper, Stacy Sommer, Drew Pavlacky, Kiran Kashi, Kasi Subbu, and Adlina Paramarta etc. should be acknowledged for a wonderful life in Department of Coatings and Polymeric Materials, North Dakota State University.

Depart of Energy and Department of Coatings and Polymeric Materials, NDSU are acknowledged for the financial support to my research.

DEDICATION

I dedicate the completion of this dissertation to my parents and my sisters. Their sincere support and their dedication to their sons and their younger brother gave me the opportunity with the higher education of completing this Doctorate of Philosophy.

TABLE OF CONTENTS

LIST OF TABLES

LIST OF FIGURES

Figure Page

NOMENCLATURE

$SCCO_2$……Supercritical carbon dioxide

UV……Ultraviolet

PVC……Pigment volume concentration

CPVC……Critical pigment volume concentration

VOC……Volatile organic compound

DC……Direct current

AC……Alternate current

EIS……Electrochemical impedance spectroscopy

ENM……Electrochemical noise measurement

SEM……Scanning electron microscopy

TEM……Transmission electron microscopy

AFM……Atomic force microscopy

XRD……X-ray diffraction

XPS……X-ray photoelectron spectroscopy

IR……Infrared Spectroscopy

DHS……Dilute Harrison's solution-0.35wt% $(NH_4)_2SO_4$ and 0.05wt% NaCl solution

DMA……Dynamic mechanical analysis

P130……Polyoil 130, a liquid polybutadiene

PCP……Polychloroprene

tBPO……tert-Butyl peroxide

MEK……Methyl ethyl ketone

ZnRP……Methyl ethyl ketone

PVD……Physical vapor deposition

SCE……Saturated calomel electrode

Simonkolleite……$ZnCl_2 \cdot 4Zn(OH)_2$

SVET……Scanning vibrating electrode technique

PDS……Potentiodyanmic polarization scan

DI water……Deionized water with a resistivity of 18.2MΩ·cm at 25˚C

1. INTRODUCTION TO ORGANIC COATINGS

1.1. Motivation

Steel is the most commonly used material for the construction of bridges, buildings, automotive parts, ships, and other structures. With high strength, high ductility, and great toughness as its advantages, steel, one of metallic materials, is inevitable to corrosion even in most outdoor atmospheres [1]. Severe environments, such as salted sea water [2], increase steel corrosion much more significantly. Synergistic corrosion modes, such as in combination with fatigue [3], could lead to faster deterioration of steel structures. All these corrosion behaviors could cause steel structures fail catastrophically. The consequences include limited structure lifetime, destroyed aesthetic, huge cost for maintenance, and most importantly, safety issue and loss of human life. A recent accident close to North Dakota State University was the collapse of I-35W Bridge across the Mississippi River on August 1st, 2007 [4], shown in Figure 1.1. It killed 13 and injured 121 others. Around 140,000 vehicles per day had to detour to cross the Mississippi River, which increased travel time till September 18th, 2008. With the economic loss around $17 million in 2007 and $43 million in 2008 [5], and the new bridge construction cost approximately $234 million [6], the total cost of the collapse was around $300 million. Steel structure protection for its corrosion mitigation is vital to avoid and/or decrease all these losses and tragedies.

Intensive research has been done for steel structure protection to minimize corrosion behaviors and to increase lifetime. Corrosion process usually happens when steel structures are under exposure to corrosive environments, commonly oxygen and water. Irrespective with different types of corrosion phenomena, such as uniform corrosion, pitting corrosion, crevice corrosion, and erosion corrosion, corrosion protection can be divided into three categories,

Figure 1.1. The collapsed I-35W bridge with vehicles on. With permission from [4].

shown in Table 1.1. The first category of corrosion protection is to modify steel structure itself to increase corrosion resistance. In this category, the composition of iron alloys can be adjusted to resist corrosive environments. Steel structures could be well maintained for corrosion vulnerable sites to decrease corrosion rates. The second category of corrosion protection is to change external environments to decrease corrosion rates. In this category, the corrosive chemicals should be minimized. The protection such as inhibitors and cathodic current can be applied. The third category of corrosion protection is to apply protective coatings. In this category, protective coatings not only minimize maintenance efforts required for corrosion protection, but also separate steel structures from corrosive environments, as well as stopping the spread of the corrosion. With all these corrosion protection methods for steel structures, organic coatings have been found to be one of the most effective ways, especially cost-effective ways, of preventing corrosion activities practically [7].

Table 1.1. Corrosion protections of steel structures [8]

Categories	Concepts	Examples
Steel structure	Modification of metals	Stainless steel and steel alloys
	Modification of metal surfaces	Avoid crevices Avoid galvanic corrosion Clean corrosion defects
External environments	Decreasing oxidizing factors	Boiling water to decrease oxygen concentration Purifying water to decrease salt concentration pH adjustment
	Adding protection factors	Cathodic protection Anodic protection Inhibitors
Protective coatings	Inorganic coatings	Vitreous enamels Portland cement coatings Chemical conversion coatings
	Metallic coatings	Electroplating Galvanizing
	Organic coatings	Paints Plastic linings

1.2. Organic Coatings

Organic coatings are basically coatings with polymeric binder systems, including, but not limiting to, paints, vanishes, and plastics. Most of them are used for corrosion protection to save money for the maintenance and the replacements as a big contribution to the world economy. In the years 2006 to 2012, organic coatings had a total value of shipments around $20 billion/year [9], half of which would be used for corrosion protection. Design of organic coatings towards improving the performance of corrosion control is not only an electrochemistry issue but also an economic issue.

1.2.1. Composition of Organic Coatings

Organic coatings usually include organic polymer binders, pigments, additives, and solvents. Organic polymer binders are used to form continuous film not only adhering to the

coated structure, but also integrating coatings together, as well as governing the properties of organic coatings. Pigments are primarily used to provide aesthetic appearance, while they could also change the properties of organic coatings dramatically and affect the corrosion protection of organic coatings significantly. Additives are used to modify some properties of organic coatings to ease coatings applications and to add functionalities of coatings. Solvents will evaporate in the final coatings. However, they are very critical in the process of applying coatings. The details of each ingredient are introduced in the followings.

Binder, usually organic polymer, is the main and required ingredient of organic coatings. It supplies both cohesion force and adhesion force, which influences mechanical properties, gloss properties, and water resistance properties. It is responsible for coating integrity, which is the main characteristic for protection of coatings. There are different binder systems, such as acrylic resins, alkyd resins, epoxy resins, polyurethanes. Different binder systems have different mechanical, thermal, ultraviolet (UV)-resistance, and water-resistance properties, shown in Table 1.2. Binder selection will depend on coatings applications, service environments as well as compatibilities with other components of coatings.

Pigments are incorporated into the coatings to contribute color, opacity, and protection. Color match of organic coatings is unlimited in the choice of pigment selections. However, the metamerism will appear unless the exact same pigments are selected. Pigments are also used to modify mechanical properties, such as to increase hardness, and to decrease ductility. The cost of coatings can be decreased with the incorporation of pigments. Commonly used pigments are titanium dioxide for white color and UV resistance. Pigment volume concentration (PVC) is pigment volume divided by dry coating volume, which is an important factor for coatings properties. Critical pigment volume concentration (CPVC) is a special point of PVC, when the

binder is only enough to fill the voids between pigment particles. Most properties of coatings, such as mechanical properties, optical properties, and diffusion properties, will change abruptly at CPVC. CPVC is dependent on pigment type, size and its distribution, while it is irrelative to binder systems. However, with poor dispersion of pigments in binder systems, PVC at some part of coatings (localized PVC) is not in agreement with PVC for whole coating system (global PVC), shown in Figure 1.2.

Table 1.2. Common polymer binder systems [10]

Binder	Advantages	Disadvantages
Epoxy	Good adhesion Good corrosion resistance Good chemical resistance Good mechanical properties	Low UV resistance
Acrylic	High flexibility High weathering resistance High chemical resistance Hydrolytic stability High solid content	Low hardness Low abrasion resistance
Alkyd	Controllable molecular weight Controllable functional groups Water dispersible High solid content	Low hydrolytic stability
Polyurethane	High gloss Hydrolytic stability Good weathering resistance Good mechanical properties Good chemical resistance	High cost Toxicity
Drying oils	Natural materials Low cost Auto-oxidation	Yellowing on aging Poor film properties
Phenolic	High abrasion Good chemical resistance Good water resistance	Toxicity Intrinsic color Brittle

Additives are very necessary for good coating formulation. Although very low in concentration, it could alter properties of coating formulation tremendously. Common additives include, but are not limited to, catalysts, pH controls, coalescents, thickeners, surfactants,

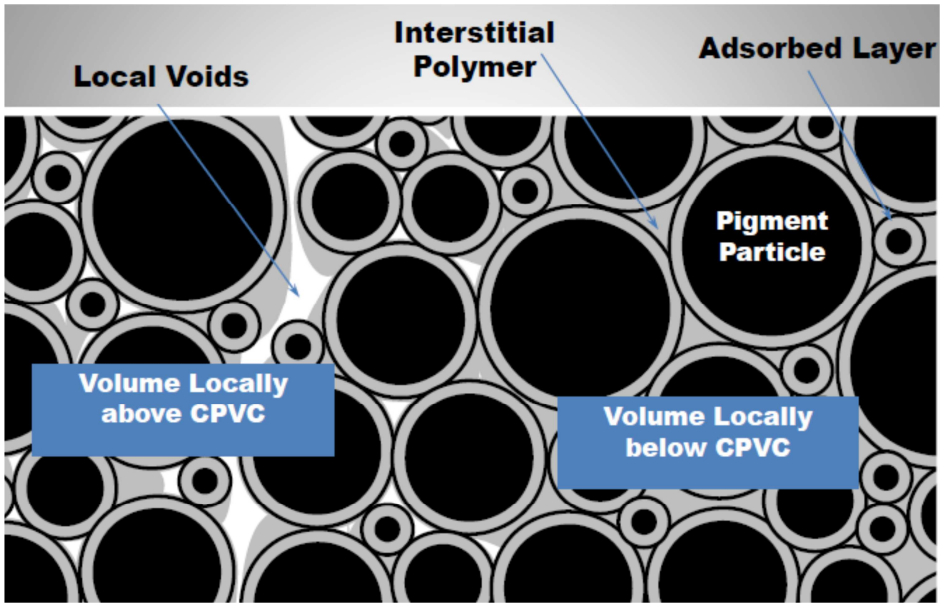

Figure 1.2. Coatings with localized pigment volume concentration due to poor dispersion. With permission from [11]. Copyright 1999, Elsevier.

dispersers, and UV stabilizers. Stability is the first priority of coating formulation not only for the uniformity but also for the storage life. In this case, dispersing agents can stabilize particle suspensions and help form homogenous particle suspensions by ionic stabilization and/or steric stabilization. Surfactants could reduce surface energy of particle surfaces, which could increase the compatibility between binder systems and particles. However, surfactant could cause foaming problem. Anti-foaming agent is used to decrease foaming issues. Thickeners produce coatings with high low-shear viscosity, which could also increase stability of coatings. In cold place such as North Dakota, organic coatings can freeze, which causes particle separation due to thermodynamics. To produce good freeze-thaw stability, anti-freeze will be needed. Wetting ability is important to increase adhesion property. In this case, surfactants can help organic coating formulations to wet substrates. Flowing property is critical for coating application. In this case, thickeners help organic coatings with appropriate viscosity for flowing, spreading and leveling. In the film formation process, coalescent agent can help film formation at a low

temperature by reducing the glass transition temperature of organic coatings. In the service condition, UV stabilizer can increase durability of organic coatings and service lifetime.

Solvents are usually used to dissolve organic binders to ease the application process. They will strongly determine the viscosity of coating formulations, which are very critical for different application methods. Solubility parameter [12], the square root of the cohesive energy density of the solvent, is a good approximation for solvent selection. Evaporation rate of solvents will affect the reaction of binder systems and the formation of final coatings. Surface tension of solvents will affect the wetting ability of both binders to pigments and coating formulations to substrates. Conductivity of solvents will be required within a specific range for electrostatic spray. However, volatile organic compounds (VOCs) should be minimized for environmental protection. In order to decrease VOCs, powder coatings have no solvents inside, while latex coatings and water-borne coatings are using water as the solvent.

Organic coatings with the four ingredients will be designed by the choice of formulation properties, film properties, and the cost of the ingredients to make good manufacturing processes, with steps of premixing, grinding, letting down, and curing.

1.2.2. Application of Organic Coatings

The goal of coating applications is to produce a continuous, defect free and uniform film with good adhesion properties. Organic coatings form to wet the substrate, to level on the substrate, to cure with solvent evaporation, and to solidify on the substrate. Surface preparation is the essential first step to apply any type of organic coatings and the key factor to coating effectiveness. Surface preparation is not only to clean the surface to avoid contaminations, but also to increase adhesion between coatings and substrates. The surface preparation includes solvent cleaning, mechanical treatment, conversion coatings, and stripping of existing coatings.

Solvent cleaning will remove contaminates, such as oils and greases. Mechanical treatment will not only clean the surface, but also can increase the roughness of the surface to help the adhesion. Conversion coatings, such as anodizing and phosphating, usually use chemicals to react with substrates in order to create a new physical surface for better adhesion. Stripping is used to scrape and to remove existing coatings off. With appropriated surface preparation, adhesion properties can be increased by mechanical interlocking, interdiffusion of chains, electrical interactions, and chemical interactions, shown in Figure 1.3.

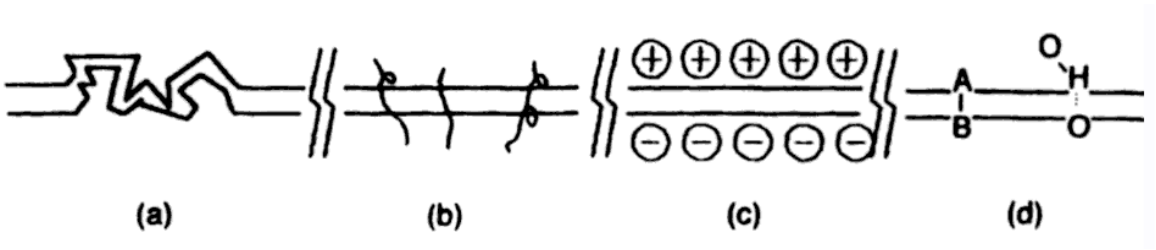

Figure 1.3. Mechanism to increase adhesion properties, (a) Mechanical interlocking; (b) Polymer diffusion; (c) Electrostatic attraction; (d) Chemical bonds. With permission from [13]. Copyright 1998, John Wiley & Sons Ltd.

Application of organic coatings depends on coating type and its properties, especially viscosity property. Organic coatings can be solid for the powder coating technique. It also can be gaseous to be sprayed. Most organic coatings are in liquid form, applied by brushes, paint rollers, blades, dip coating, and spray techniques, shown in Table 1.3. Industrial application methods include reverse roll coating, gravure coating, curtain coating, slot die process, dip coating, and metering rod, due to the fast processes. Pot life and viscosity are the main criteria for the applications. Spray coating is the most popular method in the industry. With robot technologies, spraying technique is also widely used in automotive industries. In the spray coating, the coating will be forced into small droplets and dries during the flying into the painted objects. Dilution of organic coatings with solvent will be used to adjust the viscosity of paint formulation and is very

critical to the quality of organic coatings. “Dry to touch”, “Dry through”, and “Dry to recoat” (ASTM D1640) are the quick ways to test coating formation.

Table 1.3. Application method of organic coatings [10,14]

Application method	Shear rates (s^{-1})	Advantages	Disadvantages
Spraying	10^3-10^6	Fast process Irregular shaped items	Overspray Faraday cage effect for electrospray with cage area not coated
Hand rolling	500	Less skills needed Good for windy conditions A smooth finish	Spatter and droplets problem
Brushing	4000-10000	Cleaning and stripping	Brush marks
Electrodeposition		Cost effective, efficient, controllable	Substrate limitation Sophisticated formulation
Dip coating	1-100	High production rates Less depend on operator skill	Not suitable for items with cavities
Curtain coating	10-10000	Uniform coating thickness	Only for flat items
Roll coating	1000-10000	High production rates	Only for flat items

1.2.3. Protection of Organic Coatings

Organic coatings are used as a protective layer for metal structures in three ways [7]: barrier protection, corrosion inhibitor protection, and cathodic protection. Barrier protection is used to protect metal structures from water, oxygen, and/or other corrosive agent penetration. Corrosion inhibitor protection is removing electrons from the metal to form passive layers. Cathodic protection is forcing metal structures into a stable region.

Barrier protection uses a physical insulating barrier to slow down the penetration of water, oxygen, and/or corrosive agents. It requires a good adhesion to keep away corrosive agents from staying on metal structure surfaces. Barrier property is usually proportional to the thickness of

organic coatings. It also depends on binder and pigment systems. For binder system, polymer structure and crosslinking density will affect permeability of gas and/or liquid. For pigment system, increasing its concentration before CPVC will improve barrier properties. Pigment type, especially aspect ratio, and pigment orientation will affect the tortuous path length, and thus affect the permeability of gas/liquid [15], shown in Figure 1.4. It supplies a new way to increase barrier properties with nanocomposite-based coatings.

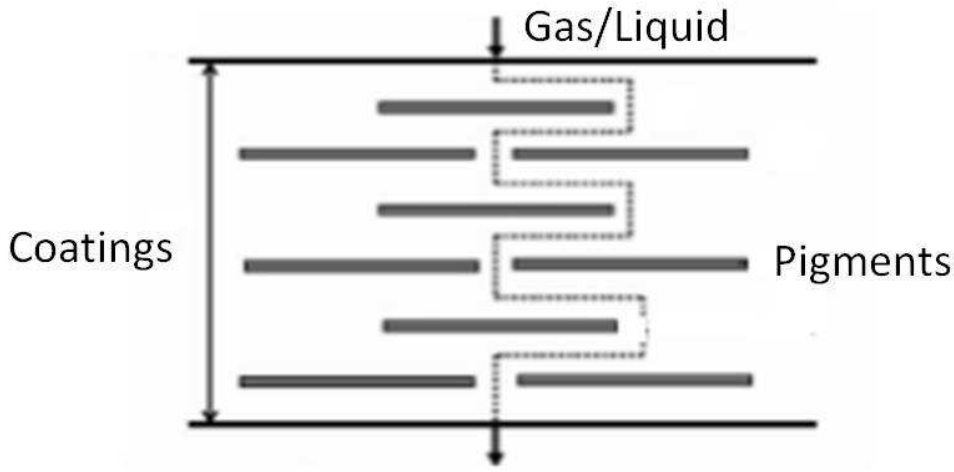

Figure 1.4. A schematic of a tortuosity-based model for the pigment effect on permeability. With permission from [15]. Copyright 2005, American Physical Society.

Organic coatings can also release inhibitor to suppress corrosion behaviors either by passivating substrates or by slowing corrosion reactions. Inhibitors can be divided into three categories: adsorption inhibitors, passivating inhibitors, and surface layer inhibitors. Adsorption inhibitors are usually polar substances adsorbing on high energy surfaces. They could also be adsorbed on surfaces by hydrogen bonding or other reactions. The adsorbed layer acts as a barrier to protect substrates. Passivation inhibitors usually use oxidizing agents to produce corrosion products at the anodic surfaces to prevent further corrosion behaviors. Surface layer

inhibitors react with metal ions forming precipitations on the surface to protect the anode. The common inhibitors are shown in Table 1.4.

Table 1.4. Common inhibitors used to control corrosion [16]

Functions	Examples	Applications
Adsorption	Amines Benzoate Thiourea Antimony trichloride	Widely used Acidic media Packaging coatings
Passivation	Nitrite Chromate Red lead Calcium plumbate	Oxidizing agents Natural oxide film
Surface layer	Phosphate Silicate Hydroxide Bicarbonate hexametaphosphate	Insoluble and stable film

Cathodic protection uses more electroactive metal pigments to protect nobler substrate, with galvanic series shown in Table 1.5 [17]. When more electroactive pigments are connected with nobler substrate, pigments are the only anode in the electrochemical reaction. These pigments are also called sacrificial metals, with zinc and magnesium as popular pigments. All corrosion process happens on pigments, while nobler substrate is protected. However, pure aluminum is insufficient to protect steel structure due to the formation of aluminum oxide film.

Smart coating [18] has now emerged as a new technology to release corrosion inhibitor when organic coatings are damaged and/or ruptured. Corrosion indicator and corrosion inhibitor are included in microcapsules, which are incorporated into paint system. These inhibitors can be released by crack propagation and/or other triggering mechanisms, such as pH change. It is a self-healing process, which could increase the lifetime of structures and decrease maintenance costs.

Table 1.5. Galvanic series in seawater [17]

More electroactive
Magnesium
Zinc
Aluminum
Steel or iron
Cast iron
Stainless steel
Copper
Silver
Titanium
Graphite
Gold
Platinum
Nobler

1.2.4. Failure of Organic Coatings

Good organic coatings are consistent in thickness, appearance and properties. The coatings should also be tough enough to withstand service environments.

Organic coatings failure comes from a formulation problem, an improper treatment of surface, an improper application, and an environment effect. Contamination is formed when some chemicals not from a coating formulation are added into the coating. Without sufficient agitation, floating will happen due to uneven distribution of pigments in the paint. With over reduced paint, curtaining of coatings will happen. Non-uniform surfaces are caused by convection cells within coating film. Orange peel is a common convection cell. Wrinkling happens when the surface coating becomes solid faster than the coating underneath. Cratering happens when the substrate surface is not clean, or the film is too thin. Migration of a color pigment and a plasticizer will cause bleeding and bloom. Poor surface treatment could also cause poor wetting, such as crawling and dewetting. Peeling and blistering (tested by ASTM D714) are commonly occurring due to improper surface treatment and/or surface adhesion failure due to

environment exposure. Chalking (tested by ASTM D4214) is the powdering surface on the coatings due to the degradation of polymer binder systems. Cracking (tested by ASTM D662) is caused by non-uniformity of coating expansion and/or contraction. Usually it happens when the coatings are not completely dry and/or cured. Erosion (tested by ASTM D662) occurs when there is an external fluid, such as water or gas. It causes a fast chalking.

When organic coating is in its service environments, organic coating will fail by electrochemical reactions with corrosive species, including mainly water and oxygen. These corrosive species will be much worse when a scribe is on the surface, resulting into cathodic disbondment and oxide lifting, shown in Figure 1.5. Cathodic disbondment is caused by cathodically generated alkalinity in reaction with binder system. These reactions and interactions disband organic coatings at interfaces. Oxide lifting happens due to anodic corrosion product accumulation. Corrosion scales for oxide lifting form mostly with alternate wetting and drying exposure.

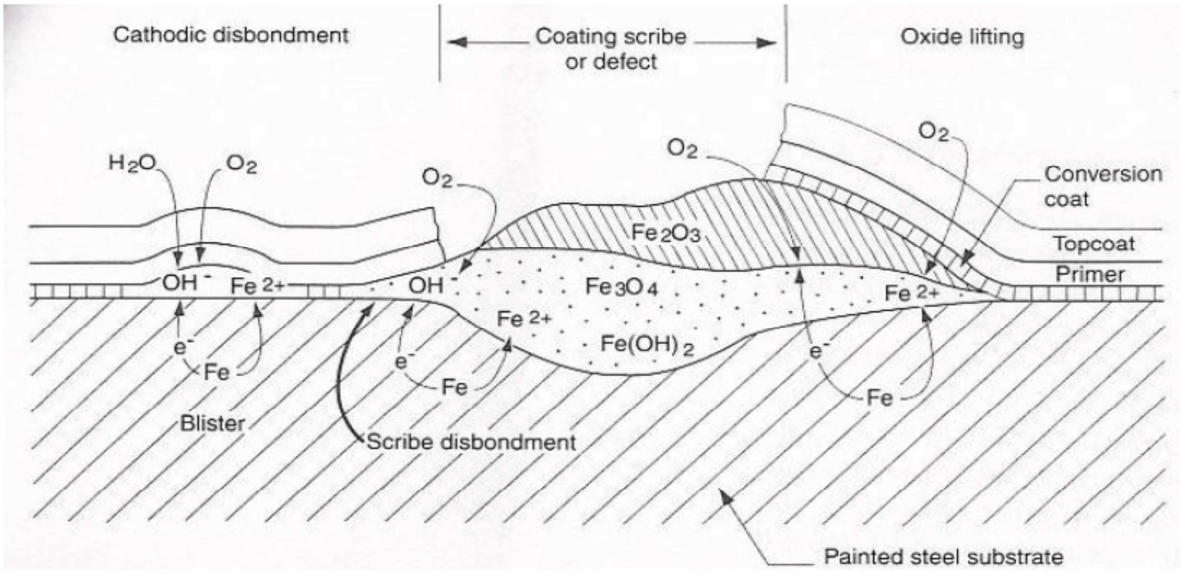

Figure 1.5. Schematic coating failure when a scribe appears. With permission from [17]. Copyright 1995, Prentice Hall.

Good maintenance is very important for organic coatings. Local failure will cause global failure easily and catastrophically. To avoid corrosion related accidents, organic coatings need to be evaluated during their service life.

1.2.5. Evaluation of Organic Coatings

After organic coatings are applied, the thickness of coating is usually the first measurement of organic coatings (instructed in ASTM E376), usually performed by Elcometer. It not only measures how thick the coating, but also evaluates the uniformity of coating. Chemical resistance tests can measure the solvent resistance of organic coatings, such as methyl ethyl ketone (MEK) double rub test (instructed in ASTM D4752). Abrasion resistance can be measured be Taber Abraser (instructed in ASTM D4060). Flexibility can be measured by Conical Mandrel test (instructed in ASTM D522) and other bending tests. Impact resistance can be measured by the pendulum impact test (instructed in ASTM D3420). Hardness can be measured by Konig pendulum hardness test (instructed in ASTM D4366) and the pencil hardness test (instructed in ASTM D3363). Adhesion test can be measured with crosshatch adhesion test (instructed in ASTM D3359), pull-off adhesion test (instructed in ASTM D4541), and pull/peel tests. Appearance is also important to organic coatings not only in aesthetics, but also in properties, such as binder system degradation. Gloss (instructed in ASTM D523) and color (instructed in ASTM D1535 and ASTM D2244) are two appearance properties due to interactions between light and organic coatings.

Electrochemical tests are the main characterization for organic coating during corrosion process. It can measure corrosion potential, corrosion current, coating electrical resistance, and coating capacitance. With direct current (DC) measurement, polarization resistance, cyclic polarization, and galvanic corrosion are standard corrosion tests. DC measurement usually gives

both potential information to show the thermodynamic tendency for an electrochemical reaction and current information to show the kinetic reaction rate on the working electrode. With alternate current (AC) measurement, electrochemical impedance spectroscopy (EIS) and electrochemical noise measurement (ENM) are standard measurements. EIS measures electrical properties of various materials in order to generate quantitative data to evaluate the quality of organic coatings. The whole coating systems could be represented by equivalent electrical circuits based on EIS data, shown in Figure 1.6. ENM measures fluctuations of potential and current generated by organic coating systems. The calculated noise resistance can be a good indicator of coating barrier property. Localization index could also be calculated to distinguish uniform corrosion and localized corrosion. Unlike DC measurements, AC measurements are nondestructive measurement and very sensitive to property changes in the coating. Scanning vibrating electrode technique, local electrochemical impedance spectroscopy, scanning ion electrode technique, and scanning polarographic electrode technique can obtain electrochemical signals with spatial resolution.

Scanning electron microscopy (SEM), transmission electron microscopy (TEM), and atomic force microscopy (AFM) could be used to investigate surface morphology of organic coatings. X-ray diffraction (XRD) and X-ray photoelectron spectroscopy (XPS) could characterize compositions of corrosion products. Infrared spectroscopy (IR) and thermal analysis can be good methods to evaluate binder property changes, such as degradation. Inductively coupled plasma and mechanical measurements can trace pigments, especially metal pigments. All these tests characterize blister contents, corrosion products, and coating degradation products in order to discover corrosion mechanisms.

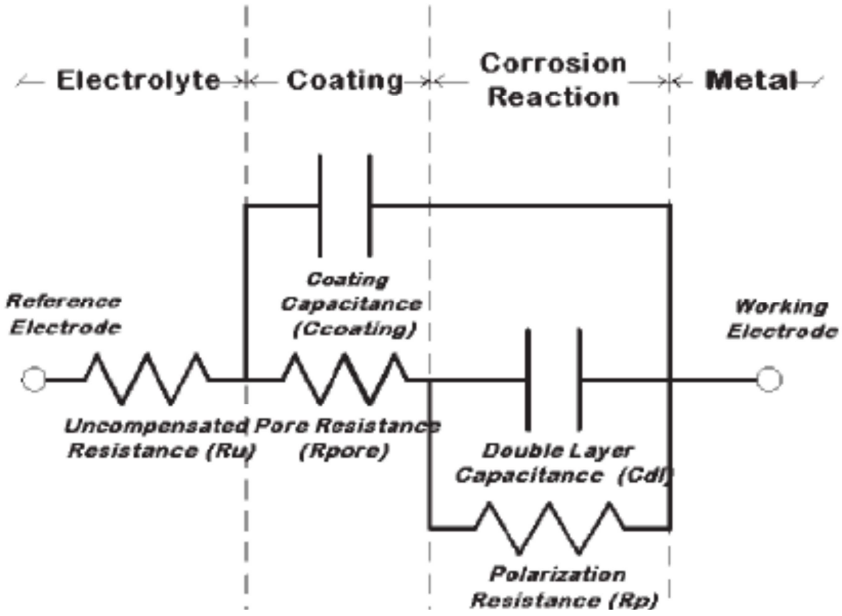

Figure 1.6. Schematic of organic coating system with equivalent electric circuits. With permission from [19]. Copyright 2004 Federation of Societies for Coatings Technology.

Accelerated weather test includes accelerated outdoor exposure and accelerated chamber tests. The accelerated outdoor exposure is usually done either in Florida with hot and humid environment or in Arizona with high UV intensity and low humidity weather. However, the test does not rely only on natural exposure, but is accelerated with facilities to provide more severe conditions. The accelerated chamber tests are using artificial weathering devices. ASTM B117 salt spray test is one of the most popular methods, which maintains a sodium chloride fog at 35˚C produced by 5% sodium chloride solution. It is a good evaluation of corrosion performance of organic coating protecting steel. However, it is not appropriate for metal-rich coatings, since it could not represent corrosive conditions that metal rich primers will be in service for. Prohesion® weather test is another popular accelerated exposure, which includes alternative wet-dry cycles. One hour drying cycle is at 35˚C, while the other wetting cycle is spraying dilute Harrison's solution at 25˚C. The corrosive conditions represent climate and acid rain situations

very well. QUV and Weather-O-Meter are another two major devices, which include ultraviolet radiation besides temperature, humidity and salts parameters. They are used to simulate natural conditions of sun, rain, and temperature. All these accelerated weather tests are to simulate real situations with a short time period. To choose a suitable accelerated weathering method is to keep corrosion mechanisms similar to the field exposure. For real industrial applications, customized accelerated weathering tests are used with optimization for field exposure simulation.

1.3. Scope of Dissertation

The focus of the dissertation was to develop organic coating formulation to protect steel structures. During the investigation, barrier protection and cathodic protection were used for organic coating formulations. Spray technique was the major application method. Sand blasting and phosphoric acid treatment were two major surface pretreatments for steel substrates. Different binder systems and pigment systems were included in the investigation to optimize organic coating formulations. With standard tests including thickness, gloss, and color, EIS was a major characterization to evaluate coating failure and deterioration. Simulated real corrosion condition and accelerated corrosion tests were used to evaluate the performance of organic coatings. Thermal and mechanical analyses, as well as surface analysis including XRD, were used to characterize corrosion products to discover corrosion mechanisms.

The dissertation consists of eleven chapters. Chapter 1 introduces the basic concept of organic coatings for the protection of steel substrates. Chapters 2, 3, 4, and 5 describe the application of organic coatings with barrier protection for pipeline steel to transport supercritical carbon dioxide. Chapter 2 introduces the background of supercritical carbon dioxide and its sequestration related corrosion problems. Chapter 3 investigates current commercial coatings used to resist supercritical carbon dioxide solvent. Chapter 4 describes design strategies for

supercritical carbon dioxide resistant polymer system and its behaviors under supercritical carbon dioxide exposure. Chapter 5 presents the conclusions and recommendations for future research. Chapters 6, 7, 8, and 9 describe the application of organic coatings with cathodic protection for water tank steels etc. Chapter 6 introduces the background of metal rich primers used for steel substrate protection. Chapter 7 describes corrosion mechanism of zinc/magnesium rich primers with different weathering conditions. Chapter 8 presents the performance of different zinc/magnesium rich primers with accelerated weathering tests. Chapter 9 presents the conclusions and recommendations for future research.

1.4. References

1. Van Droffelaar H, Atkinson JTN, Corrosion and its control: An introduction to the subject, 2nd edition; NACE International: Houston TX, 1995.
2. Al-Fozan SA, Malik AU, Effect of seawater level on corrosion behavior of different alloys, International Desalination Association World Congress Conference, Singapore, 2005.
3. Coca FJO, Tello MUL, Gaona-Tiburcio C et al., Corrosion fatigue of road bridge: A review, international Journal of Electrochemical Science, 2011, 6(8): 3438-3451.
4. Stambaugh H, Cohen H, I-35W bridge collapse and response, Technical Report, USFA-TR-166 (2007), U.S. Fire Administration.
5. Postively Minnesota, Department of Employment and Economic Development: Economic impacts of the I-35W bridge collapse. http://www.positivelyminnesota.com/Data_Publications/Data/Research_Reports/Economic_Development_Insights/Economic_Impacts_of_the_I35W_Bridge_Collapse.pdf (accessed July 10, 2012)

6. Breg S, New I-35W bridge elicits dreadful memories and pride in accomplishment, MINNPOST [Online] September 16, 2008. http://www.minnpost.com/politics-policy/2008/09/new-i-35w-bridge-elicits-dreadful-memories-and-pride-accomplishment (accessed July 10, 2012).

7. Bierwagen GP, Organic coatings for corrosion control, ACS Symposium Series 689, American Chemical Society, Washington DC, 1992.

8. Revie RW, Uhlig HH, Corrosion and corrosion control: An introduction to corrosion science and engineering, 4th edition; John Wiley & Sons, Inc., Hoboken NJ, 2008.

9. United States Census Bureau, Paints and allied products, Current Industrial Report, MA325F(10) (July 2011), U.S, Department of Commerce, Washington D.C.

10. Wicks Jr. ZW, Jones FN, Pappas SP et al., Organic coatings: Science and technology, 3rd edition; John Wiley & Sons, Inc., Hoboken NJ, 2007.

11. Bierwagen G, Fishman R, Storsved T et al., Recent studies of particle packing in organic coatings, Progress in Organic Coatings, 1999, 35(1-4): 1-9.

12. Hildebrand JH, Solubility, Journal of American Chemical Society, 1916, 38(8): 1452-1473.

13. Garbassi F, Morra M, Occhiello E, Polymer surfaces: from physics to technology, John Wiley & Sons Ltd., West Sussex, UK, 1998.

14. Regenstein L, Shearman J, Pollution prevention in metal painting and coating operations: A manual for pollution prevention technical assistance providers, Technical Report, Illinois Sustainable Technology Center TR Series-032 (1998), Northeast Waster Management Officials Association.

15. Lu CS, Mai YW, Influence of aspect ratio on barrier properties of polymer-clay nanocomposites, Physical Review Letters, 95(8)(2005), 088303-1-4.

16. http://nzic.org.nz/ChemProcesses/metals/8J.pdf (accessed July 10, 2012).

17. Jones DA, Principles and prevention of corrosion, Macmillan Publishing Company, New York NY, 1992.

18. Feng W, Patel SH, Young MY et al., Smart polymeric coatings-recent advances, Advances in Polymer Technology, 26(1), 2007, 1-13.

19. Loveday D, Peterson P, Rodgers B, Evaluation of organic coatings with electrochemical impedance spectroscopy part 2: Application of EIS to coatings, JCT Coatings Tech, 1(10), 2004, 88-93.

2. INTRODUCTION TO PIPELINE COATINGS FOR $SCCO_2$ TRANSPORTATION

2.1. Motivation

The increase in the concentrations of greenhouse gases, especially CO_2, has been identified as a major contribution to global warming. Geological sequestration of CO_2 is identified as a potential way to either mitigate or delay global warming. In the sequestration process, the transport method of choice is to transport supercritical carbon dioxide phase ($SCCO_2$) by pipeline, which is an economic and efficient way. In the meantime, transport of carbon dioxide into oil reservoirs could help enhanced oil recovery. Currently, there are around 3600 miles of CO_2 pipelines in operation in the United States [1], with more than 50 million tons of CO_2 per year transported by pipeline [2]. With huge cost of approximately a million dollars per mile of pipeline [3], the durability and lifetime of pipeline should be a big matter of concern.

However, corrosion of such pipelines would present a significant safety hazard including human death if the leakage of CO_2 occurs [4,5]. Repair of corrosion damage to pipelines is also very expensive. Some steel corrosion behaviors that might appear in the transport of supercritical carbon dioxide have been investigated [6,7,8,9]. Methods to mitigate corrosion have been developed [10,11,12], such as purification of supercritical carbon dioxide, improved composition of pipeline steels, and use of corrosion inhibitors. Little work has been published on organic coatings for $SCCO_2$ pipeline protection. Little experimental data has been obtained on the corrosion behavior when pressure of carbon dioxide is higher than 2 MPa [12]. Organic coatings to be investigated for pipeline protection relative to their integrities and to increase their service life will contribute to geological sequestration and to mitigate global warming.

2.2. Literature Review

2.2.1. Properties of Carbon Dioxide

Supercritical carbon dioxide has the properties of non-toxicity, non-flammability, cheapness, reasonably high purity, and moderate critical conditions [13,14]. The CO_2 phase diagram of CO_2 is shown in Figure 2.1. The critical temperature and pressure of carbon dioxide are $31.1\,℃$ and $7.38MPa$, respectively [15]. Under the subcritical cooled conditions CO_2 exists mainly as a liquid with a finite vapor pressure. Above the critical condition, it exists as only one phase.

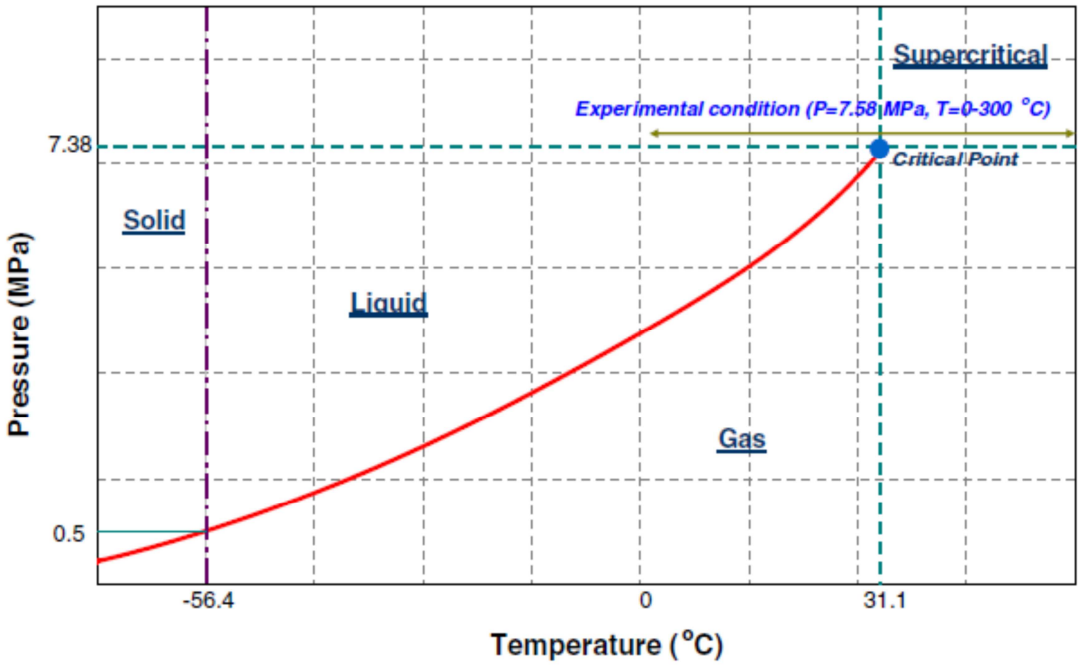

Figure 2.1. Phase diagram of carbon dioxide. With permission from [15]. Copyright 2008, Elsevier.

Physical properties of carbon dioxide, such as the density and the viscosity can be varied [16]. For example, with different temperature, the dielectric values range from 1.01 to 1.45 for gaseous CO_2 and 1.60 to 1.67 for liquid CO_2 [17]. Close to the critical point, physical properties

change rapidly with both pressure and temperature [15], shown in Figure 2.2. This makes the investigation of CO_2 effect on the pipelines difficult.

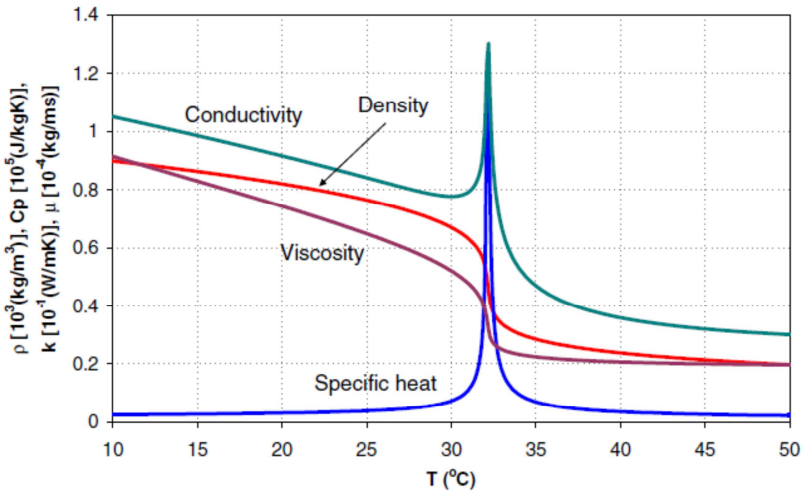

Figure 2.2. Properties change close to the critical point at 7.58MPa. With permission from [15]. Copyright 2008, Elsevier.

CO_2 under normal conditions is considered to be nonpolar and acts as a Lewis acid [18]. In the supercritical state, CO_2 behaves like a polar organic solvent [19]. This increases the solubility of many coating polymers in $SCCO_2$ and makes the design of organic coatings for $SCCO_2$ resistance quite difficult.

$SCCO_2$ has the characteristics of gas-like diffusivity and low surface tension [20, 21]. Solutes in $SCCO_2$ exhibit higher diffusivities relative to many liquid solvents so that a corrosion reaction may be faster if it can occur in such a solvent.

2.2.2. Effects of $SCCO_2$ on Pipeline Steel

CO_2 is an acid gas and can react with water to form carbonic acid. Carbonic acid corrosion of carbon steels is recognized as one of the major damages to pipelines [5], as in below.

$$Fe \rightarrow Fe^{2+} + 2e; H_2CO_3 + 2e \rightarrow CO_3^{2-} + H_2$$

$$Fe^{2+} + CO_3^{2-} \rightarrow FeCO_3$$

When CO_2 partial pressure is greater than 207kPa, carbonic acid will be produced directly [11]. Concentration of carbonic acid is important for the corrosion behavior, shown in Figure 2.3. The corrosion rate of steels increases significantly below pH 3.5 [11], since corrosion reactions mainly depend on acid reactions, which is related to carbonic acid concentration and growth of corrosion products [22]. Corrosion in carbonic acid is also more severe than hydrogen chloride under the same pH due to the additional cathodic reaction, H_2CO_3 reduction in the system [23]. High pressure and high temperature increase the corrosion rate in the case of scale free CO_2 corrosion [12], especially when the temperature is above 110^oC [22]. The formations of protective iron carbonate layers, shown in Figure 2.4, will change the kinetics of process [9]. It serves as a diffusion barrier and covers a portion of the steel surface. Iron carbonate scale growth and its protection depend primarily on the precipitation rate. The protection only occurs when the precipitation rate is higher than the corrosion rate. The higher temperature results in a higher precipitation rate, which can form a protective layer [9]. The corrosion mechanism can be shown in Figure 2.5. Fe_3C serves as the cathodic site, while the $FeCO_3$ layer serves as the protective layer.

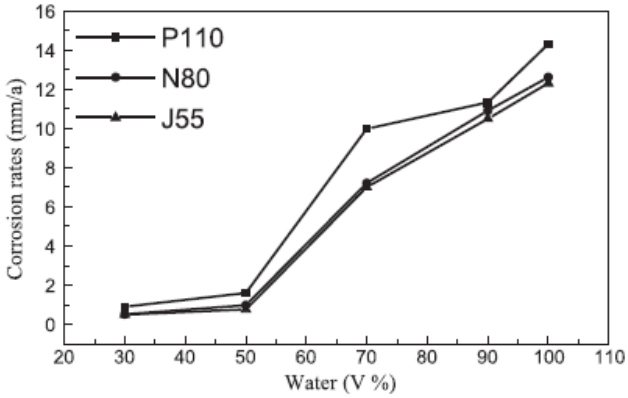

Figure 2.3. The effect of water in CO_2 on the corrosion rate of steel. With permission from [24]. Copyright 2004, Elsevier.

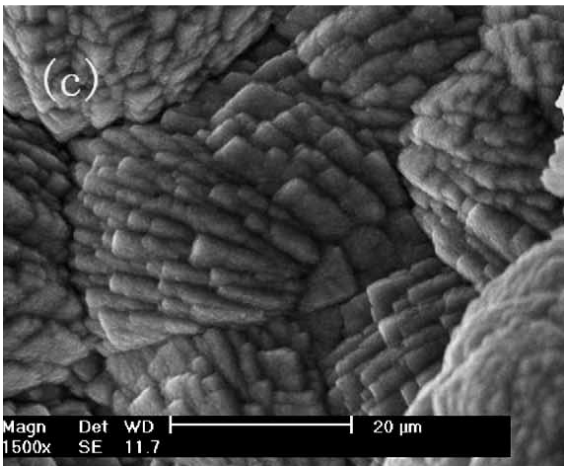

Figure 2.4. The protective layer formed by the corrosion product iron carbonate. With permission from [25]. Copyright 2004, Elsevier.

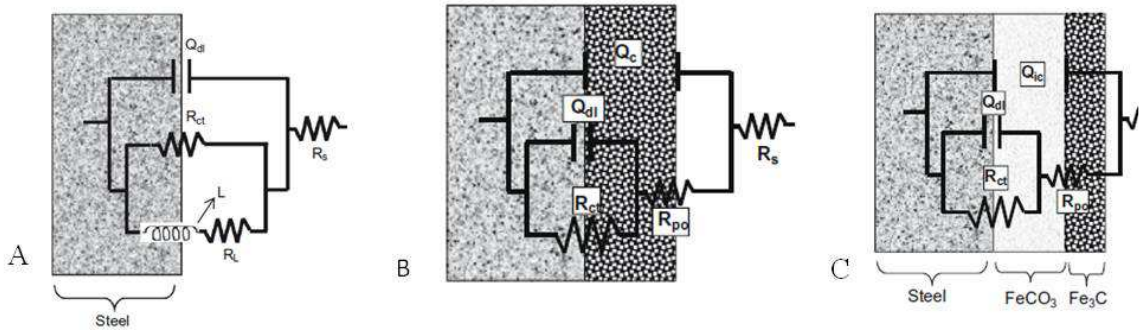

Figure 2.5. The "sweet" corrosion mechanism of steel, (A) Initial stage; (B) Developing stage; (C) Later stage. With permission from [26]. Copyright 2010, Elsevier.

Trace contamination of other gases along with $SCCO_2$ will cause accelerated corrosion [11]. H_2S can cause severe corrosion along with $SCCO_2$ even at concentrations below 1ppm [27]. Iron sulfide is formed as a corrosion product. Corrosion cracking may also happen due to the sulphide stress [28]. The presence of Acetic acid (HAc) can also affect the protective layer of iron carbonate. At 500ppm HAc, the layer becomes porous. At 2000ppm HAc, the layer appears to dissolve [29]. Corrosion behavior with SO_x and NO_x included has not been well defined [11]. However, they will increase corrosion rate dramatically [30].

2.2.3. Corrosion Protection and Characterization

Steel pipeline can be designed with zinc plating, coating, and plastic lining [31]. Organic coatings should neither be soluble into $SCCO_2$, nor absorb $SCCO_2$. $SCCO_2$ should not diffuse into the organic coatings. Drying of CO_2 can be regarded as an effective corrosion protection [32] due to lack of corrosion with pure CO_2. Pigments can be also used to entrap CO_2 [33], which could supply a new way to protect pipeline steel. Corrosion inhibitor monoethylene glycol can also be added to prevent the corrosion reactions [12]. It has been proved that at 20ppm this corrosion inhibitor can decrease the corrosion rate to 0.1mm/year at temperature around 30˚C and pressure around 7.2MPa. Hexadecylthrimethylammonium bromide was also found to provide the good corrosion protection among the inhibitors tested [34] with the corrosion rate still higher than 1mm/year.

To emulate dirty CO_2 or contaminated CO_2 in the laboratory, Barlet-Gouedard V et al. designed a vessel with water at the bottom [35]. They obtained the water saturated with CO_2 at the bottom and the wet supercritical CO_2 at the top, as shown in Figure 2.6 (a). To characterize the corrosion progress of pipeline steel exposed to $SCCO_2$, Beck J et al. put electrodes inside a vessel for in situ measurement of impedance, shown in Figure 2.6 (b) [36].

Organic coatings for corrosion protection can be evaluated by visual inspection, such as the formation of blisters [37] and over-film corrosion [38]. Gloss and color are two major methods to quantify visual appearance. There are different glosses, such as specular gloss, contrast gloss, and surface uniformity gloss [39], among which specular gloss is mostly used in the coating industrials. It depends on the surface topography, including the roughness and the lateral correlation length [40]. Gloss decreases exponentially with increasing roughness [41]. Crosslinking changes the gloss too. With the crosslinking density increasing, the gloss value

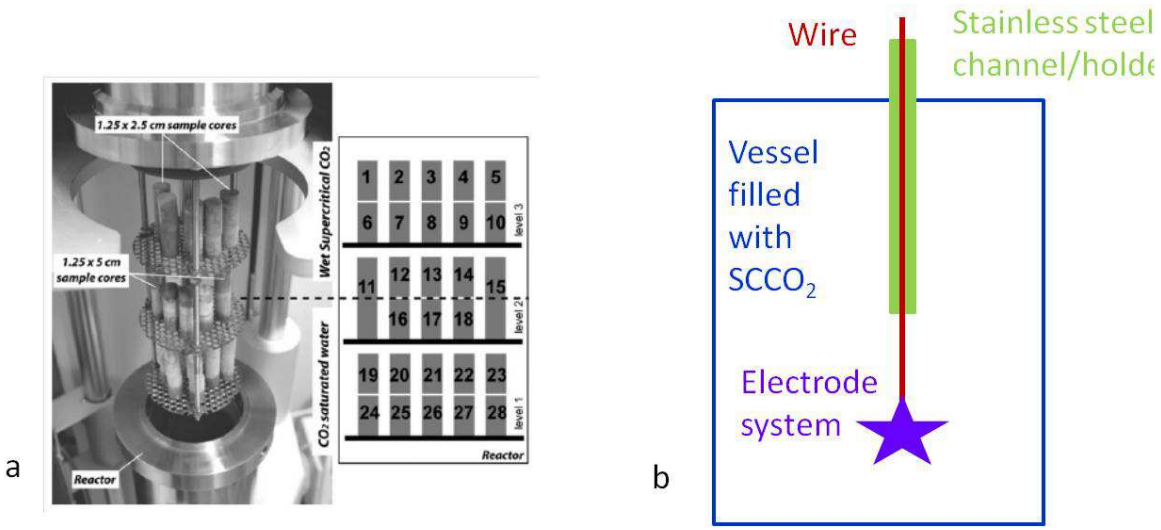

Figure 2.6. $SCCO_2$ exposure test, (a) CO_2 reaction vessel, with permission from [35], Copyright 2009, Elsevier**;** (b) Schematic of on-site EIS measurement [36].

increases initially, reaches the maximum, and decreases later [42]. However, gloss is independent to the thickness of the coatings [43]. Color is more complicated than gloss. It depends on the pigments, the binders, and the processing. The degradation of organic coatings could cause the discoloration (whitening) [44] due to pigment bleaching. Color also changes to be yellowing due to the weathering process [45]. Chroma decreases with the increase of surface roughness [46]. Color changes by crosslinking density. As crosslinking density increases, the color value increases initially and reaches a plateau [47]. The color difference also increases as the amplitude of fluctuation increases [48]. Color does depend on the thickness of coating until it reaches infinite optical thickness [43].

Barrier properties of organic coatings can be evaluated by weight and thickness tests, pressure decay method, frequency modulation and chromatographic methods, in order to check solubility of polymers in $SCCO_2$ and diffusivity of $SCCO_2$ in polymers [49]. Spectroscopy methods can also be used to check solubility due to the interaction of groups of bonds changing

the vibrations [17]. The influence of $SCCO_2$ on organic coatings can be evaluated by thermal analysis due to the plasticization of organic coatings [50], as shown in Figure 2.7.

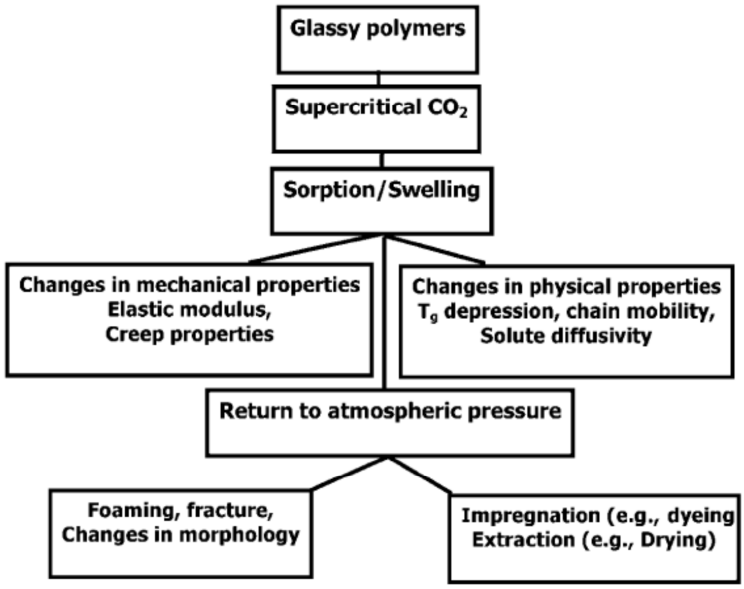

Figure 2.7. The effect of $SCCO_2$ on polymers. With permission from [50]. Copyright 2006, Taylor & Francis.

Corrosion behaviors of pipeline steel exposed to $SCCO_2$ can utilize electrochemical impedance spectroscopy (EIS) to determine corrosion mechanisms [36, 51], infrared spectroscopy methods to identify the corrosion products [51], and surface analysis methods to measure the corrosion product morphologies and compositions [51]. EIS was a good method to determine corrosion process if passive layer was formed, degraded and reformed [25, 36].

2.3. Scope of Investigation

The focus of this part of the thesis was to develop organic coatings with barrier protection for pipeline steel to transport supercritical carbon dioxide. During the investigation, the following studies were carried out.

1. Commercial coatings and designed coatings were both investigated and compared to select better corrosion mitigation properties.
2. Test protocols for $SCCO_2$ resistance were developed. During the exposure, temperature and pressure of $SCCO_2$, and exposure period to $SCCO_2$ were considered as variable parameters. After the exposure, thickness, weight, color, gloss, and impedance were considered as evaluation parameters.
3. Failure mechanisms were discussed. Failure modes were discovered especially by visual results. Failure mechanisms were related to properties of organic coatings in order for future design.

The part of investigation consists of four chapters. Chapter 2 describes the research background of the pipeline steel with $SCCO_2$. Chapter 3 describes corrosion behaviors of several commercial coatings exposed to $SCCO_2$. Chapter 4 describes the design of organic coatings and characterizations of the behaviors of these organic coatings in $SCCO_2$. Finally, chapter 5 gives the conclusions of this part of the study and recommendation for future research.

2.4. References

1. Vann A, Parfomak PW, Regulation of carbon dioxide sequestration pipelines: Jurisdictional issues, CRS report for Congress, RL34037 (April 15, 2008).
2. Carbon Capture and Storage http://www.cgenpower.com/kgh/kgh_transport_storage.html#, (Accessed August 1, 2012).
3. Bergman P, Overview of U.S. Department of Energy research subprogram in CO_2 capture, re-use and disposal, Waste Management, 1997, 17(5-6): 289-293.

4. Elgin B, The dirty truth about clean coal, Business Week, June 18, 2008. http://www.businessweek.com/stories/2008-06-18/the-dirty-truth-about-clean-coal (accessed August 1, 2012).
5. Barrie J, Brown K, Hatcher PR et al., Carbon dioxide pipelines: A preliminary review of design and risks, Greenhouse Gas Control Technologies 7, 2005, 1, 315-320.
6. Altoe PG, Pimenta CF, Moulin CF et al., Evaluation of oilfield corrosion inhibitors in CO_2 containing media: A kinetic study, Electrochimica Acta, 1996, 41(7-8): 1165-1172.
7. Bai ZQ, Chen CF, Lu MX et al., Analysis of EIS characteristics of corrosion of well tube steels with corrosion scales, Applied Surface Science, 2006, 252(20): 7578-7584.
8. Lin GF, Zheng MS, Bai ZQ et al., Wear resistance of CO_2 corrosion product scale formed at high temperature, Journal of Iron and Steel Research International, 2006, 13(5): 47-52.
9. Nesic S, Key issues related to modeling of internal corrosion of oil and gas pipelines- A review, Corrosion Science, 2007, 49(12): 4308-4338.
10. Udvardi G, Gerecs L, Ouchi Y et al., CO_2 dehydration scheme aids Hungarian EOR project, Oil and Gas Journal, 1990, 88(43): 74-79.
11. Thomas DC, Benson SM, Impact of SO_x and NO_x in flue gas on CO_2 separation, compression and pipeline transmission, Carbon Dioxide Capture for Storage in Deep Geologic Formations, 2005, 2: 955-981.
12. Seiersten M, Kongshaug KO, Materials selection for capture, compression, transport and injection of CO_2, Carbon Dioxide Capture for Storage in Deep Geologic Formations, 2005, 2: 937-953.

13. Esteki M, Rezayat M, Ghaziaskar HS et al., Application of QSPR for prediction of percent conversion of esterification reactions in supercritical carbon dioxide using lease squares support vector regression, J. Supercritical Fluids, 2010, 54 (2): 222-230.

14. Liu ZT, Sun ZF, Liu ZW et al., Benzylated modification and dyeing of ramie fiber in supercritical carbon dioxide, Journal of Applied Polymer Science, 2008, 107(3): 1872-1878.

15. He S, Kim WS, Jackson JD, A computational study of convective heat transfer to carbon dioxide at a pressure just above the critical value, Applied Thermal Engineering, 2008, 28(13): 1662-1675.

16. Breitenbach A, Mohr D, Kissel T, Biodegradable semi-crystalline comb polyesters influence the microsphere production by means of a supercritical fluid extraction technique, Journal of Controlled Release, 2000, 63(1-2): 53-68.

17. Canelas DA, Burke ALC, DeSimone JM, Carbon dioxide as a continuous phase for polymer synthesis, Plastics Engineering, 1997, 53(12): 37-40.

18. Gohres JL, Shukla CL, Popov AV et al., Effects of solute structure on local salvation and solvent interactions: results from UV/Vis Spectroscopy and molecular dynamics simulations, J. Phys. Chem. B, 2008, 112(47): 14993-14998.

19. Nguyen QT, Baird DG, An improved technique for exfoliating and dispersing nanoclay particles into polymer matrices using supercritical carbon dioxide, Polymer, 2007, 48(23): 6923-6933.

20. Hwang TY, Lee SM, Ahn Y et al., Development of polypropylene-clay nanocomposite with supercritical CO2 assisted twin screw extrusion, Korea-Australia Rheology Journal, 2008, 20(4): 235-243.

21. Kondoh E, Fukuda J, Deposition kinetics and narrow-gap-filling in Cu film growth from supercritical carbon dioxide fluids, J. Supercritical Fluids, 2008, 44(3): 466-474.

22. Zheng YC, Gao KW, Schmitt G et al., Water effect on steel under supercritical CO2 condition, NACE Corrosion 2011 Conference & Expo, 11378, Houston, TX, 2011.

23. Song FM, A comprehensive model for predicting CO2 corrosion rate in oil and gas production and transportation systems, Electrochimica Acta, 2010, 55(3): 689-700.

24. Cui ZD, Wu SL, Li CF et al., Corrosion behavior of oil tube steels under conditions of multiphase flow saturated with super-critical carbon dioxide, Materials Letters, 2004, 58(6): 1035-1040.

25. Wu SL, Cui ZD, Zhao GX et al., EIS study of the surface film on the surface of carbon steel from supercritical carbon dioxide corrosion, Applied Surface Science, 2004, 228: 17-25.

26. Farelas F, Galicia M, Brown B et al., Evolution of dissolution processes at the interface of carbon steel corroding in a CO_2 environment studied by EIS, Corrosion Science, 2010, 52(2), 509-517.

27. de Visser E, Hendriks C, Barrio M et al., Dynamic CO_2 quality recommendations, International Journal of Greenhouse Gas Control, 2008, 2(4): 478-484.

28. Vandeginste V, Piessens K, Pipeline design for a least-cost router application for CO_2 transport in the CO2 sequestration cycle, International Journal of Greenhouse Gas Control, 2008, 2(4): 571-581.

29. Nazari MH, Allahkaram SR, The effect of acetic acid in the CO_2 corrosion of grade X70 steel, Materials and Design, 2010, 31(9): 4290-4295.

30. Choi YS, Nesic S, Effect of water content on the corrosion behavior of carbon steel in supercritical CO_2 phase with impurities, NACE Corrosion 2011 Conference & Expo, 11377, Houston, TX, 2011.

31. Akasaki H, Progress in pipe and tube technology and its future prospect: Application and manufacturing, Nippon Steel Technical Report, No. 90, July 2004.

32. Bratfos HA, Leinum BH, Torbergsen LE et al., Journal of Pipeline Engineering, 2007, 6(3): 161-172

33. Lastoskie C, Caging Carbon Dioxide, Science, 2010, 330(6004): 595-596.

34. Zheng YC, Gao KW, Schmitt G, Inhibition of steel corrosion under aqueous supercritical CO_2 conditions, NACE Corrosion 2011 Conference & Expo, 11378, Houston, TX, 2011.

35. Barlet-Gouedard V, Rimmele G, Porcherie O et al., A solution against well cement degradation under CO_2 geological storage environment, International Journal of Greenhouse Gas Control, 2009, 3(2): 206-216.

36. Beck J, Lvov S, Fedkin M et al., Electrochemical system to study corrosion of metals in supercritical CO_2 fluids, NACE Corrosion 2011 Conference & Expo, 11380, Houston, TX, 2011.

37. Schneider O, Kelly RG, Localised coating failure of epoxy coated aluminum alloy 2024-T3 in 0.5M NaCl solutions: comparison of conventional electrochemical techniques and microelectrochemical methods, Corrosion Engineering Science and Technology, 38(2003), 119-128.

38. Shreepathi S, Guin AK, Naik SM et al., Service life prediction of organic coatings: electrochemical impedance spectroscopy vs actual service life, Journal of Coatings Technology and Research, 8(2011), 191-200.

39. Lozano RD, A new approach to appearance characterization, Color Research and Application, 31(2006), 164-167.

40. Arino I, Kleist U, Mattsson L et al., On the relation between surface texture and gloss of injection-molded pigmented plastics, Polymer Engineering and Science, 45(2005), 1341-1356.

41. Briones V, Aguilera JM, Brown C, Effect of surface topography on color and gloss of chocolate samples, Journal of Food Engineering, 77(2006), 776-783.

42. Zhao QL, Li XG, Gao J, Aging of ethylene-propylene-diene monomer (EPDM) in artificial weathering environment, Polymer Degradation and Stability, 92(2007), 1841-1846.

43. Solah VA, Crosbie GB, Huang S et al., Measurement of color, gloss, and translucency of white salted noodles: effects of water addition and vacuum mixing, Cereal Chemistry, 84(2007), 145-151.

44. Kiguchi M, Kataoka Y, Matsunaga H et al., Surface deterioration of wood-flour polypropylene composites by weathering trials, Journal of Wood Science, 53(2007), 234-238.

45. Capanescu C, Cincu C, Evaluation of UV inhibitors in polyester gelcoats, Advances in Polymer Technology, 22(2003), 365-372.

46. Briones V, Aguilera JM, Brown C, Effect of surface topography on color and gloss of chocolate samples, Journal of Food Engineering, 77(2006), 776-783.

47. Zhao QL, Li XG, Gao J, Aging of ethylene-propylene-diene monomer (EPDM) in artificial weathering environment, Polymer Degradation and Stability, 92(2007), 1841-1846.

48. Bierwagen GP, Estimation of film thickness nonuniformity effects on coating optical-properties, Color Research and Application, 17(1992), 284-292.

49. Tomasko DL, Li HB, Liu DH et al., A review of CO2 applications in the processing of polymers, Ind. Eng. Chem. Res., 2003, 42(25): 6431-6456.

50. Chehroudi B, Supercritical fluids: nanotechnology and select emerging applications, Combust. Sci. and Tech., 2006, 178(1-3): 555-621.

51. Han JB, Carey JW, Zhang JS, Effect of debonded interfaces on corrosion of mild steel composites in supercritical CO_2-saturated brines, NACE Corrosion 2011 Conference & Expo, 11376, Houston, TX, 2011.

3. INVESTIGATION OF COMMERCIAL COATINGS EXPOSED TO $SCCO_2$

3.1. Introduction

As stated in section 2.2.2, sweet corrosion may occur in $SCCO_2$ transport. When some contaminations or dirty $SCCO_2$ exist, most often from SO_x, NO_x, and H_2S, the environment of $SCCO_2$ fluid becomes acidic. With all these factors considered, corrosion behaviors of pipeline steel exposed to $SCCO_2$ are caused by these acidic environments. Organic coatings to protect pipeline steel from corrosion exposed to $SCCO_2$ should thus be acid resistant. $SCCO_2$ transport may need pumping flue gas to geological storage sites, mostly oil fields. Gas and/or oil may be remaining in $SCCO_2$ fluid without sufficient purification process. Organic coatings with corrosion protection for pipeline steel thus need to be very chemically resistant. With fluid transported, organic coatings may encounter with erosion-corrosion problems, and thus should also have high abrasion resistance. With all these factors considered from Table 1.2, epoxy and phenolic coating systems were selected for initial investigation of commercial organic coatings corrosion behaviors when exposed to $SCCO_2$.

In this chapter, the barrier properties of organic coatings are investigated. Two different conditions of $SCCO_2$ were applied for corrosion test. One is $SCCO_2$ at $32℃ - 7.58MPa$, while the other is $SCCO_2$ at $40℃ - 10.00MPa$. As stated in section 2.2.3, organic coating failure can be investigated by visual inspection. The high solubility and diffusivity of $SCCO_2$ will not only change surface roughness but also change adhesion force between pigments and binders. Therefore gloss and color values could change and were measured in the exposure process. Barrier properties were evaluated by weight and thickness change. Thickness and weight measurement have also been done for $SCCO_2$ effects on organic coatings. EIS was utilized as the

major tool to characterize corrosion behaviors and to evaluate barrier properties of organic coatings.

3.2. Experimental Methods

3.2.1. Materials

TZ™ 904 coating, DevChem™ 253 coating, Scotchkote™ 345 coating, and Scotchkote™ 323 coating were four commercial coating systems selected for $SCCO_2$ exposure investigations.

TZ™ 904 is a high performance coating from Chevron Phillips Chemical Company and is a high-build modified epoxy coating engineered to provide outstanding resistance for steel structures in corrosive environments (http://www.cpchem.com/bl/specchem/en-us/tdslibrary/TZ_904_TDS_v808.pdf).

Devchem™ 253 is a two-component epoxy novolac coating from International Paints (http://www.duspec.com/DuSpec2/product/ProductDocumentSearchController.htm?documentFormat=pdf&systemSetId=13&productCode=253&documentType=datasheet&submit=Get+Document). DevChem™ 253 is claimed to have an exceptional resistance to a wide range of chemicals and solvents. DevChem™ 253 is typically used for industrial storage and process chemical tanks and pipelines, high pressure crude oil pipes and separation tanks. DevChem™ 253 is also used as a protective coating for highly corrosive environments.

Scotchkote™ 323 is a two-component system designed to protect steel pipe and other metal surfaces from the harsh effects of corrosion and can be used as internal lining (http://multimedia.3m.com/mws/mediawebserver?mwsId=SSSSSu7zK1fslxtU4Y_xMYtxev7qe17zHvTSevTSeSSSSSS--). This coating is resistant to damage by acids and bases in the pH range of 2 to 14. Scotchkote™ 323 is also resistant to hydrocarbons and many solvents.

Scotchkote™ 345 is a liquid one-part phenolic primer designed for application to metal surfaces prior to top coating with Scotchkote fusion bonded epoxy (FBE- which is high temperature applied epoxy powder coatings, the current industry standard for the protective layers closest to the metal.) coating (http://solutions.3m.com/wps/portal/3M/en_US/Corrosion/Protection/Products/Catalog2/?PC_7_RJH9U523001R40I49E2FVI20E3_nid=L7QJ75BXFQbe7C5QZ78847gl).

S36 steel panels, purchased from Q-Lab, were used as the substrate in these following coating studies. Hexane, purchased from Sigma-Aldrich, was used as the degreasing agent for steel panel preparation. Toluene, purchased from Sigma-Aldrich, was used as the solvent for TZ™ 904 coating preparation. Xylenes, purchased from Sigma-Aldrich, were used as the viscosity adjuster for spray application. Ammonia sulfate and sodium chloride, purchased from Sigma-Aldrich, were used in dilute Harrison's solution (DHS) preparation. All these Sigma-Aldrich chemicals were reagent grade. CO_2 gas was purchased from PRAXAIR with >99% purity.

3.2.2. Characterizations

An Elcometer 345 FS film thickness gauge was used to measure the thickness of organic coatings on steel S36 substrate. An X-Rite SP 64 color spectrophotometer was used to measure the color coordinates of $L^*a^*b^*$ using a D65 light source with 10 degree observer. It took 10 points on each surface. The average color value of $L^*a^*b^*$ was used to describe the color of the coatings. The color difference change on exposure was calculated by

$$\Delta E = \sqrt{(\Delta L^*)^2 + (\Delta a^*)^2 + (\Delta b^*)^2}; \text{where } \Delta L^* = L^* - L_0^*; \Delta a^* = a^* - a_0^*; \Delta b^* = b^* - b_0^*$$

where $(L_0^* a_0^* b_0^*)$ are for the original color values. A Mettler Toledo AL 204 was used for weight measurement. A BYK-Gardner micro-TRI Gloss meter was used to measure the gloss with angle

of 20 degrees, 60 degrees, and 85 degrees. The measurement took 3 points on the surface for each angle. The average gloss value was used to describe the gloss of the coatings. A Gamry Potentiostat Reference 600 was used for EIS testing. The electrolyte was DHS, which comprised of 0.35wt% $(NH_4)_2SO_4$ and 0.05wt% NaCl in distilled water. EIS data were collected for 100kHz to 0.01Hz frequency range with a 10mV rms amplitude at 10points/dec.. Dynamic mechanical analysis (DMA) is using tensile measurement of the film with the size around $15 * 5 * 0.4mm$ by DMA Q800. The temperature ranges from the room temperature to 275^oC with the rate of $5^oC/min$.

3.2.3. Experimental Set-up

Organic coatings were applied on steel substrates both by drawdown and spray techniques. For drawdown films, steel substrates were sanded using #320 and #600 sand papers and degreased by hexane. For spray methods, steel substrates were sand blasted with aluminum oxide and degreased by hexane. Organic coatings with the four commercial coating formulations were prepared as described in Table 3.1. For the four commercial coating systems, TZ™ 904 and

Table 3.1. Organic coating formation of four commercial formulations

Organic coatings	Materials	Operation methods	Curing conditions
TZ™ 904	1:1 volume ratio of TZ™ 904 R and H	8 mils drawdown with toluene adjusted viscosity	24 hours at room temperature
		Spray with toluene adjusted viscosity	
DevChem™ 253	4:1 volume ratio of DevChem™ 253 base and convertor	8 mils drawdown with xylenes adjusted viscosity	5 days at room temperature
		Spray with xylenes adjusted viscosity	
Scotchkote™ 323	2:1 volume ratio of Scotchkote™ 323 part A and part B	Spray	24 hours at room temperature
Scotchkote™ 345	One component	Spray	30 minutes at 240°C

DevChem™ 253 were applied by both drawdown and spray techniques. The formulations were adjusted for proper application by toluene and xylenes, respectively. Scotchkote™ 323 and Scotchkote™ 345 were applied only by spray techniques, because during the investigation, spray techniques were discovered to provide better barrier properties than drawdown techniques. The films were sprayed at different thickness to investigate thickness effect on film properties.

Supercritical carbon dioxide exposure was performed using the set-up presented in Figures 3.1 and 3.2. The coated sample panels were put into the high pressure test vessel. The vessel was immersed in a water bath at approximately 4^{o}C. The vessel was first evacuated and then filled with carbon dioxide gas. The process was repeated three times to ensure there was no contamination from remaining air. After this the vessel was filled with around 0.5 Kg of carbon dioxide (the CO_2 tank was placed on a scale to monitor the weight), with the pressure monitored to approximately 6.8 MPa. With the system tightly sealed, the recirculator started to rise temperature of water bath to the preset temperature. The temperature of $SCCO_2$ was monitored by a thermo couple inserted in the vessel, as shown in Figure 3.2 B. Care was taken to adjust the ventilated valve to release the pressure to a predefined pressure, monitored by the pressure gage attached to the vessel, shown in Figure 3.2 B. After adjustments, the predefined pressure was maintained. The coated panels were held under those conditions for different periods. In this investigation, two conditions of $SCCO_2$ were chosen. One was $SCCO_2$ at $32℃ - 7.58MPa$, very close to critical point of carbon dioxide. The other is $SCCO_2$ of $40℃ - 10.00MPa$, close to real condition often used for transportation for $SCCO_2$.

Figure 3.1. A complete reaction set-up of $SCCO_2$ exposure test.

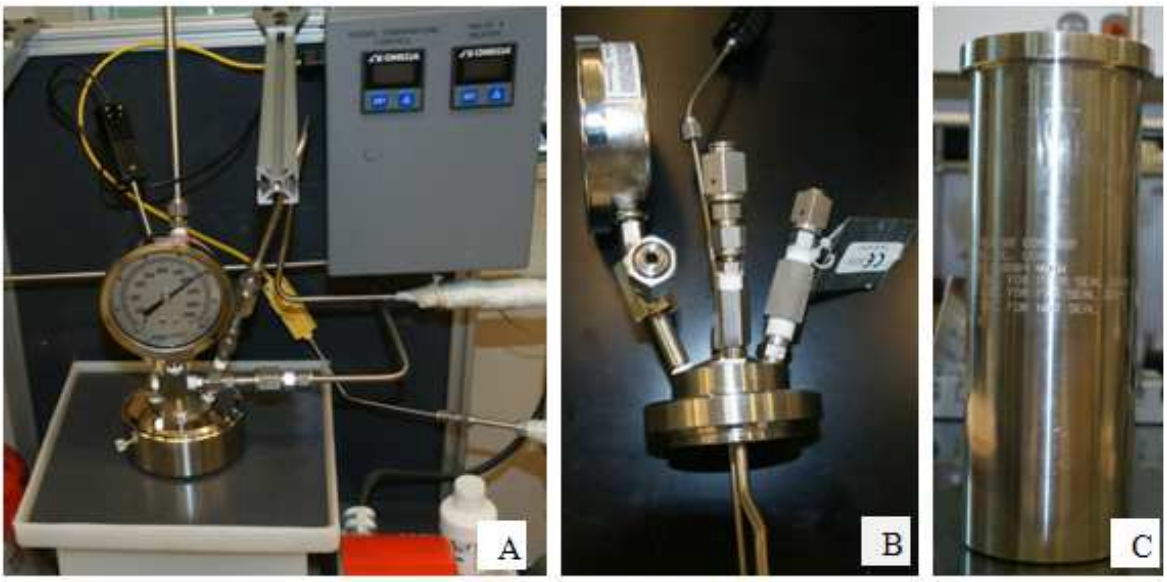

Figure 3.2. The parts of the reaction set up. (A) the assembled vessel; (B) the top part of the vessel; and C: the bottom part of the vessel.

3.3. Results and Discussions

3.3.1. Performance of TZ™ 904 Coatings

The preparation of the different coating samples is described in Table 3.2. The nomenclature follows the rule of "coating-application method-thickness" to represent each coating system. Four types of samples were prepared. The samples were exposed to $SCCO_2$. Then they were evaluated by visual inspections and EIS characterizations.

Table 3.2. Samples of TZ™ 904 coatings

Sample	Name	Application method	Thickness/μm
1	TZ-D-107μm	Drawdown	107
2	TZ-S-63μm	Spray	63
3	TZ-S-145μm	Spray	145
4	TZ-S-313μm	Spray	313

Pictures of these films before and after exposure to supercritical conditions are given in Figure 3.3. TZ-D-107μm exposed to $SCCO_2$ of 35℃ and 10.9MPa for 48 hours had many smaller blisters formed on the surface, while TZ-S-313μm exposed to $SCCO_2$ of 40℃ and 10.00MPa for 24 hours had several larger blisters formed. All the other samples were unchanged under exposure to $SCCO_2$ of both 32℃ and 7.58MPa for 24 hours and 40℃ and 10.00MPa for 24 hours. The measured thickness changes with the exposure are shown in Figure 3.4. TZ-D-107μm had a lot of blisters on the surface, which made the thickness measurement not accurate. Although TZ-S-313μm had blisters on the surface, thickness measurements were avoiding these locations. With all these samples, thickness did not change significantly. It was a sign of neither significant sorption of carbon dioxide in the coating nor significant dissolution of coating into $SCCO_2$. Regarding appearance change, gloss at 60 degrees decreased, as shown in Figure 3.5. Color difference in b value and in ΔE value increased after exposure, shown in Figure 3.6. All these changes in gloss and color might be due to increasing

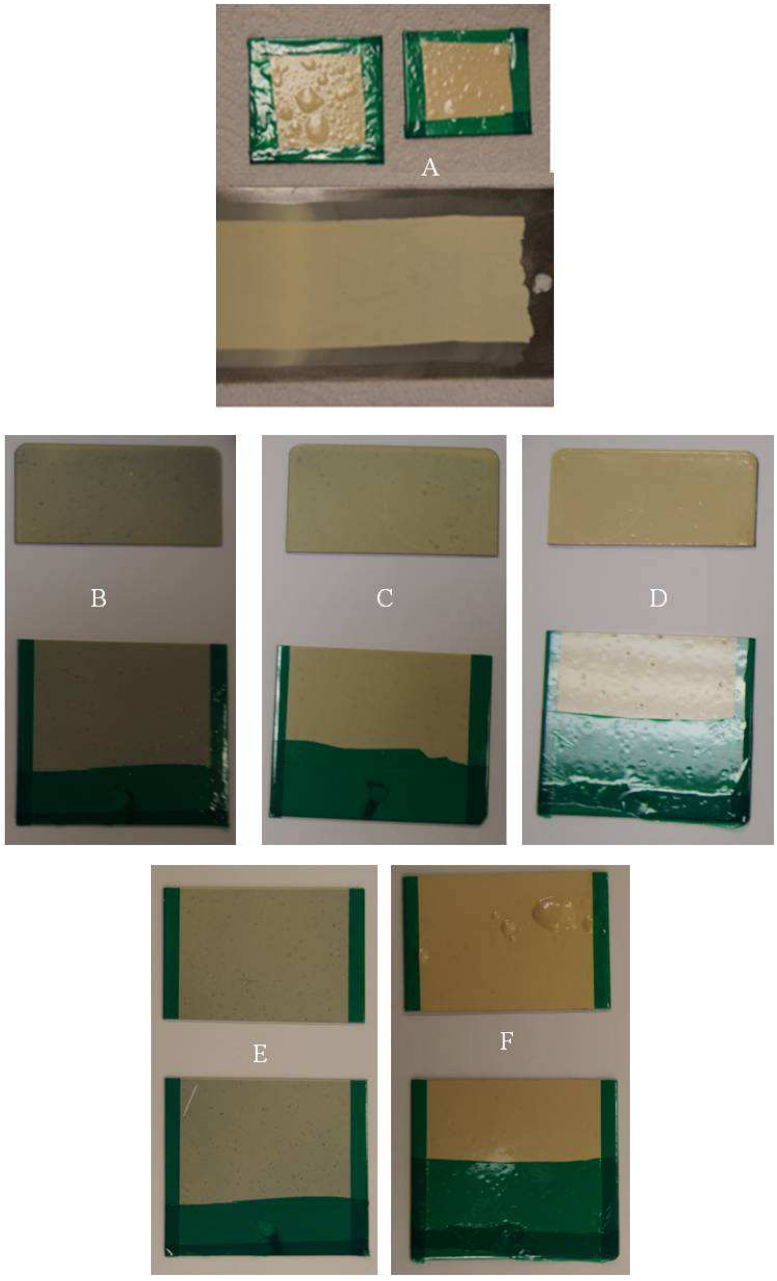

Figure 3.3. The above: coated small panels after exposure to $SCCO_2$; and the below: unexposed original panels. (A) TZ-D-107µm exposed to $SCCO_2$ of 35℃ and 10.9MPa for 48 hours. (B) TZ-S-63µm; (C) TZ-S-145µm; and (D) TZ-S-313µm exposed to $SCCO_2$ of 32℃ and 7.58MPa for 24 hours. (E) TZ-S-63µm; and (F) TZ-S-313µm exposed to $SCCO_2$ of 40℃ and 10.00MPa for 24 hours. (Note: the samples had to be cut to be able to fit inside the pressure vessel).

roughness, because roughness increases color difference but decreases gloss [1,2]. Color difference in b value increasing usually represents polymer degradation [3].

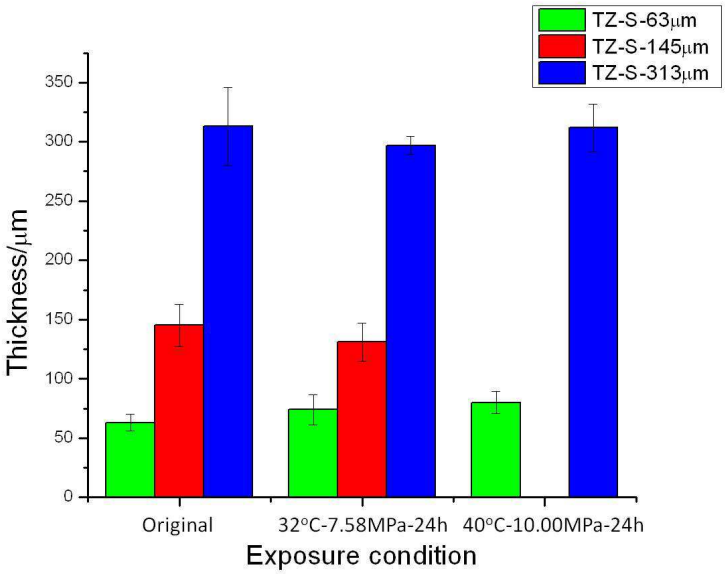

Figure 3.4. Thickness change with different exposure conditions.

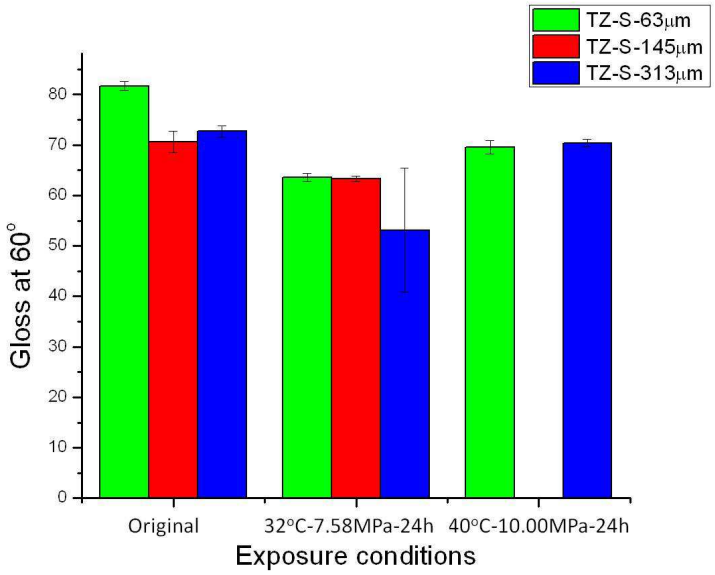

Figure 3.5. Gloss change with different exposure conditions.

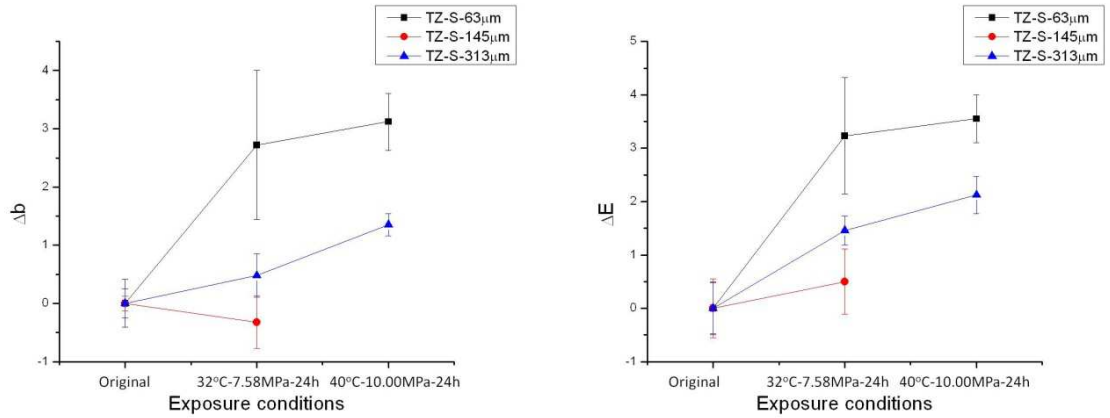

Figure 3.6. Color value change with different exposure conditions

Electrochemical impedance spectroscopy is shown in Figure 3.7. For TZ-D sample, the impedance became lower after the exposure due to electrolyte penetration. It was in accordance with the blister formation and increased in diffusion coefficient from porosity. The exposure to $SCCO_2$ had less influence to the impedance of the thicker coatings. The resistance decreased with the more severe exposure conditions in $SCCO_2$. With the thicker coatings, the percentage of decrease was smaller. The impedance values at high frequencies of EIS measurement remained relatively constant through exposure.

From the above results, although the thickness of coatings did not change significantly, visual inspections showed blisters formed in coatings. The gloss of the coatings decreased. Color of the coatings changed in yellowing. Impedance of coatings decreased. All indicated that $SCCO_2$ did have some effects on TZ™ 904 coatings. Since $SCCO_2$ has low viscosity and high diffusivity, it could diffuse into coatings and deteriorated coatings. Thinner coatings showed more changes, because thinner coatings were affected more by $SCCO_2$ diffusion. The diffusion path of $SCCO_2$ may be used as the electrolyte penetration path to decrease impedance. The

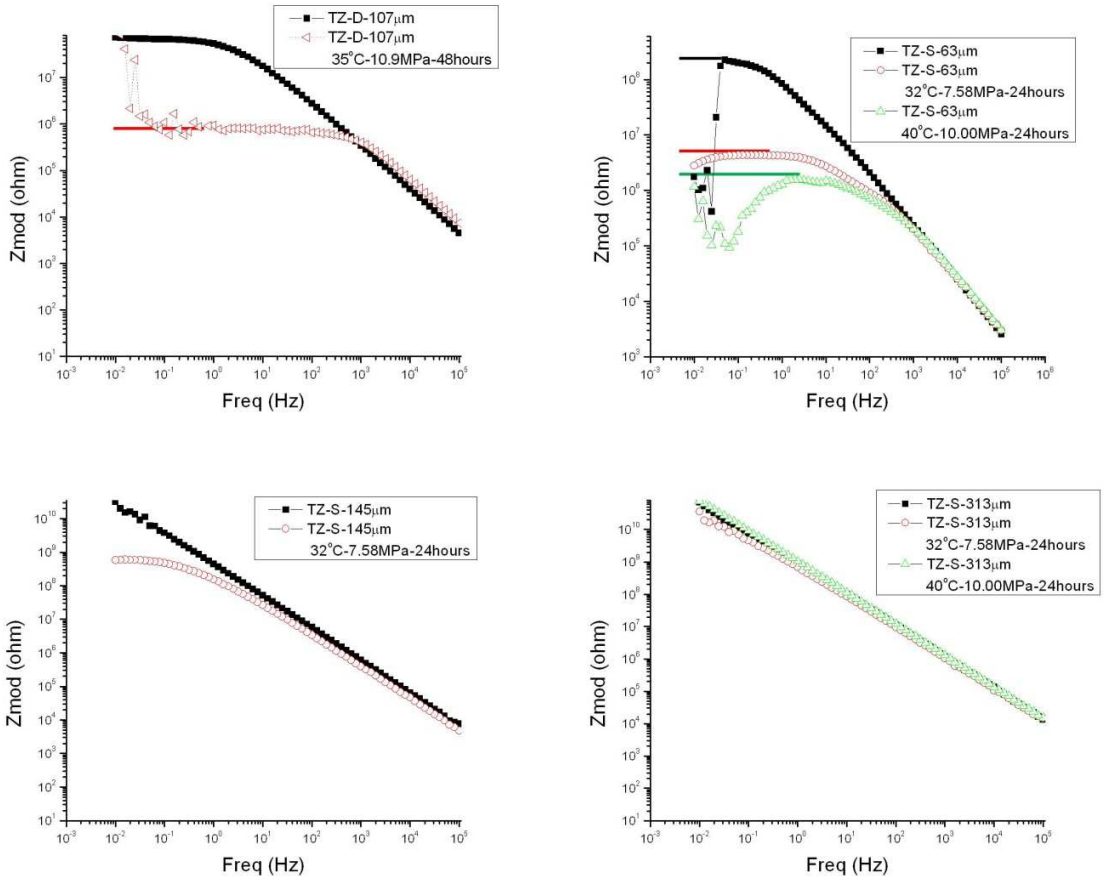

Figure 3.7. Electrochemical impedance spectroscopy of TZ™ 904 coatings with various exposure conditions. (The solid line represents the possible actual spectroscopy)

diffusion of $SCCO_2$ made the surface rougher and made the barrier properties of organic coatings worse, especially for thinner coatings.

However, blisters formed in the films in different ways. Blisters formed in TZ-D-107μm sample and the TZ-S-313μm sample, the thickest coating. The blisters formed due to $SCCO_2$ diffusion into organic coatings and inadequate diffusion out of organic coatings once pressure was released. Compared with other coatings, the TZ-D-107μm coating had low adhesion, which allowed $SCCO_2$ to diffuse into the film to displace it at the interface. The TZ-S-313μm coatings were thick enough so that $SCCO_2$ could not diffuse out of the coating film when pressure was released. However, this situation only happened at 40℃ and 10.00MPa for 24 hours. The

reason might be the low pressure at 7.58MPa was not high enough to form blisters on the coating surfaces. So blisters were formed on the surface when the force caused by the pressure of the trapped CO_2 in coatings was higher than the adhesion force.

3.3.2. Performance of DevChem™ 253 Coatings

The different coating films are studied in Table 3.3. Three types of samples were prepared. The samples were exposed to $SCCO_2$. Then they were evaluated by appearance measurements, visual inspection and EIS characterization.

Table 3.3. Samples of DevChem™ 253 coatings

Sample	Name	Application method	Thickness/μm
1	DV-D-74μm	Drawdown	74
2	DV-S-52μm	Spray	52
3	DV-S-159μm	Spray	159

Pictures of organic coatings before and after exposure to supercritical conditions are given in Figure 3.8. DV-D-74μm exposed to $SCCO_2$ of 35℃ and 10.9MPa for 48 hours had many pores formed on the surface. DV-S-159μm had several blisters formed on the surface after exposure to $SCCO_2$ of both 32℃ and 7.58MPa for 24 hours and 40℃ and 10.00MPa for 24 hours. DV-S-52μm remained the same under exposure to $SCCO_2$ of both 32℃ and 7.58MPa for 24 hours and 40℃ and 10.00MPa for 24 hours. The thickness changes with the exposure are given in Figure 3.9. With all these samples, thickness did not change significantly. It was a sign that neither significant sorption of carbon dioxide in the coating nor significant dissolution of coating into $SCCO_2$. Regarding appearance changes, gloss at 60 degrees decreased, shown in Figure 3.10. The b value and in ΔE value increased after exposure for DV-S-52μm, shown in Figure 3.11. For DV-S-52μm, organic coatings had aging behavior with exposure, and surface roughness increased. For DV-S-159μm, gloss decreased,

while color difference first increased and then decreased. The reason might be caused by the increasing crosslinking density [3].

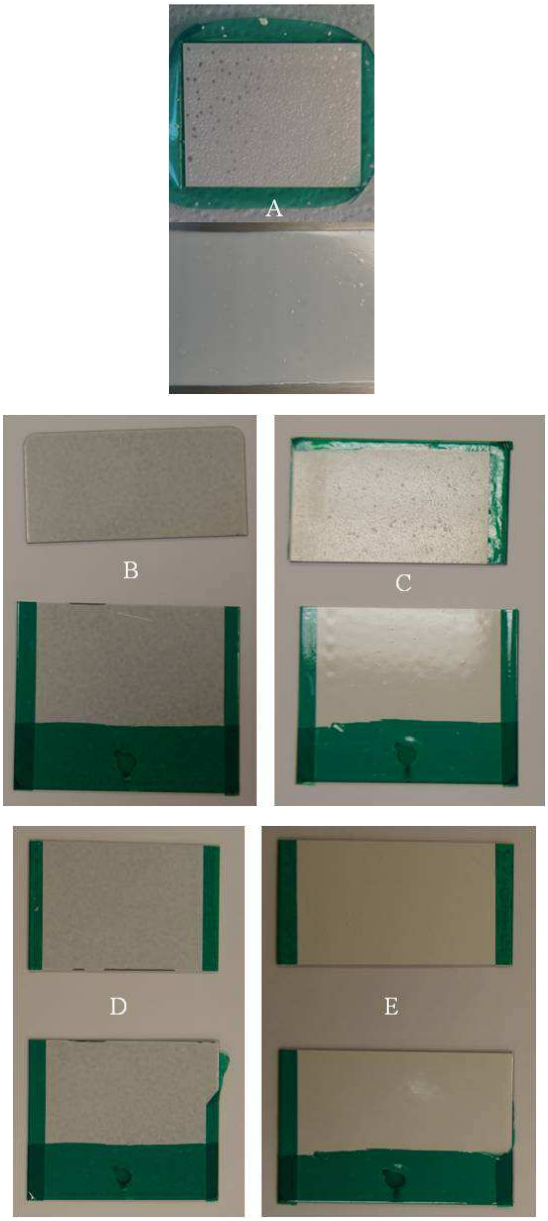

Figure 3.8. The above: coated small panels after exposure to $SCCO_2$ and the below: unexposed original panels. (A) DV-D-74µm exposed to $SCCO_2$ of 35℃ and 10.9MPa for 48 hours. (B) DV-S-52µm; and (C) DV-S-159µm exposed to $SCCO_2$ of 32℃ and 7.58MPa for 24 hours. (D) DV-S-52µm; and (E) DV-S-159µm exposed to $SCCO_2$ of 40℃ and 10.00MPa for 24 hours. (Note: the samples had to be cut to be able to fit inside the pressure vessel).

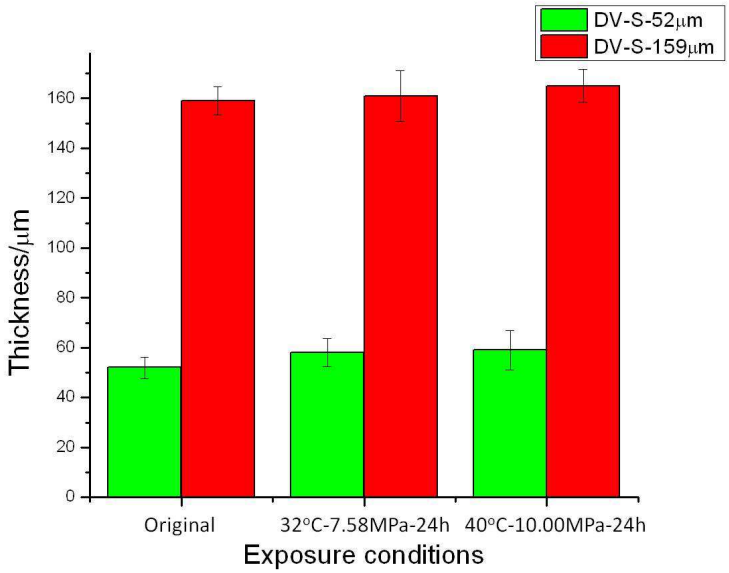

Figure 3.9. Thickness change with different exposure conditions.

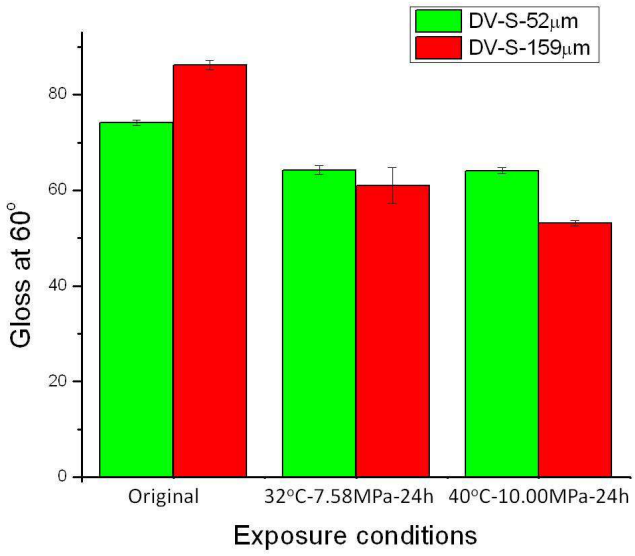

Figure 3.10. Gloss change with different exposure conditions.

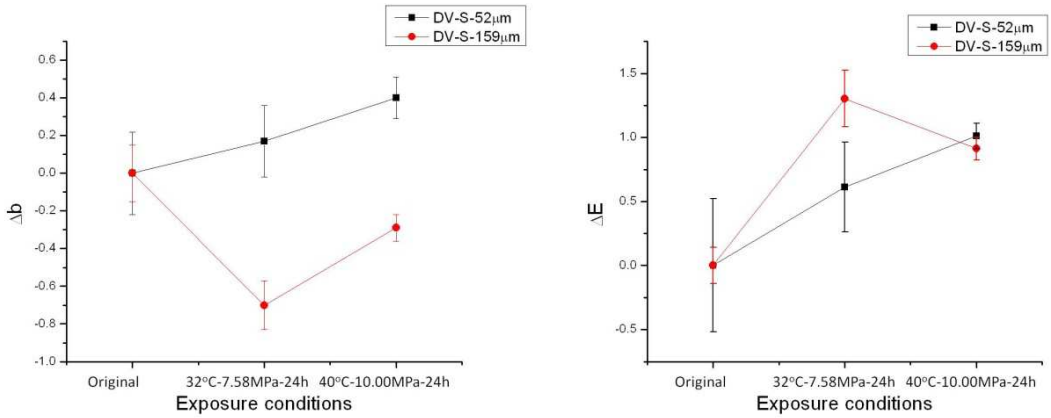

Figure 3.11. Color value change with different exposure conditions.

Electrochemical impedance spectroscopy is shown in Figure 3.12. . DV-D-74µm sample had porous structure on the surface, which yielded high error results for our type of EIS test. The impedance decreased with exposure to $SCCO_2$ of 32℃ and 7.58MPa for 24 hours. However, the impedance increased with exposure to $SCCO_2$ of 40℃ and 10.00MPa for 24 hours. For DV-D-159µm sample, the impedance even became higher than the original untreated sample.

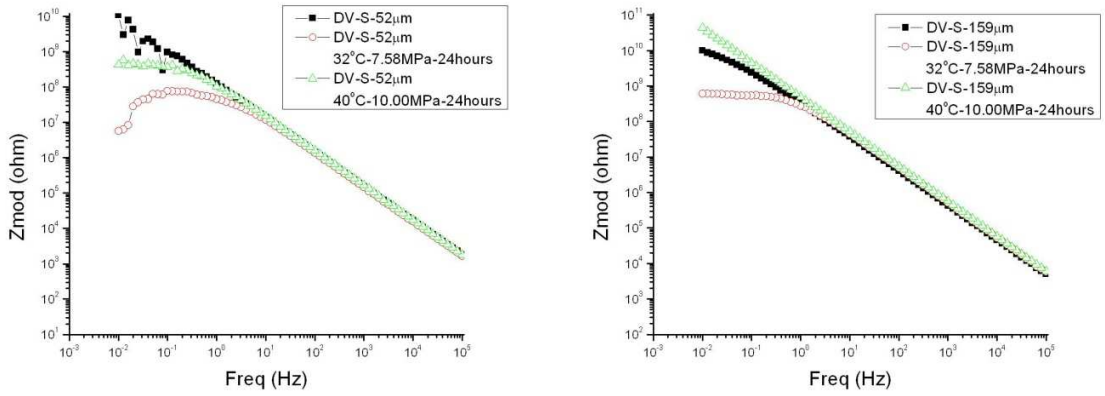

Figure 3.12. Electrochemical impedance spectroscopy of DevChem™ 253 coatings with various exposure conditions.

The porous structure formed on DV-D-74µm instead of blisters, due to brittle organic coatings, which could not withstand blister formation. For DV-S-52µm and DV-S-159µm

samples, coatings were either thin enough for $SCCO_2$ to diffuse out or had good adhesion between interfaces which decreased CO_2 trapped at the interface. The thicker coatings DV-S-159µm showed less color difference with exposure. The impedance of DV-S-159µm after exposure was even higher than the original coatings. The reason might be further crosslinking reaction with $SCCO_2$ as the plasticization. At the lower pressure and lower temperature condition, $SCCO_2$ was not enough to relax epoxy chain to enhance crosslinking density. The crosslinking reaction kept CO_2 trapped in the coating to form blisters on surface of the coatings.

3.3.3. Performance of Scotchkote™ 323 Coatings

Different coating systems are described in Table 3.4. The nomenclature follows the rule of "coating-application method-thickness" to represent each coating systems. Three types of samples were prepared. The samples were exposed to $SCCO_2$. Then they were evaluated by visual inspections and EIS characterizations.

Table 3.4. Samples of Scotchkote™ 323 coatings

Sample	Name	Application method	Thickness/µm
1	S323-S-35µm	Spray	35
2	S323-S-65µm	Spray	65
3	S323-S-172µm	Spray	172

Pictures of organic coatings before and after exposure to $SCCO_2$ of 32℃ and 7.58MPa for 24 hours are given in Figure 3.13. S323-S-35µm and S323-S-65µm samples did not have any blister on the surface up to 41 hours. However, S323-S-172µm sample started to form blister on the surface at 6 hours. The blisters increased with longer exposure time. Thickness and weight change with the exposure are shown in Figure 3.14. Thickness did not have any significant change with the periods investigated. However, weight showed a little decrease with 6 hour exposure and after that remained the same. Gloss changes with the

Figure 3.13. Coated panels with different exposure time to $SCCO_2$ of 32℃ and 7.58MPa for 24 hours. A: S323-S-35µm; B: S323-S-65µm; and C: S323-S-172µm.

exposure are shown in Figure 3.15. For S323-S-172µm sample, gloss could not be measured because sample was cut and too small for gloss measurement. For S323-S-35µm and S323-S-65µm samples, gloss at 60^o was decreasing initially up to 6 hour exposure and reached a plateau after 6 hour exposure. However, gloss at 85^o was staying almost the same except a decrease at 6 hour exposure. Color difference is shown in Figure 3.16. Δb value remained almost zero until 6

hour exposure, increased sharply around 6 hour exposure, and reached a plateau after 12.5 hour exposure. Color difference showed the similar trend with Δb value. The thick coatings showed higher Δb value and ΔE value eventually.

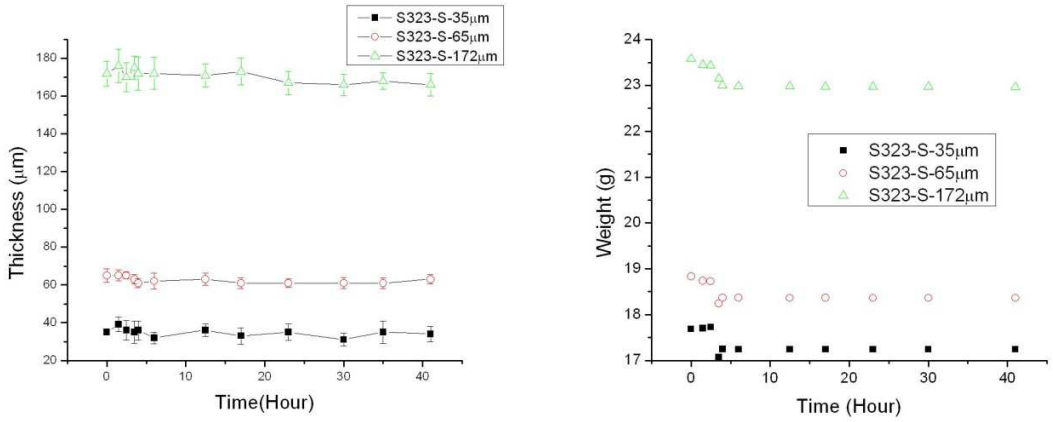

Figure 3.14. Thickness and weight change due to different periods of exposure.

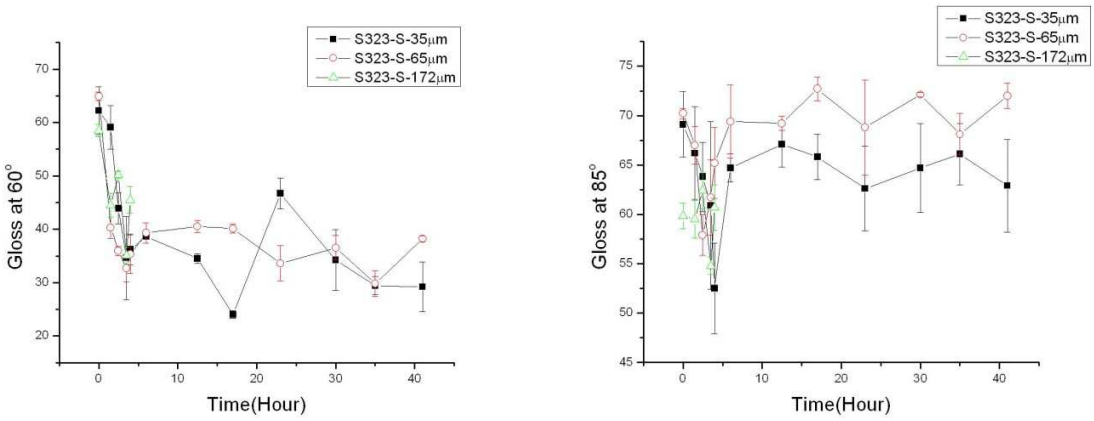

Figure 3.15. Gloss change due to different periods of exposure.

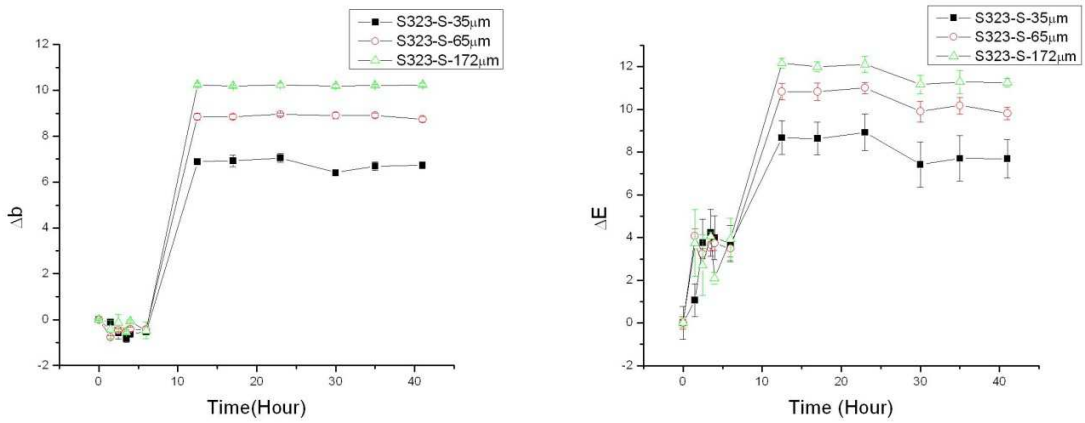

Figure 3.16. Color change due to different periods of exposure.

Electrochemical impedance spectroscopy is shown in Figure 3.17. S323-S-35µm sample showed continuous decrease in impedance. S323-S-65µm sample showed around the same impedance until 30 hour exposure. Around 41 hour exposure, impedance started to decrease. S323-S-172 µm sample showed high impedance until 6 hours. Then the impedance decreased until 31 hours. After that, the impedance started to increase. With low frequency impedance, shown in Figure 3.18, the thicker coatings had higher impedance, which showed better barrier properties. Impedance for S323-S-35µm increased at 6 hour exposure, decreased after it, and kept almost the same. Impedance for S323-S-172µm had a fluctuate impedance at 0.01Hz after 6 hour exposure, because EIS cell fell onto blistered areas.

With the above results, properties of organic coating changed abruptly with 6 hour exposure, including gloss, color difference, and impedance. Gloss decrease, color difference increase, and impedance increase showed that crosslinking reaction happened. With thicker organic coatings, S323-S-65µm and S323-S-172µm only displayed gloss decrease and color difference increase. The impedances kept almost constant. The reason might be crosslinking reaction for thicker coating was slow. It was not enough to increase the impedance, but only

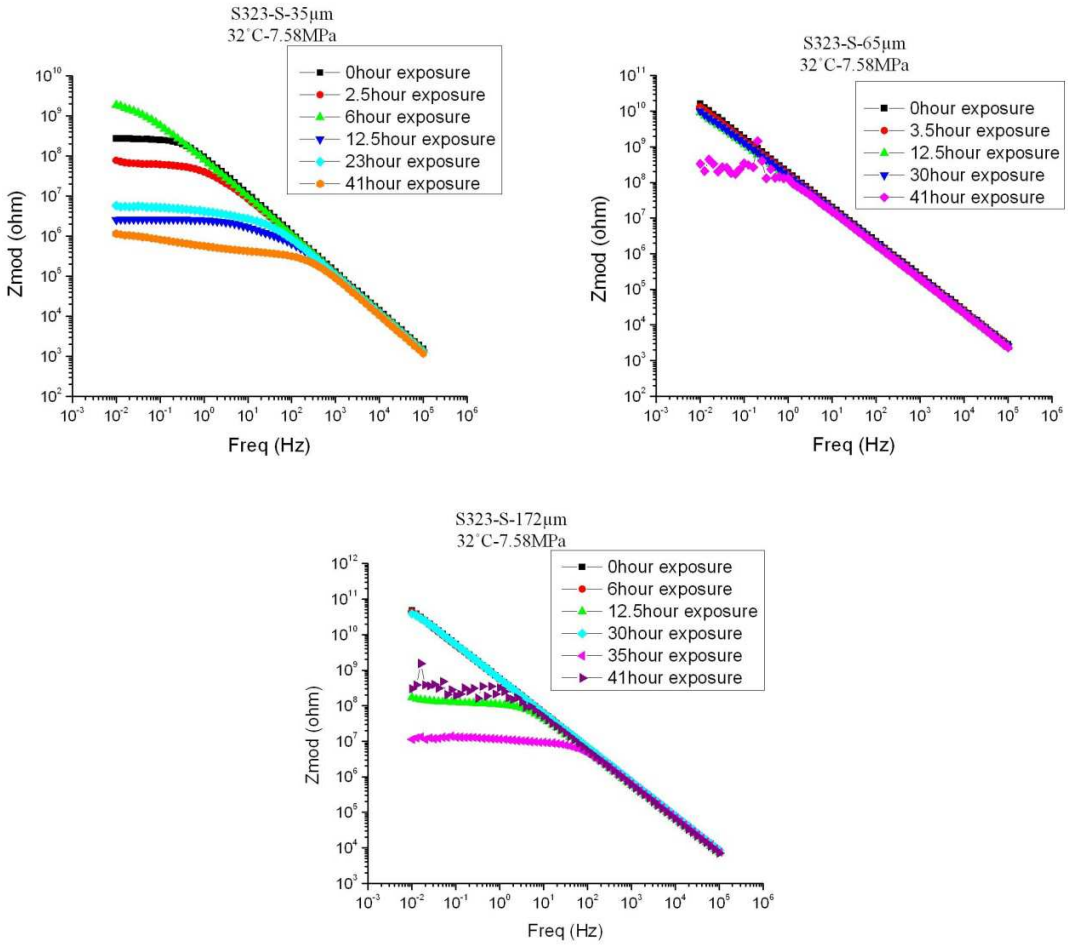

Figure 3.17. Electrochemical impedance spectroscopy of Scotchkote™ 323 coatings with different periods of exposure.

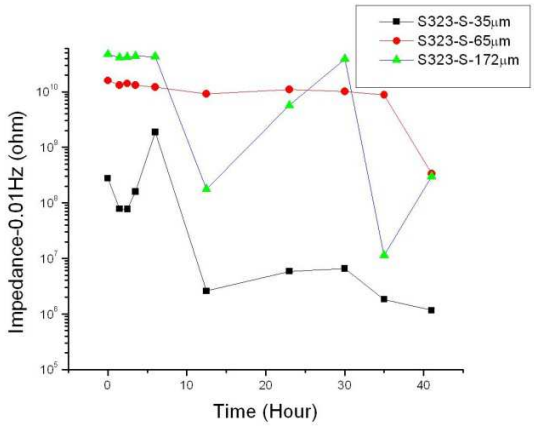

Figure 3.18. Impedance at f=0.01Hz for Scotchkote™ 323 with exposure to $SCCO_2$.

enough to compensate the impedance decrease with the exposure of $SCCO_2$. For S323-S-35µm, after 6 hour, organic coating had enough crosslinking density to stabilize organic coating with exposure to $SCCO_2$.

Another observation was that thicker coatings tended to have a high color difference. The reason was due to the extraction of phthalo green [4]. It increased b value of color value. The thicker coatings tended to lose more colored pigment during the exposure. After 6 hours, the crosslinking density increased to eliminate the extraction to keep color difference constant. The extraction of pigment could cause porous structure, which was also proven by the diffusion controlled process in a certain time of exposure, shown in Figure 3.19.

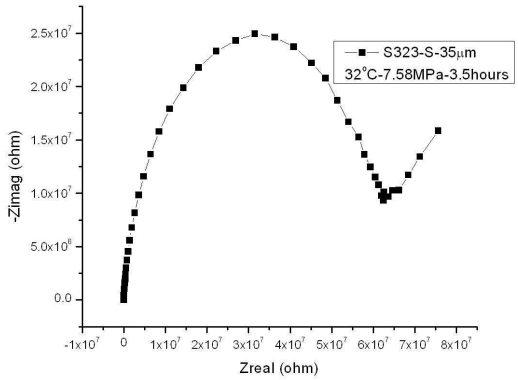

Figure 3.19. Nyquist plot of electrochemical impedance spectroscopy of S323-S-35µm exposed to $SCCO_2$ for 3.5 hours.

The third observation was gloss at 60^o decreased, while gloss at 85^o did not change significantly. The reason was that gloss was mainly depending on the roughness of samples [5]. From Billmeyer equation,

$$h = \frac{\lambda}{cosi};$$

the larger angle was sensitive to the higher roughness. In this situation, surface roughness did not change enough to affect the gloss value especially at 85°. So the gloss at 85° did not change a lot, with only the gloss at 60^o decreasing.

3.3.4. Performance of Scotchkote™ 345 Coatings

Different coating systems are described in Table 3.5. The nomenclature follows the rule of "coating-application method-thickness" to represent each coating systems. Three types of samples were prepared. The samples were exposed to $SCCO_2$. Then they were evaluated by visual inspections and EIS characterizations.

Table 3.5. Samples of Scotchkote™ 345 coatings

Sample	Name	Application method	Thickness/µm
1	S345-S-15µm	Spray	15
2	S345-S-50µm	Spray	50
3	S345-S-180µm	Spray	180

Pictures of the film before and after exposure to supercritical conditions are given in Figure 3.20. At the two conditions of $SCCO_2$, with three samples of different thickness, the samples were in good condition. There was neither blister nor pores formed on the surface. The changes in film thickness and weight are shown in Figure 3.21. There is almost no change during the exposure for any of the coatings independent of thickness. Thickness and weight remained constant, which indicated that the coatings were neither imbibing CO2 nor dissolving CO2. Gloss changes with the exposure are shown in Figure 3.22. Gloss at 60^o showed a lot of fluctuations during the exposure, while gloss at 85^o showed less fluctuations than gloss at 60^o. However, gloss did not change significantly. The variations might be dependent on the surface roughness, which might be caused by the effect of $SCCO_2$ on Scotchkote™ 345. There was no significant influence but surface roughness change. Color difference shown in Figure 3.23

confirmed that $SCCO_2$ did not post significant effect on organic coatings due to the stability of color value.

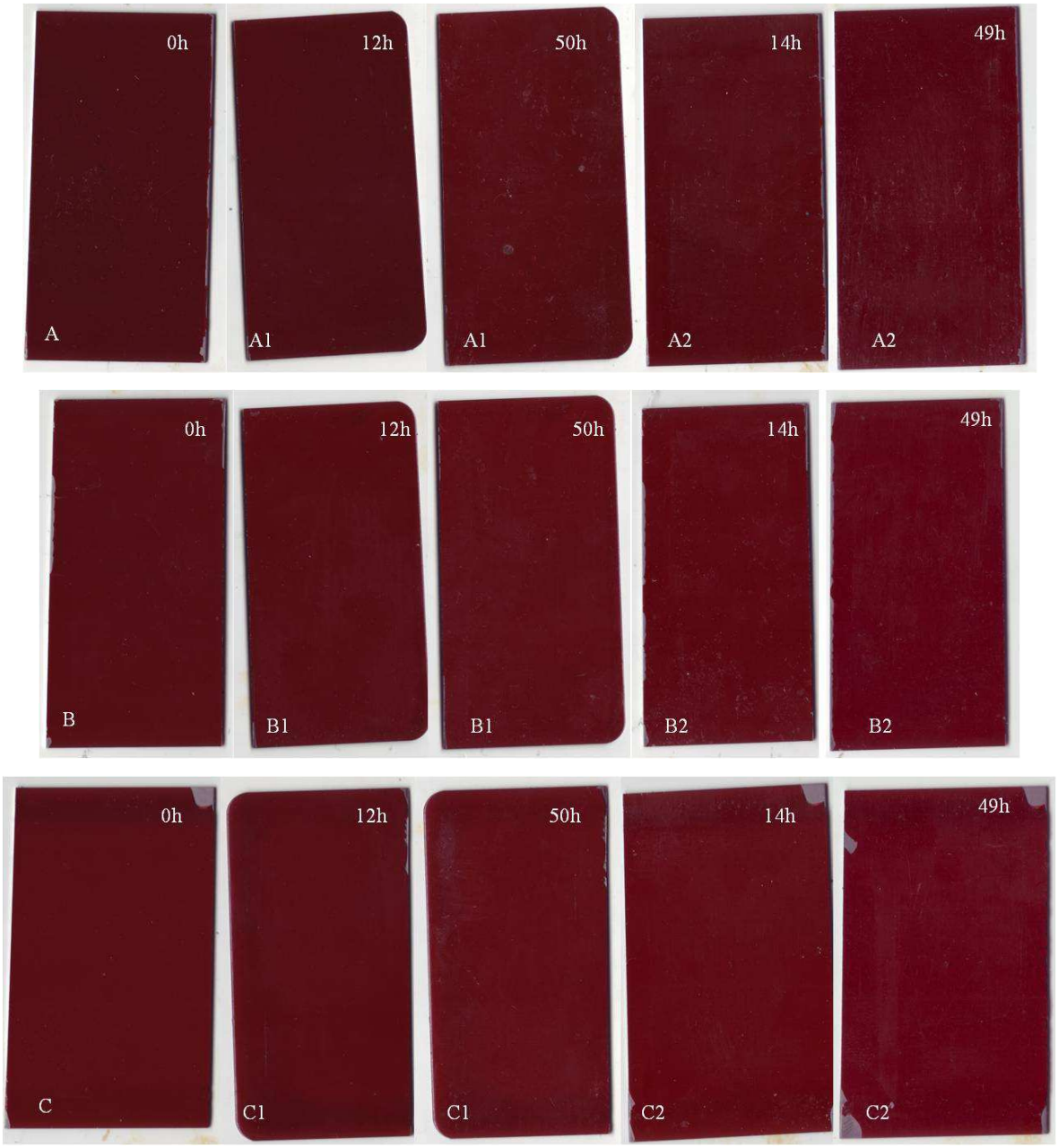

Figure 3.20. Coated panels with different exposure time to $SCCO_2$. (A) S345-S-15μm; (B) S345-S-50μm; and (C) S345-S-180μm. Numbers after the sample sign are exposure conditions, while 1 represents 32℃ and 7.58MPa, and 2 represents 40℃ and 10.00MPa.

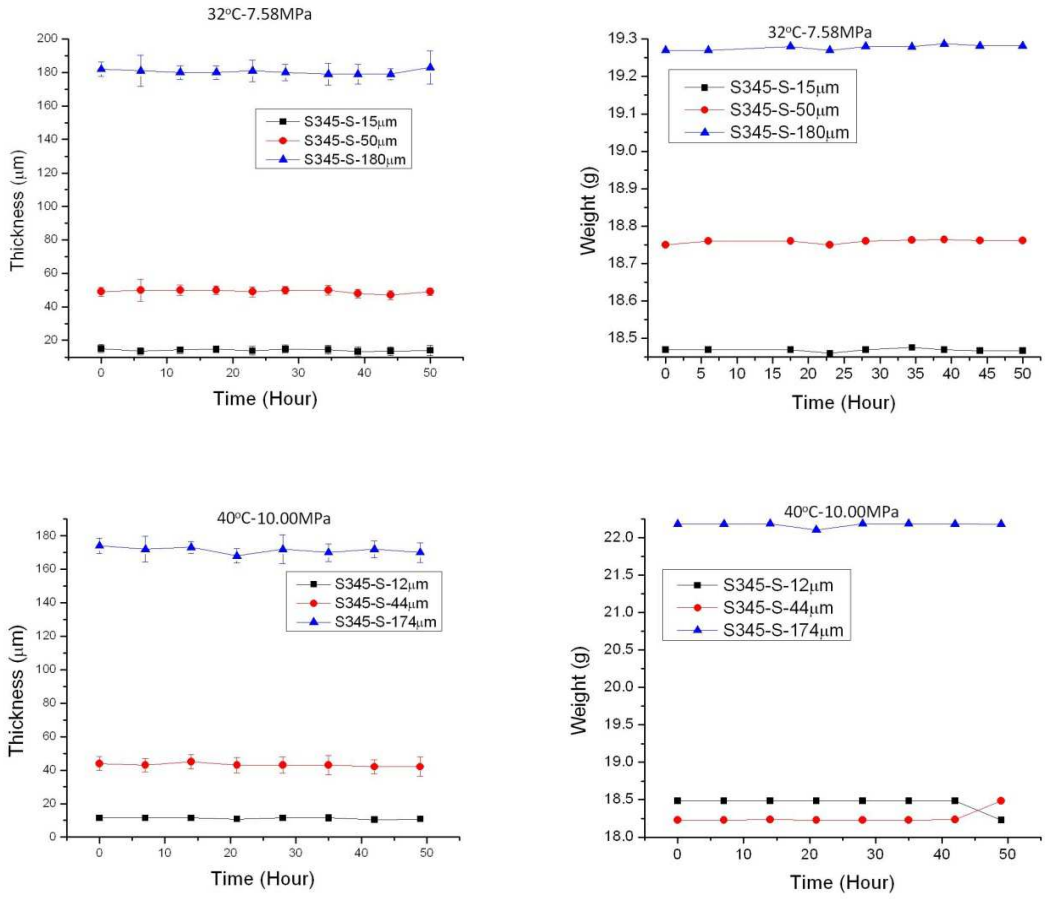

Figure 3.21. Thickness and weight change due to different periods of exposure and different exposure conditions.

Electrochemical impedance spectroscopy is shown in Figure 3.24. S345-S-180μm and S345-S-174μm samples did not show any change with exposure time. S345-S-50 μm sample did not show any change with exposure time up to 44 hours. With 50 hour exposure, impedance decreased dramatically. Impedance of S345-S-44 μm sample decreased a little, increased a little, and decreased again. S345-S-15μm sample showed a continuous decrease in impedance, while S345-S-12 μm sample kept its impedance disregarding the exposure period. However, the electrochemical kinetics did change. $SCCO_2$ of $40℃ - 10.00MPa$ showed much more effects than $SCCO_2$ of $32℃ - 7.58MPa$ to Scotchkote™ 345 coatings. However, when the coating was

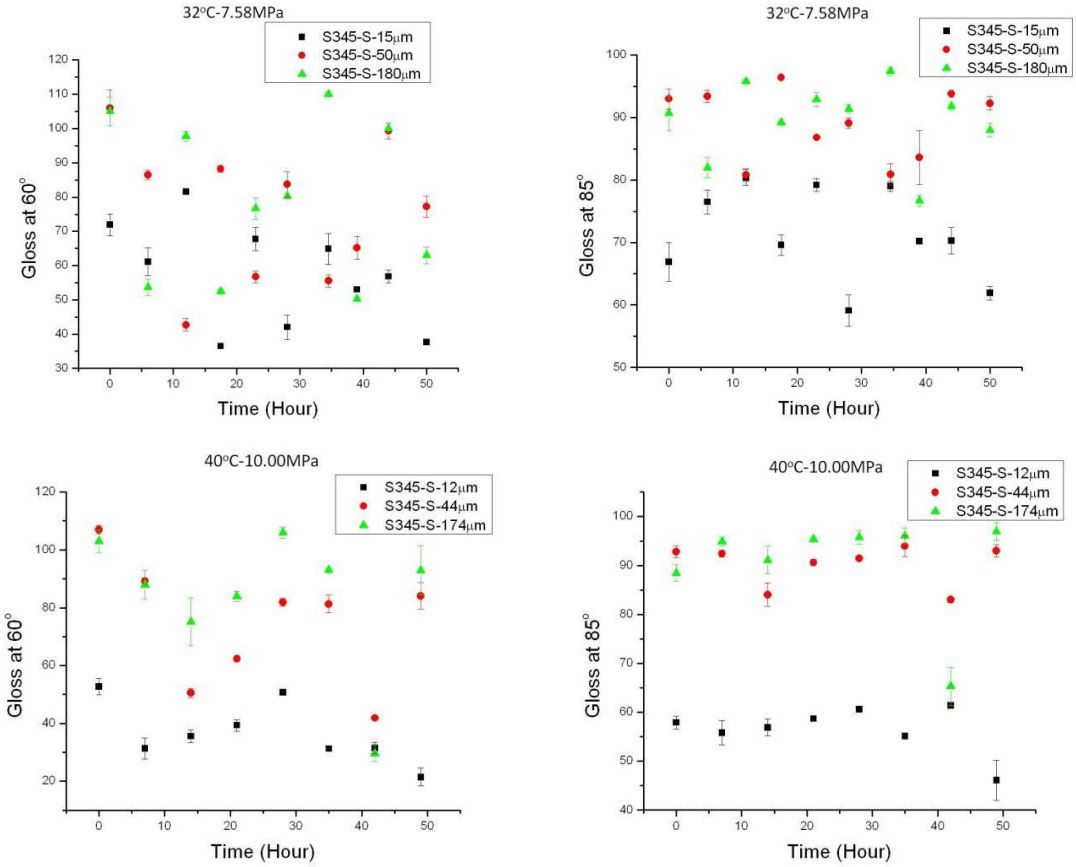

Figure 3.22. Gloss change due to different periods of exposure and different exposure conditions.

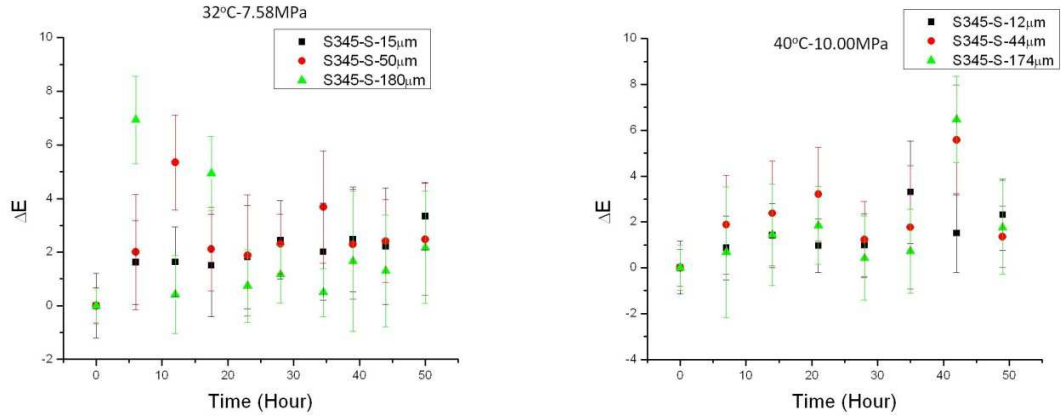

Figure 3.23. Color difference due to different periods of exposure and different exposure conditions.

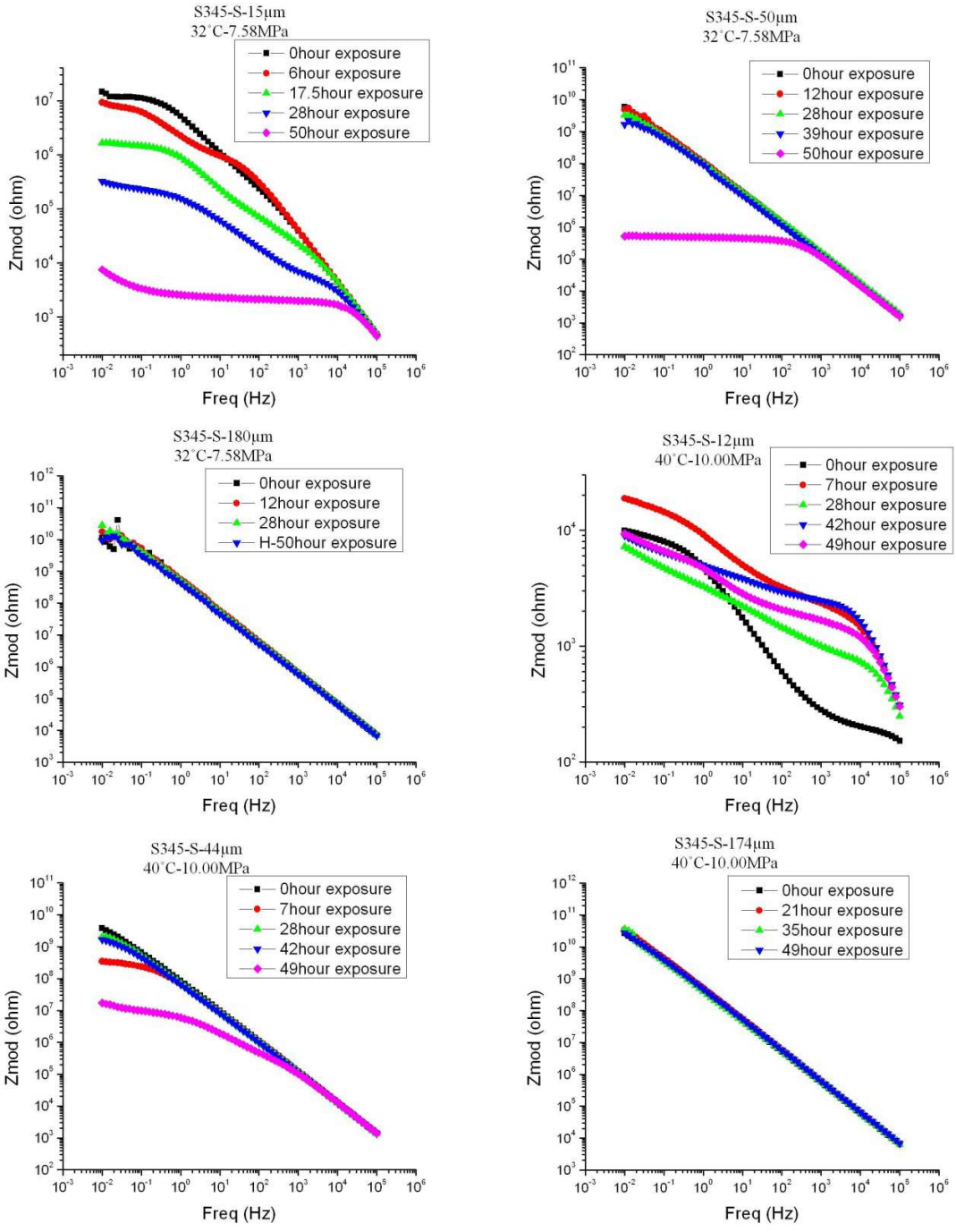

Figure 3.24. Electrochemical impedance spectroscopy of Scotchkote™ 345 coatings with different periods of exposure, and different conditions of exposure.

thick enough, for example around 180µm, organic coatings showed very good barrier properties up to 50 hours exposure for both conditions, due to constant impedances. With low frequency

impedance, shown in Figure 3.25, the thicker coating had higher impedance, which proved a better barrier property. S345-S-50 µm and S345-S-44 µm had impedance value close to S345-S-180 µm and S345-S-174 µm, respectively. Around 50µmthickness was good enough for barrier properties of organic coatings. S345-S-12 µm had impedance value of around 10^4ohm and kept constant, because it was close to bare metal impedance [6]. It was a good example to investigate the failure mechanism of organic coatings.

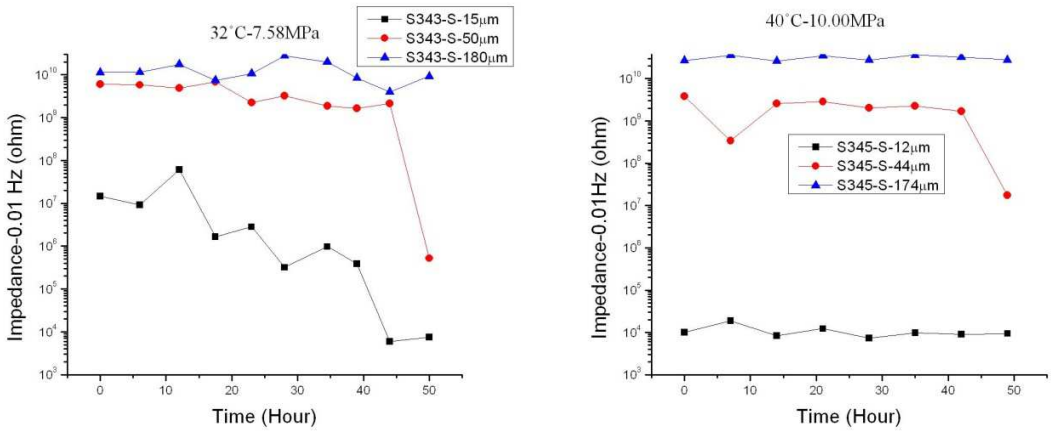

Figure 3.25. Impedance at f=0.01Hz for Scotchkote™ 345 with exposure to $SCCO_2$ of different periods and different conditions.

From the above results, the appearance of Scotchkote™ 345 coatings did not change as well as thickness and weight of the coatings, although gloss values did have fluctuations, possibly due to roughness fluctuations. Impedance of thicker coatings than 50µm did not change significantly up to 50 hours exposure to $SCCO_2$ of both $32℃ - 7.58MPa$ and $40℃ - 10.00MPa$. For thin coating samples, S345-S-15µm and S345-S-12µm showed decreased impedance value at low frequency with time of exposure elapsed, although no appearance change. It showed that $SCCO_2$ still had influence on organic coatings to deteriorate coatings. To investigate the influence on organic coatings, Nyquist plots were shown in Figures 3.26 and 3.27

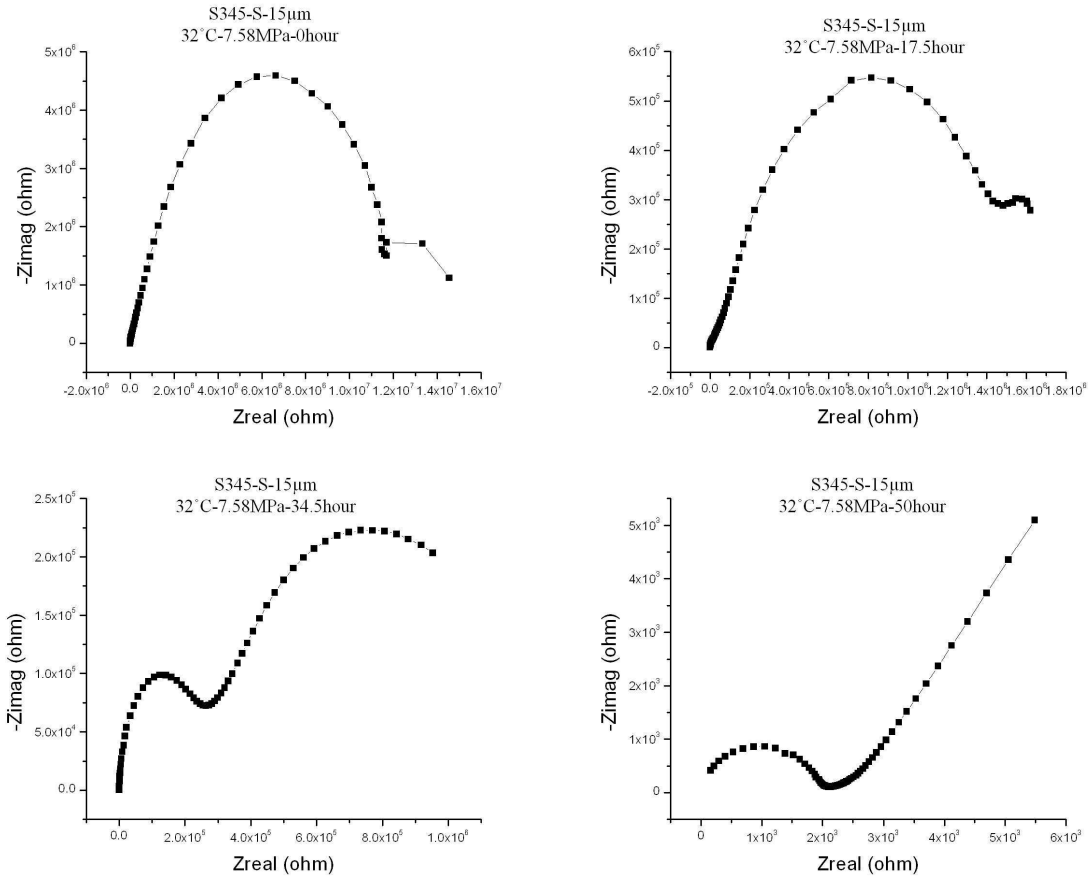

Figure 3.26. Nyquist plot of electrochemical impedance spectroscopy of S345-S-15µm exposed to $SCCO_2$ for different periods.

for samples S345-S-15µm and S345-S-12µm, respectively. It could be seen that for both samples, initially, one semicircle changed into two semicircles. The first semicircle tended to become small, while the second semicircle tended to become big. The first semicircle was attributed to organic coatings, while the second semicircle was attributed to protective film formed on the surface [7]. For S345-S-15µm immersed in $SCCO_2$ of $32℃ - 7.58MPa$, the second semicircle started around 17.5 hour. For S345-S-12µm immersed in $SCCO_2$ of $40℃ - 10.00MPa$, the second semicircle started around 7 hour. It showed $SCCO_2$ of $40℃ - 10.00MPa$ posted much more significant affect than $SCCO_2$ of $32℃ - 7.58MPa$ for pipeline steel.

Eventually, with the organic coating deterioration, the protective film could not cover the damaged sites. Porous structures formed with the proof of diffusion controlled process shown in Nyquist plots. While S345-S-15µm samples had porous structure around 50hour exposure, S345-S-12µm had porous structure around 42 hours. For S345-S-12µm sample, the protective film still could be found for 42 hour exposure. With 49 hour exposure, the protective film indicated continuous growth.

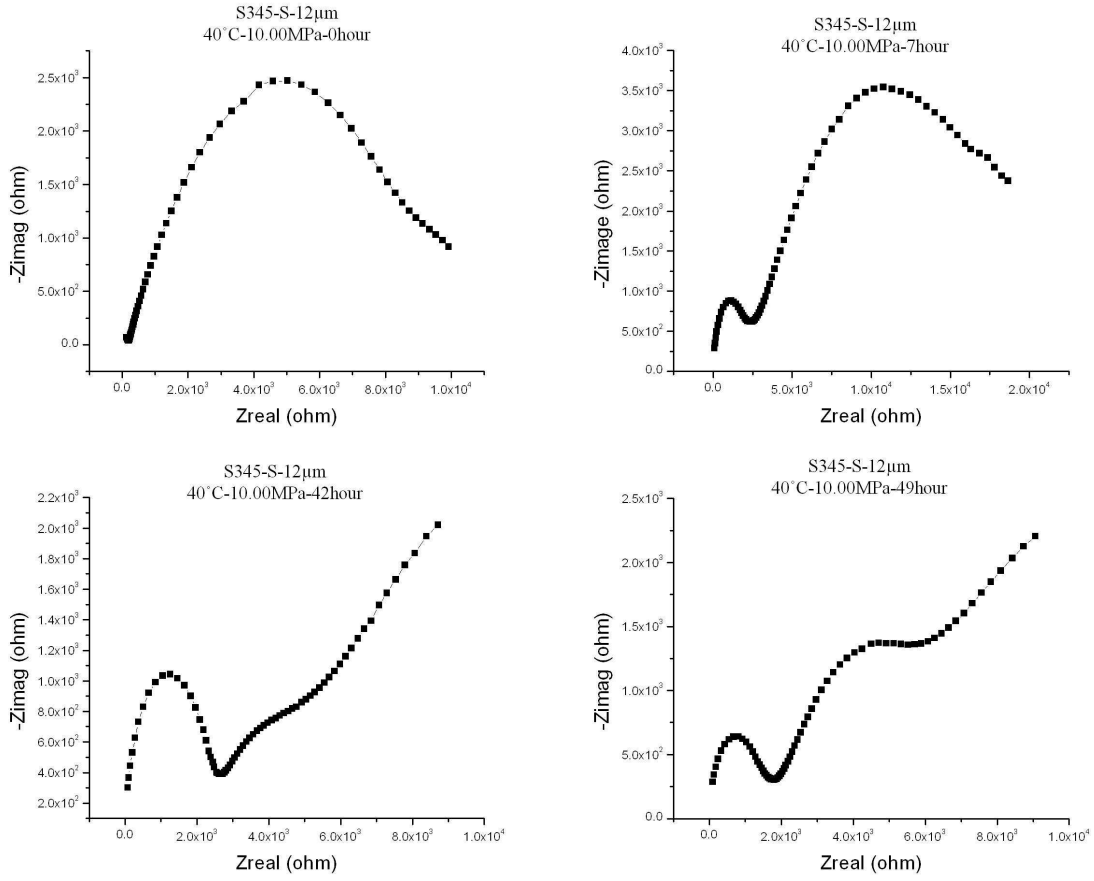

Figure 3.27. Nyquist plot of electrochemical impedance spectroscopy of S345-S-12µm exposed to $SCCO_2$ for different periods.

3.3.5. Thermal Mechanical Analysis of Commercial Coatings

Dynamical mechanical analysis results are shown in Table 3.6. Sctochkote™ 345 coatings had the highest glass transition temperature and the highest modulus retention. With the highest glass transition temperature, Sctochkote™ 345 coatings had the highest restriction for molecular mobility, which was good for $SCCO_2$ resistance [8]. With highest modulus retention, Sctochkote™ 345 coatings had the highest restriction even with $SCCO_2$ plasticization.

Table 3.6. Dynamic mechanical analysis of commercial coatings

Coatings	Glass transition temperature (^oC)	Storage modulus before T_g (MPa)	Storage modulus after T_g(MPa)	Modulus retention (%)
TZ™ 904	53	340	5	1.47
DevChem™ 253	75	1700	25	1.47
Sctochkote™ 323	75	3485	50	1.43
Sctochkote™ 345	167	730	120	16.44

3.3.6. Corrosion Mechanism of Commercial Coatings Exposed to $SCCO_2$

The blistering underneath the coating may be caused by the following mechanism (Figure 3.28). Blister formation occurs when the coating no longer releases CO2 and returns to having barrier film properties after being made very permeable by exposure to SCCO2. From the blister formation mechanism, the diffusion coefficient of the coatings returns to a low value, especially for the CO_2 gas, which retained at the interface and formed blisters. The results showed blister formed on the surface of the thickest coatings in each coating systems, due to the diffusion length was the longest to make it the most difficult to diffuse out. The porous structure formed due to the brittleness of the coating causing the blister to rupture and to form pores on the surface. The thinner coatings happened to have more pores on the surface, due to the poorer mechanical properties. With the mechanism, adhesion force is very important to maintain the integrity of the

coating film. Drawdown film was more vulnerable for blister formation than spray coating due to the lower adhesion force. Higher pressure and higher temperature can make the diffusivity easier, which are also easier for the blister formation.

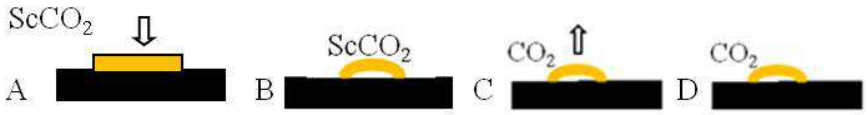

Figure 3.28. Proposed mechanism of blister formation. (A) SCCO2 diffuses into the coatings; (B) SCCO2 saturates the coating; (C) CO_2 diffuses out of the coatings when pressure is reduced to atmospheric pressure; and (D) Remaining CO_2 changes into gaseous phase and causes blistering with extreme volume increase.

When $SCCO_2$ diffused into the substrates, two reactions would compete into each other. One was $SCCO_2$ deteriorating organic coatings by blister and pore formation. The other one was corrosion products formed at the interface. The first one would decrease impedance, while the latter one would increase impedance. High temperature and high pressure of 42^{o}C and 10.00MPa would increase both reactions, and the competition of the two reactions.

3.4. Conclusions

Investigation of commercial organic coatings exposed to $SCCO_2$ has been done here. In the investigation, a test protocol for $SCCO_2$ resistance was developed. Organic coatings for the protection of pipeline steel were exposed to $SCCO_2$ of two conditions, $32℃ - 7.58MPa$ and $40℃ - 10.00MPa$. Different periods of exposure were studied to evaluate lifetime of organic coatings. During the tests, visual inspections were done to check blister and porous structure formation. Color and gloss measurements were used to confirm the visual inspections. Weight and thickness measurement were used to check the solubility of $SCCO_2$ inside the organic coatings and the dissolution of organic coatings into $SCCO_2$. For the corrosion process, EIS was mainly used to characterize coating failure and corrosion behaviors.

During the investigation, there are several conclusions listed in the followings.

1. Adhesion of organic coating to steel substrate was critical to supercritical carbon dioxide exposure. Good adhesion helped $SCCO_2$ resistance.
2. High pressure and high temperature of $SCCO_2$ in exposure chamber increased the rate of corrosion processes.
3. Long time exposure to $SCCO_2$ resulted into organic coating deterioration.
4. Thicker organic coatings had better barrier protection, but were vulnerable to blister formation.
5. Thinner organic coatings had less barrier property, but were useful to investigate failure mechanisms.
6. Blister was formed due to carbon dioxide trapped at the interface. The thick coatings were vulnerable to blister formation.
7. The competition of the barrier property between the deterioration of organic coatings and the corrosion product formation at the interface was increased with the high temperature and the high pressure of $SCCO_2$.

3.5. References

1. Briones V, Aguilera JM, Brown C, Effect of surface topography on color and gloss of chocolate samples, Journal of Food Engineering, 2006, 77: 776-783.
2. Bierwagen GP, Estimation of film thickness nonuniformity effects on coating optical-properties, Color Research and Application, 1992, 17: 284-292.
3. Zhao QL, Li XG, Gao J, Aging of ethylene-propylene-diene monomer (EPDM) in artificial weathering environment, Polymer Degradation and Stability, 2007, 92, 1841-1846.

4. Sattler KD, Handbook of nanophysics: Functional nanomaterials, CRC Press, 2011, Boca Raton, FL.

5. Arino I, Kleist U, Mattsson L et al., On the relation between surface texture and gloss of injection-molded pigmented plastics, Polymer Engineering and Science, 2005, 45, 1341-1356.

6. Loveday D, Peterson P, Rodgers B, Evaluation of organic coatings with electrochemical impedance spectroscopy. Part 2: Application of EIS to coatings, JCT CoatingsTech, 2004, 1(10): 88-93.

7. Wu SL, Cui ZD, Zhao GX et al., EIS study of the surface film on the surface of carbon steel from supercritical carbon dioxide corrosion, Applied Surface Science, 2004, 228(1-4): 17-25.

8. Sawan SP, Shieh YT, Su JH, Evaluation of the interaction between supercritical carbon dioxide and polymeric materials, LA-UR-94-2341, (URL: http://www.turi.org/content/view/full/4603)

4. INVESTIGATION OF DESIGNED COATINGS EXPOSED TO $SCCO_2$

4.1. Introduction

In order to design protective coatings for $SCCO_2$ transportation, coatings must be resistant to $SCCO_2$. Due to high solvency of $SCCO_2$, it can dissolve many polymers. Research has shown that intermolecular interactions between polymer segments and $SCCO_2$ are much more responsible for miscibility than hydrostatic pressure [1], although the solvency of CO_2 in general increases with the pressure [2]. There are three mechanisms regarding the solubility [1]. The first is the electron donor-acceptor mechanism. The second is the specific interaction, such as $SCCO_2$ and polymer dipoles. The third is the electrostatic interactions, such as SCCO2 and polymer π systems. In these cases, carbonyl or ether groups that are either in the backbone or on side chains can specifically interact with $SCCO_2$. Polymers that are often difficult to dissolve in other fluids such as fluorine-substituted polymers and silicon based polymers are dissolved in $SCCO_2$, this being especially true for perfluoroalkyl ethers and acrylates [1]. The solvency of $SCCO_2$ increases with the increasing content of polar groups in the polymer, due to the increased polarity of $SCCO_2$ compared with its subcritical fluid [1]. However, hydroxyl end groups decrease polymer solubility [3]. Polymer chain entanglement confined free volume will restrict a limit for the solvency of $SCCO_2$ [4]. Chain flexibility aids dissolution. High crystalline polymers have a low solubility due to the condensed structure and much slower transport processes [1]. For the semicrystalline polymers, the solubility occurs mainly in the amorphous regions. Polymers of molecular weight higher than 20000g/mol will have a negligible solubility. Literature review for the potential candidate for $SCCO_2$ resistant polymers is given in Table 4.1.

Table 4.1. Potential candidate for $SCCO_2$ resistant polymer

Polymer	Experimental conditions	Visual sampling due to exposure to $SCCO_2$	Polymer property related to $SCCO_2$ resistance	Reference
Poly(vinyl chloride)	2000/3000psi, 40/70^oC	A light dissolution	High dipole C-Cl	[5]
Polypropylene	2000/3000psi, 40/70^oC	A light yellow	High crystallinity	[5]
Polyethylene, Teflon	2000/3000psi, 40/70^oC	Some bubbles	High crystallinity	[5]
Nylon 66	2000/3000psi, 40/70^oC		High crystallinity	[5]
Copolymer with poly(methacrylic acid)		SCCO2 insoluble		[6]
High branched phenol		SCCO2 insoluble		[6]
Surface modified polystyrene by carboxylic acid group	1232-2857psi, 40-60 ^oC	SCCO2 resistant	Static repulsion	[7]
Higher fraction of hard segment of poly(urethane)	1000-3000psi, 42 ^oC	Low sorption of SCCO2	High restriction	[8]

The candidates to be $SCCO_2$ resistant should not have CO_2-philic groups (interpreted as the CO_2 functions under $SCCO_2$ conditions), such as fluorinated groups, siloxane groups, ester groups, and ether groups. High crystallinity or high crosslinking are favored final film structures Aliphatic polymer is better than aromatic polymer, since the benzole group can have electron-electron interaction with $SCCO_2$. Our designed polymer should be resistant not only for $SCCO_2$ but also for "dirty" $SCCO_2$ ($SCCO_2$ captured in a co-sequestration mode or compressed from incompletely cleaned flue gas). With slight water contamination of $SCCO_2$, any corrosion that might occur has been shown to be more severe [9]. To decrease water effect on the corrosion, the target polymer was designed to be water insoluble as a component of its barrier protection, because total water permeability is dependent on film thickness, diffusion coefficient and solubility in the coating barrier polymer.

A crosslinked liquid natural rubber (Figure 4.1) was designed as the main binder for $SCCO_2$ resistance. From the structure, it is aliphatic without any CO_2-philic group. It is also hydrophobic to resist water contamination. With crosslinking, this polymer becomes more CO_2-resistant and water-resistant, and increases its strength, functions important to coating matrix candidate. In addition, liquid natural rubber is inexpensive and relatively easy to process. An organic peroxide compound, such as dicumyl peroxide, could crosslink the free double bond in the liquid natural rubber. This is described extensively in the literature on rubber compounding for commercial and tire use. The sulfur-crosslinking natural rubber, usually used for tires, could be swollen in $SCCO_2$ with crosslinking density around $10^7 mol\ L^{-1}$ [10]. With the organic peroxide compound used for the crosslinking reaction, the shorter crosslinked branch than the sulfur will make the rubber stiffer, which would be better for SCCO2 resistant [11].

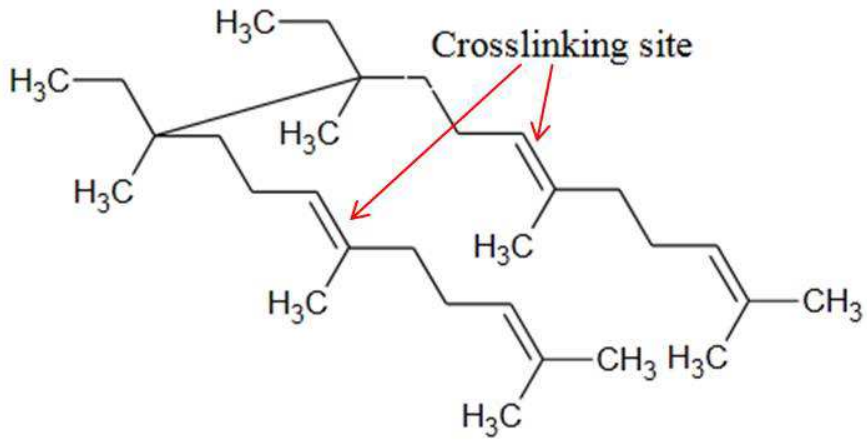

Figure 4.1. The molecular structure of the crosslinked natural rubber

Polybutadiene, an aliphatic polymer and crosslinkable, can serve as a $SCCO_2$ resistant polymer as well as a good barrier polymer. The crosslinking process will increase the cohesive strength, which should increase $SCCO_2$ resistance. The liquid polybutadiene can be crosslinked by both sulfur and peroxide, such as dicumyl peroxide. The difference between the two processes is the covalent bonds in between, where in the sulfur process the covalent bonds are polysulfidic-

carbon bonds and in the peroxide process the covalent bonds are carbon-carbon bonds. Higher Tg can be obtained for the sulfur-crosslinked polybutadiene at the same crosslink density [12]. The polybutadiene rubber can also be crosslinked by exposure to radiation, such as electron beam or ultraviolet radiation [13]. The UV curable formulation needs a photosensitive group present such as an acrylic. However, this could be detrimental to the $SCCO_2$ resistance property [14]. To make good adhesion to the metal and the primer, which is good for eliminating the blister formation on the coatings caused by the exposure to $SCCO_2$, rubber hydrohalide, hydrochloride rubber, or cyclicized rubber are strongly recommended [15]. Polychloroprene is chosen in the formulation, since it could be prepared in-situ, and bought by commercial trade name of “neoprene” [15]. Another reason is that polychloroprene can be functionalized in the corrosion preventing coating compositions [16, 17].

In this chapter, different coating formulations were prepared and tested for their barrier properties and $SCCO_2$ resistances in order to find the appropriate coating formulation for pipeline.

4.2. Experimental Methods

4.2.1. Materials

Polyoil™ 130 (P130), a non-hydolysable liquid polybutadiene (http://corporate.evonik.com/en/products/search-products/Pages/product-details.aspx?pid=22351&pfcat=5043), was obtained from EVONIK Industries. It is a highly reactive crosslinkable binder. Polychloroprene (PCP) was purchased from Bayer Materials Science(http://bayermaterialsciencenafta.com/products/index.cfm?mode=grades&pp_num=EB7C4E4A-9321-3303-8B3789A0E86FCC74&o_num=14). The initiator tert-Butyl peroxide (tBPO)

was obtained from Sigma-Aldrich. Methyl ethyl ketone (MEK), purchased from Sigma-Aldrich, was used to dissolve polychloroprene. Other materials used were the same from section 3.2.1.

4.2.2. Characterizations

Characterizations were the same from section 3.2.2. Visual inspection was used to evaluate surface appearance, especially blisters and pores. Gloss and color measurements were also used to evaluate the surface appearance. Thickness and weight measurements were used to evaluate the absorption of $SCCO_2$ in organic coatings and the dissolution of organic coatings in $SCCO_2$. EIS was used to measure the impedance of organic coatings to evaluate the barrier properties of organic coatings.

4.2.3. Experimental Set-up

The formulation table is shown in Table 4.2. The formulation has primer base polybutadiene with the initiator tert-butyl peroxide as the crosslinking agent too. To increase the adhesion between the primer and the substrate, polychloroprene was added into the formulation. Xylenes was used as the solvent to adjust the viscosity of the formulation for spray application.

Table 4.2. The formulation of $SCCO_2$ resistant coating

Part A		Part B	
Materials	Functions	Materials	Functions
Polybutadiene	Primer base	Polychloroprene	Adhesion promoter
Tert-Butyl peroxide	Crosslinking agent	Solvent: Xylenes	Viscosity adjustor

The parameters used to control the coating crosslinking density, adhesion property, and mechanical properties are shown in Table 4.3. In the experimental set-up, curing time was selected for the completely crosslinking reactions. The curing time was 30 minutes. Viscosity was adjusted for spray application. So the parameters considered were ratio of primer to initiator, ratio of primer to polychloroprene, and temperature. The initiator was added 2% and 6% weight

percent of binders. Polychloroprene was added 12.5% and 37.5% weight percent of binders. Temperature was selected to be 100˚C and 200˚C.

Table 4.3. The control variables for the coating preparation

Variables	Functions
Ratio of primer to initiator	The crosslinking density and the reaction speed
Ratio of primer to polychloroprene	Adhesion property and mechanical properties
Temperature	The reaction speed
Time	The crosslinking density
Solvent	The reaction speed

4.3. Results and Discussions

Different coating systems are described in Table 4.4. The nomenclature follows the rule of "Polyoil™ 130-polychloroprene weight percent-tert-butyl peroxide weight percent-curing temperature-thickness" to represent each coating systems. For example, 2wt% tBPO-P130 curing at 100˚C with thickness of 37μm can be named as P130-0-2-100-37μm sample. Eight types of samples were prepared. The samples were exposed to $SCCO_2$. Then they were evaluated by visual inspections and EIS characterizations.

4.3.1. Performance of P130 Coatings with A Different Amount of Initiator

Visual pictures of P130 coatings cured at 100^{o}C for 30 minutes with 2wt% and 6wt% initiators are shown in Figure 4.2. The round spots on the surface of the panels were under DHS, which was used for our EIS testing. For both samples P130-0-2-100-37μm and P130-0-6-100-29μm, they did not have any blisters formed on the surface when they were exposed to $SCCO_2$ of 32˚C-7.58MPa. However, they both started to form blisters on the surface after 7 hours exposure to $SCCO_2$ of 40˚C-10.00MPa. With the exposure time increasing, the blisters became bigger and more. From Chapter 3, $SCCO_2$ of 40˚C-10.00MPa was more severe than $SCCO_2$ of 32˚C-7.58MPa. It was the reason why blisters formed when sample panels were exposed to

Table 4.4. Samples of specialty coatings

Formulation	Description	Curing conditions	Thickness (µm)
1	2wt% tBPO- P130	100^{o}C for 30min	37 (P130-0-2-100-37µm)
2	2wt% tBPO- P130	200^{o}C for 30min	21 (P130-0-2-200-21µm) 51(P130-0-2-200-51µm) 92(P130-0-2-200-92µm)
3	6wt% tBPO- P130	100^{o}C for 30min	29 (P130-0-6-100-29µm)
4	6wt% tBPO- P130	200^{o}C for 30min	12 (P130-0-6-200-12µm) 36(P130-0-6-200-36µm) 99(P130-0-6-200-99µm)
5	2wt% tBPO- 12.5wt% PCP in P130	200^{o}C for 30min	19 (P130-12.5-2-200-19µm) 36(P130-12.5-2-200-36µm) 87(P130-12.5-2-200-87µm)
6	2wt% tBPO- 37.5wt% PCP in P130	200^{o}C for 30min	36 (P130-37.5-2-200-36µm) 62(P130-37.5-2-200-62µm) 94(P130-37.5-2-200-94µm)
7	6wt% tBPO- 12.5wt% PCP in P130	200^{o}C for 30min	44 (P130-12.5-6-200-44µm) 67(P130-12.5-6-200-67µm) 124(P130-12.5-6-200-124µm)
8	6wt% tBPO- 37.5wt% PCP in P130	200^{o}C for 30min	21 (P130-37.5-6-200-21µm) 72(P130-37.5-6-200-72µm) 151(P130-37.5-6-200-151µm)

$SCCO_2$ of 40˚C-10.00MPa. So the organic coatings could withstand $SCCO_2$ of 32˚C-7.58MPa, but not strong enough to withstand $SCCO_2$ of 40˚C-10.00MPa. The sample P130-0-6-100-29µm had less blisters on the surface than the sample P130-0-2-100-37µm, due to the higher crosslinking density. Thickness and weight did not show significant change, shown in Figure 4.3.

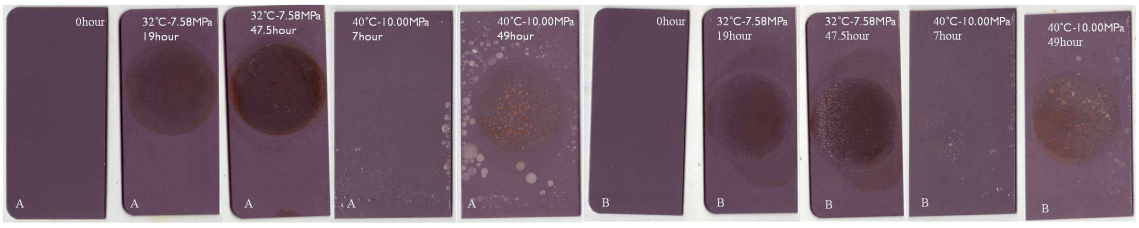

Figure 4.2. Coated panels with different exposure time to $SCCO_2$. (A) P130-0-2-100-37µm; and (B) P130-0-6-100-29µm.

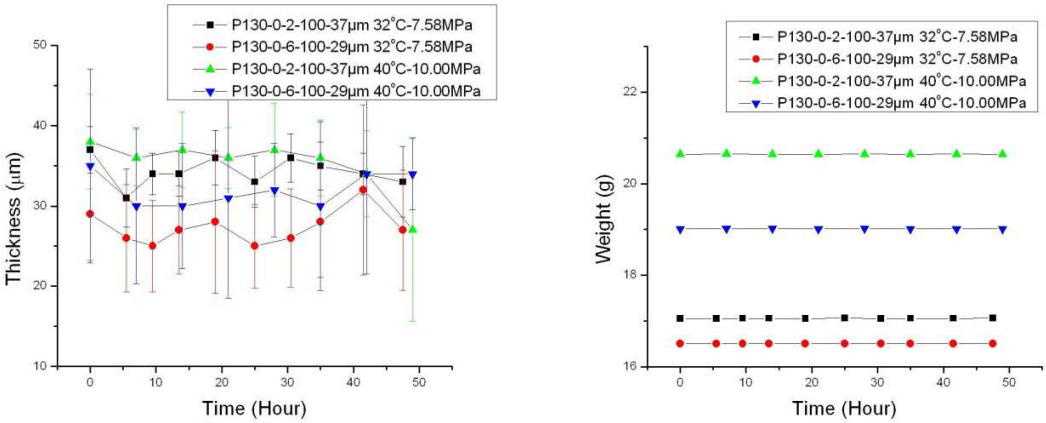

Figure 4.3. Thickness and weight change with different exposure time to $SCCO_2$ for P130 coatings.

Electrochemical impedance spectroscopy is shown in Figure 4.4. For both samples P130-0-2-100-37μm and P130-0-6-100-29μm, the impedance showed the decrease trend with the exposure time increasing. It meant that the barrier properties were lost during the exposure. For P130-0-2-100-37μm sample with exposure to $SCCO_2$ of 32˚C-7.58MPa, the impedance increased a little bit around 25 hour exposure, decreased, increased a lot around 47.5 hour exposure. The increase in impedance at 25 hour exposure might be caused by the crosslinking density increase due to $SCCO_2$ diffusion. For P130-0-6-100-29μm sample, there was not such an increase. The reason was that P130-0-6-100-29μm sample had a higher crosslinking density than P130-0-2-100-37μm. The increase in impedance at 47.5 hour exposure might be caused by the corrosion product formed on the interface. For more severe condition of $SCCO_2$ of 40˚C-10.00MPa, both coating samples showed deterioration. There was an increase for sample P130-0-6-100-29μm at 14 hour exposure, due that the crosslinking density was increased. For sample P130-0-2-100-37μm, the deterioration was more severe than crosslinking density increase, which resulted into a continuous decrease in impedance.

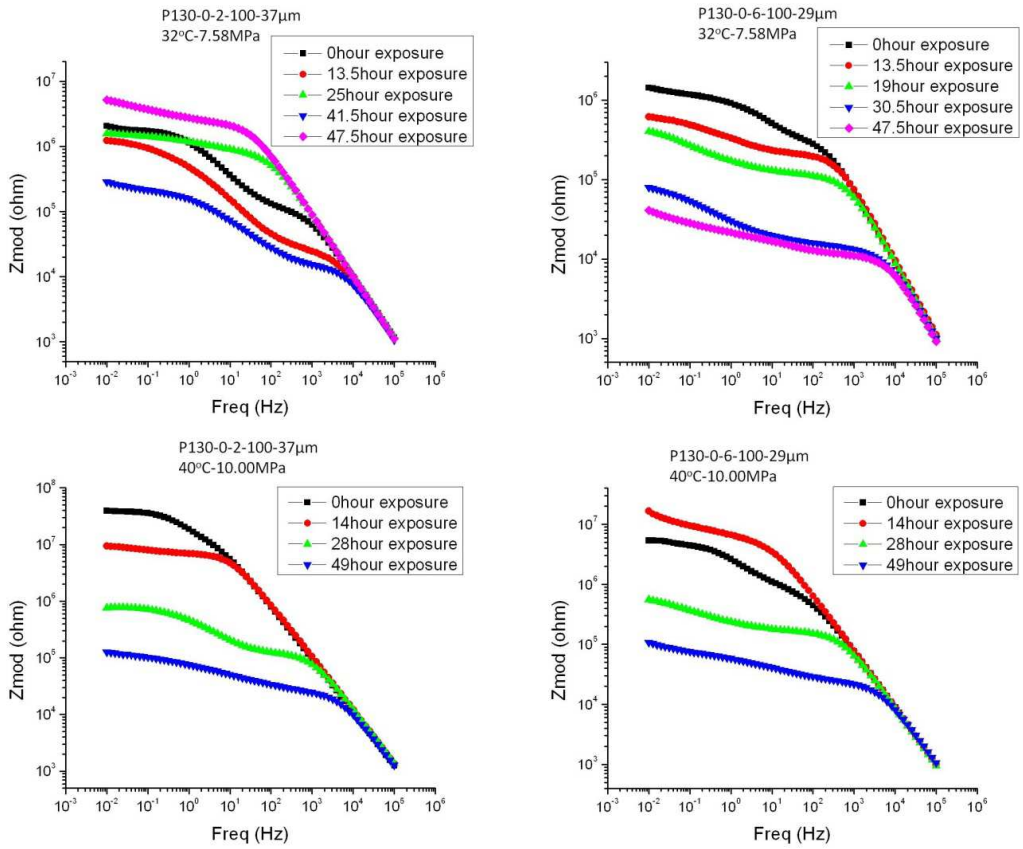

Figure 4.4. Electrochemical impedance spectroscopy of P130 coatings with different periods of exposure, and different conditions of exposure.

Due to the blister formation with exposure to $SCCO_2$ of 40˚C-10.00MPa, another set of samples with curing temperature 200˚C and curing time 30 minutes were prepared. Visual pictures are shown in Figure 4.5. There was no blister on the surface. It indicated that with high crosslinking temperature, organic coatings had better barrier properties. Weight and thickness did not have significant change during the exposure, shown in Figure 4.6. For samples of P130-0-2-200-92µm and P130-0-6-200-99µm, wrinkles were shown on the surface, which caused the thickness to increase. The reason might be caused by the shrinkage by the further crosslinking reaction, while the adhesion was not enough to withstand the shrinkage.

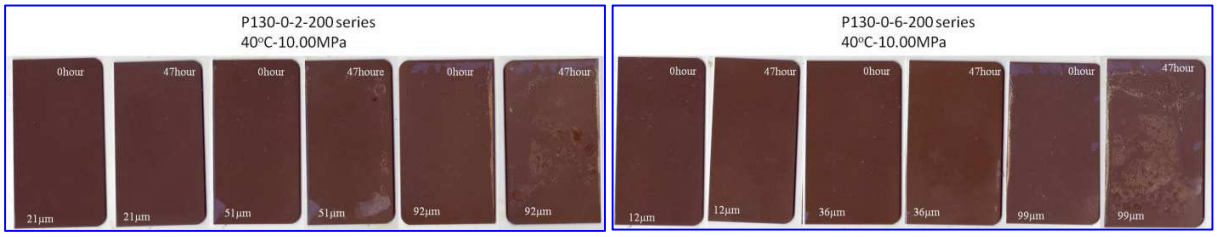

Figure 4.5. Coated panels with different exposure time to $SCCO_2$. Left: P130-0-2-200 series with different thickness of 21µm, 51µm, and 92µm. Right:P130-0-6-200 series with different thickness of 12µm, 36µm, and 99µm.

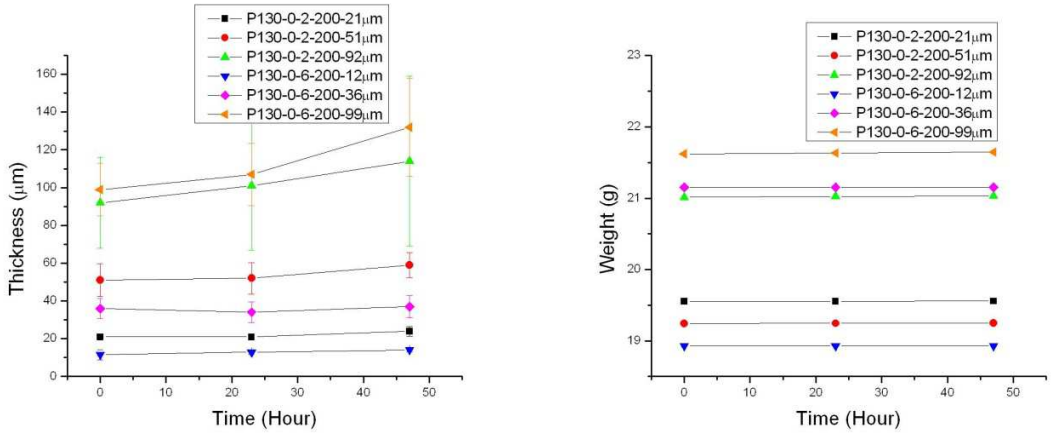

Figure 4.6. Thickness and weight change with different exposure time to $SCCO_2$ of 40˚C-10.00MPa for P130 coatings.

Electrochemical impedance spectroscopy is shown in Figure 4.7. For both series P130-0-2-200 and P130-0-6-200, the thicker coatings had better barrier properties. For thin coating samples P130-0-2-200-21µm, P130-0-6-200-12µm, and P130-0-6-200-36µm, impedance did not change significantly. For medium thick coating sample P130-0-2-200-51µm, impedance increased and maintained. For thick coating samples P130-0-2-200-92µm and P130-0-6-200-99µm, impedance decreased a lot and maintained. For thin coatings, barrier property did not change for the investigated time exposure. However, the further crosslinking reaction did not change the barrier property significantly. For medium thick coatings, the further crosslinking reaction increased barrier property and impedance. For thick coatings, the adhesion failure caused barrier property to be poor.

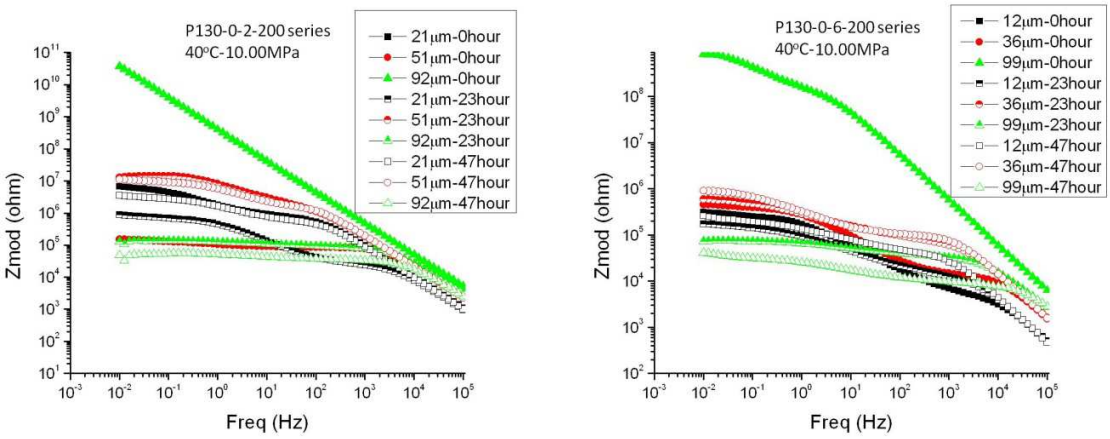

Figure 4.7. Electrochemical impedance spectroscopy of P130 coatings with different periods of exposure.

The higher curing temperature increased the performance of coatings significantly, which eliminated blister formation on the coatings. The medium thickness around 50μm provided the best performance, due to the synergistic effect by little crosslinking reaction shrinkage and little $SCCO_2$ effect on adhesion failure. The high concentration of initiator increased the performance a little, but not significantly.

4.3.2. Performance of P130-PCP Coatings

Visual pictures of P130-PCP coatings are shown in Figure 4.8. With the addition of PCP into coating formulations, wrinkles disappeared with the exposure. PCP increased adhesion force between coatings and steel substrates, which decreased wrinkle problems. However, the hardness of organic coatings was so brittle as to be peeled off and/or be scratched, as shown in Figure 4.8C. The reason was that PCP had poor tear strength [18], especially with aging [19], and low resilience [20]. As shown in Figure 4.9, weight and thickness of samples did not change significantly. However, P130-12.5-6-200 series and P130-37.5-6-200 series showed a little increase in thickness. It might be due that the high crosslinking density deteriorated the adhesion force [21, 22], which caused wrinkling problems and/or blisters, and increased the thickness. The

scratches on P130-12.5-6-200 series and the wrinkles on P130-37.5-6-200 series confirmed the adhesion force failures.

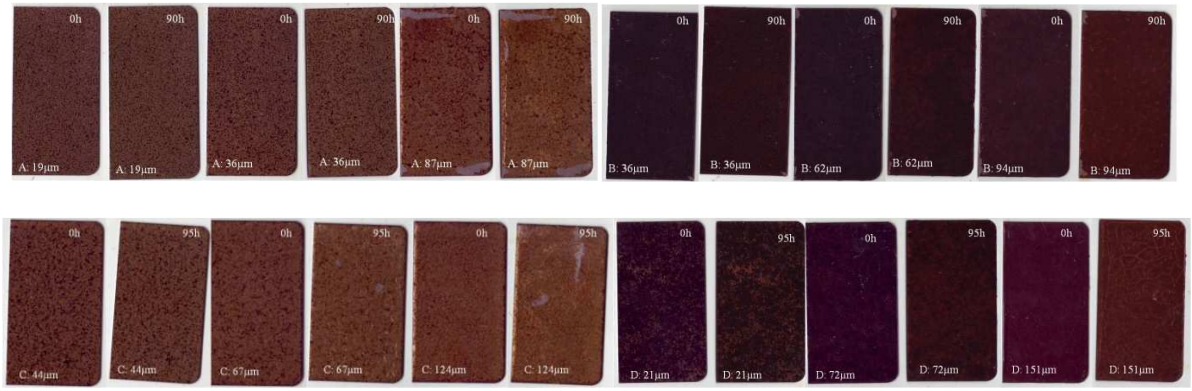

Figure 4.8. Coated panels with different exposure time to $SCCO_2$ of 40˚C-10.00MPa. (A) P130-12.5-2-200 series; (B) P130-37.5-2-200 series; (C) P130-12.5-6-200 series; D: P130-37.5-6-200 series.

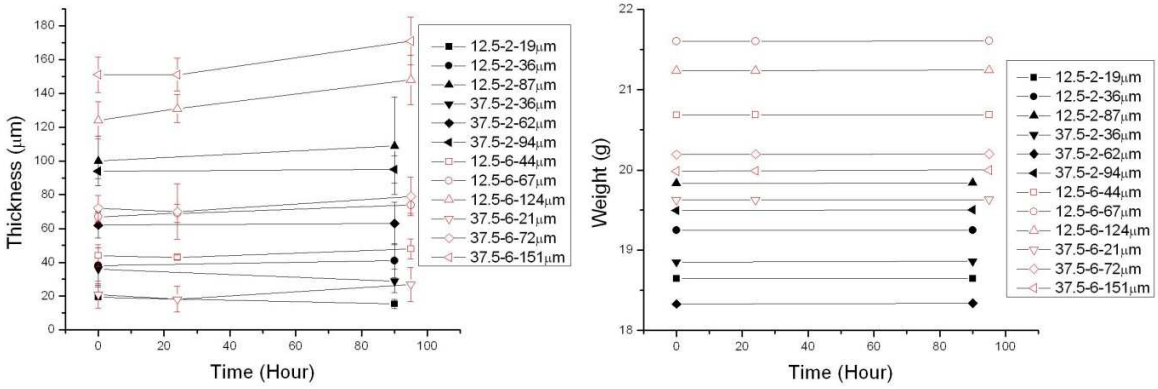

Figure 4.9. Thickness and weight change with different exposure time to $SCCO_2$ of 40˚C-10.00MPa for P130-PCP coatings. The samples were all using P130 and cured at 200˚C. The legends shown in the figure were in short for sample names by taking the second, the third, and the fifth out.

Electrochemical impedance spectroscopy is shown in Figure 4.10. With 2wt% initiator, for thin coatings, such as P130-12.5-2-200-19μm, P130-12.5-2-200-36μm, and P130-37.5-2-200-36μm, the impedance did not change significantly. However, for thick coatings, such as P130-12.5-2-200-87μm, P130-37.5-2-200-62μm, and P130-37.5-2-200-94μm, the impedance

decreased a lot with exposure. With 6wt% initiator, after 24 hour exposure, the impedances were almost the same for all samples, except P130-12.5-6-200-44µm. The decreased impedance might be due to the adhesion deteriorations. The adhesion failure was caused by the internal stress of organic coatings by crosslinking reactions. The thicker coatings usually had a bigger internal stress. So P130-12.5-6-200-44µm and P130-37.5-6-200-21µm sample did not change a lot in impedance. However, P130-37.5-6-200-21µm sample had low impedance due to the self-crosslinking of PCP and possible phase separation of PCP and P130 [23].

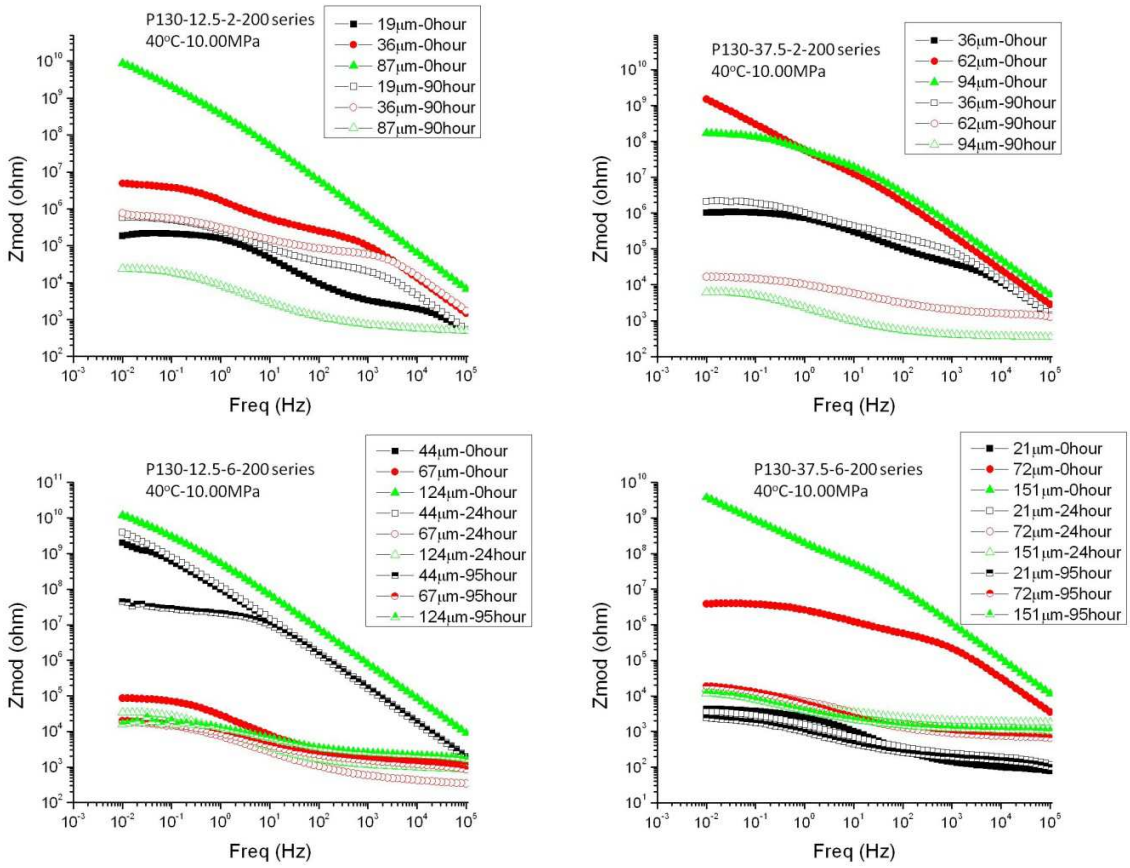

Figure 4.10. Electrochemical impedance spectroscopy of P130-PCP coatings with different periods of exposure.

Polychloroprene incorporated increased the performance of organic coatings, especially adhesion property. However, self-crosslinking reaction of polychloroprene and phase miscibility

of PCP with P130 made the formulation more complicated than P130 system itself. Organic coatings were brittle and had possible phase separation. High concentration of 37.5wt% PCP would cause phase separation, which decreased impedance and barrier property. High concentration of 6wt% BPO would result into high crosslinking reaction rate, which caused a large internal stress. With a large internal stress in organic coatings, interface adhesion could be deteriorated, which also decreased impedance and barrier property.

4.3.3. Thermal Mechanical Analysis of Designed Coatings

Dynamical mechanical analysis results are shown in Table 4.5. The coating formulations had a high glass transition temperature and high modulus retention. With high modulus retention, organic coatings still had good mechanical properties and restrictions with $SCCO_2$ plasticization, which was good for $SCCO_2$ resistance. For P130 series organic coatings, the glass transition temperature was higher than P130-PCP composite organic coatings. The reason might be PCP was more reactive than P130, which lower P130 crosslinking density and the glass transition temperature. However, the high concentration of PCP around 37.5wt%, the modulus retention was high. The reason was that PCP was more rigid than P130. With the consideration of adhesion property and the internal stress caused by crosslinking reaction, PCP incorporation would be good for $SCCO_2$ resistance. However, the optimization of PCP concentration should be done to develop the better organic coatings.

4.4. Conclusions

Two sets of organic coatings with eight formulations were prepared in the chapter. One was P130 organic coatings, while the other one was P130-PCP composite organic coatings. P130-PCP composite organic coatings had better adhesion property to increase the performance

Table 4.5. Dynamic mechanical analysis of designed coatings

Coatings	Glass transition temperature (^oC)	Storage modulus before T_g (MPa)	Storage modulus after T_g(MPa)	Modulus retention (%)
P130-0-2-200 series	121	250	50	20.00
P130-0-6-200 series	145	115	25	21.74
P130-12.5-2-200 series	105*	200	30	15.00
P130-37.5-2-200 series	102*	100	25	25.00
P130-12.5-6-200 series	87*	350	50	14.29

* Two glass transitions showed in DMTA test, while the lower glass transition selected here to explain $SCCO_2$ resistance.

of organic coatings exposed to $SCCO_2$. However, P130-PCP composite organic coatings might have poorer mechanical properties.

For P130 organic coatings, 6wt% BPO was better than 2wt% BPO. 200^{o}C curing temperature was much better than 100^{o}C curing temperature. All these were attributed to the higher crosslinking density. For P130-PCP composite organic coatings, it would increase $SCCO_2$ resistance. However, phase separation and mechanical properties also played important roles on the performance to resist $SCCO_2$ besides crosslinking density, which made thickness an indicator to evaluate the coating performance. Around 50μm organic coatings produced good barrier properties.

4.5. References

1. Tomasko DL, Li HB, Liu DH et al., A review of CO2 applications in the processing of polymers, Ind. Eng. Chem. Res., 42(2003), 6431-6456.
2. Canelas DA, Burke ALC, DeSimone JM, Carbon dioxide as a continuous phase for polymer synthesis, Plastics Engineering, 53(1997), 37-40.

3. Bray CL, Tan B, Wood CD et al., High throughput solubility measurements of polymer libraries in supercritical carbon dioxide, Journal of Materials Chemistry, 15(2005), 456-459.
4. Li YG, Park CB, Li HB et al., Measurement of the PVT property of PP/CO2 solution, Fluid Phase Equilibria, 270(2008), 15-22.
5. Sawan SP, Shieh YT, Su JH, Evaluation of the interaction between supercritical carbon dioxide and polymeric materials, LA-UR-94-2341, (URL: http://www.turi.org/content/view/full/4603)
6. McCluskey GE, Lee JK, Sha J et al., Synthesis and processing of organic materials in supercritical carbon dioxide, MRS Bulletin, 34(2009) 108.
7. Cabanas A, Enciso E, Carbajo MC et al., Effect of supercritical CO_2 in modified polystyrene 3D latex arrays, Langmuir, 22(21)(2006) 8966.
8. Briscoe BJ, Kelly CT, The effect of structure on gas solubility and gas induced dilation in a series of poly(urethane) elastomers, Polymer, 1996. 37(15), 3405
9. Song FM, A comprehensive model for predicting CO2 corrosion rate in oil and gas production and transportation systems, Electrochimica Acta, 55(2010) 689.
10. Kojima M, Tosaka M, Ikeda Y, Chemical recycling of sulfur-cured natural rubber using supercritical carbon dioxide, Green Chemistry, 6(2004) 84.
11. Rindfleisch F, DiNoia TP, McHugh MA, Solubility of polymers and copolymers in supercritical CO2, J. Phys. Chem., 100(1996) 15581.
12. Huang R, Salmen L, Stenberg B, Effects of the type of crosslink on viscoelastic properties of natural rubber, Journal of Polymer Science, Part B: Polymer Physics, 34(1996), 1997-2006.

13. Bradehl TD, Leverty HW, Smith RL et al., Solventless compounding and coating of non-thermoplastic hydrocarbon elastomers, USP 5539033, Jun. 23, 1996.

14. Phinyocheep P, Duan S, Ultraviolet-curable liquid natural rubber, Journal of Applied Polymer Science, 78(2000), 1478-1485.

15. Smith WC, Elizabeth NJ, Adhesion of butyl rubber to metal, USP 2471905, May. 31, 1949

16. Nagelschmidt R, Rudolph A, Corrosion preventing coating compositions for metals comprising a chlorine containing organic polymer as film former, a copper compound and a tertiary organic heterocyclic base, USP 2860118, Nov. 11, 1958

17. Burton SA, Ross R, Corrosion protection with elastomers-an investigation of cathodic protection effects on elastomeric coated pipelines and risers, Corros. Prev. Control., 34(1987), 45-50.

18. Yeh MH, Hwang WS, High mechanical properties of polychloroprene/montmorillonite nanocomposites, Materials Transactions, 2006, 47(11): 2753-2758.

19. Anh TH, Vu-Khanh T, Effects of thermal aging on fracture performance of polychloroprene, Journal of Materials Science, 2005, 40(19): 5243-5248.

20. Menon ARR, Visconte LLY, Studies on blends of polychloroprene and polybutadiene rubber containing phosphorylated cardanol prepolymer: Melt rheology, cure characteristics, and mechanical properties, Journal of Applied Polymer Science, 2006, 102(4): 3195-3200.

21. Loctite, The design guide for bonding rubber and thermoplastic elastomers, Henkel Corporation, Rocky Hill, CT: 2005.

http://www.henkelna.com/us/content_data/14105_LT2662_Loctite_Design_Guide_Bonding_Rubber_Thermoplastic_Elastomers.pdf, accessed on October 2nd, 2012.

22. Galliano A, Bistac S, Schultz J, The role of free chains in adhesion and friction of poly(dimethylsiloxane) (PDMS) networks, The Journal of Adhesion, 2003, 79(10): 973-991.

23. Zhang P, Huang GS, Qu LL et al., Study on the self-crosslinking behavior based on polychloroprene rubber and epoxidized natural rubber, Journal of Applied Polymer Science, 2011, 125(2): 1084-1090.

5. CONCLUSIONS AND FUTURE RECOMMENDATIONS

5.1. Conclusions

With the investigation,3M Scotchkote™ liquid phenolic primer 345 has been proved as a good candidate to transport $SCCO_2$ at various pressure and temperature when thickness of coating was above 50μm. Designed Polyoil™ 130-based polymer systems, cured at 200℃, showed a good candidate, when thickness of coatings were around 50 μm. The incorporation of polychloroprene improved $SCCO_2$ resistance. However, the optimization of concentration of polychloroprene needed to be defined.

During the project, different coating systems and various exposure conditions have been investigated. Following conclusions can be obtained.

1. Four commercial coatings and one designed coating system have been studied to show the sequence of the ability to resistance $SCCO_2$, Commercial coating S345> Designed Polyoil™ 130-based coating systems>Commercial TZ™ 904 coating~ Commercial S323 coating ~ Commercial DevChem™ 253 coating. The reason was attributed to adhesion properties and barrier properties. The barrier properties were dependent on the restriction of polymer chains, which was modified by the crosslinking reaction and the crosslinking density. The crosslinking reactions were evaluated by dynamic mechanical analysis with glass transition temperatures and storage modulus retention before and after glass transition temperature.

2. Blister formation was due to diffusivity of $SCCO_2$ and CO_2, while porous structure formed when coatings were not resilient to stand for pressure in blisters. Blister formed easier with thicker coating, higher temperature of $SCCO_2$, higher pressure of $SCCO_2$, and longer exposure time. Porous structure formed easier with thinner coating, higher temperature of

$SCCO_2$, higher pressure of $SCCO_2$, and more brittle coating. Increasing interfacial adhesion would decrease blister formation and porous structure formation.

3. Besides barrier property failure, $SCCO_2$ with trace contaminations, such as water, would cause corrosion products at the interface, which could increase impedance of organic coatings and supply the new barrier for substrate protections.

4. Curing conditions will affect barrier properties of coatings. More initiator and higher curing temperature would increase crosslinking density, which will increase barrier properties. Internal stress caused by curing process, especially for thick coatings, would be harmful to barrier properties and to properties of resistance to $SCCO_2$. Phase separation of blend coatings would be also harmful to barrier properties.

5.2. Recommendations for Future Research

In order to further develop protective coatings for pipeline to transport $SCCO_2$, more experimental studies can be implemented. Suggestions on experiments are as followings.

1. Field test is very important to evaluate organic coatings performance. These organic coatings should be applied on actual pipelines. The results can be used to verify the application of organic coatings. In the field test, sensors can be developed to monitor organic coatings failure for maintenance.

2. Organic coating formulations, especially P130-PCP composite organic coatings, should be optimized to improve the performance when exposed to $SCCO_2$. Pigments are also useful for barrier properties. Pigmented formulation should also be investigated, such as iron oxide in Scotchkote™ 345 system.

3. An on-site test system can be built to evaluate the corrosion process and the failure process of organic coatings, for example, a built-in EIS test system can be set up inside the high pressure vessel to evaluate the barrier property of organic coatings.

4. Dirty-$SCCO_2$, $SCCO_2$ with trace contaminations, such as H_2S, H_2O, SO_x, and NO_x, are the real gas flue from power plants. The performance of organic coatings to resist this dirty-$SCCO_2$ should also be evaluated.

6. INTRODUCTION TO ZINC-MAGNESIUM RICH PRIMERS

6.1. Motivation

Zinc rich primers (ZnRPs) have been used to protect iron and steel substrates since 1836, initially developed by Stanislas Sorel [1]. They are used as the corrosion protection for marine structures, highway bridges, water tanks, ground vehicles and other structures with immersion of salted water and mild chemicals. However, the cathodic protection of zinc (Zn) particles has a finite period with the gradual depletion of zinc particles. The barrier protection of zinc rich primer is not durable, due to the porous structure of its corrosion products. Underfilm corrosion is very common as a cause of failure in zinc rich primers [2].

Zinc rich primers need improvement to extend their protective life time. Modifications in the primers, such as polymer binder [3], the Zn pigment itself [4, 5, 6, 7], including size, type and pigment volume concentration, additives [8], extenders [9, 10, 11], and even solvents [12] may be used to develop high performance Zn rich primers. Mixing as a powder and/or alloying Magnesium (Mg) with Zinc powders for the protection primer could increase the protective life time of Zn rich primer [13]. However, Zn-Mg rich primers for ferrous substrates have not been well developed and commercialized. Design optimization of Zn-Mg pigmented coating formulations need to be performed in order to improve corrosion protection for industrial applications.

6.2. Literature Review

6.2.1. Zn-Mg Layer Studies

Although Mg powder and Zn powder were used in Mg rich primers [14] and Zn rich primers [1], respectively, Zn-Mg rich primers have not been studied based on Mg powder and Zn powder mixture for such coating formulations. Galvanizing coatings are commonly used as

protective coatings, either by electrodeposition or hot dipping. Mg has been added into the galvanizing layers [15, 16, 17] and shown to give enhanced corrosion resistance as thin metal layers. These layers showed dendritic formation, which could help alter iron/zinc intermetallic formation. It has been also postulated that Mg may be precipitated out of Zn crystals due to the low solubility of Mg in Zn-Mg systems [17]. Physical vapor deposition (PVD) of Mg over Zn layers is another way to prepare Zn-Mg coatings [18, 19]. In the process, Zn was initially coated on the steel, and then Mg was subsequently deposited on Zinc layer and inter-diffused into zinc layer to form the composite coatings. Another way to prepare protective Zn-Mg layers is to use direct alloying Zn and Mg. The alloyed particles $MgZn_2$ can be used to form coating layers [20]. Another type of alloyed particles Mg_2Zn_{11} has been found in the galvanizing process and PVD process [21, 22].

Although the pretreatment for Mg powder with the carbonation has been showed to increase the corrosion resistance of Mg rich primers [14], the pretreatment for Zn powder with corrosion inhibitors or an organosilane has not shown any significant effect on corrosion resistance [23]. Surface treatments of steel substrates may increase the corrosion resistance by improving the adhesion properties of coatings formed on such materials.

Although the studies on Zn/Mg layers over steel showed an enhanced protection, the films were formed either on a laboratory scale [18] or on a complicated process [17].

6.2.2. Zn-Mg Layer Corrosion Tests

Natural weather exposures are actual corrosion tests to evaluate the corrosion resistance performance of Zn-Mg rich layers. However, it requires a long time to finish such evaluations, usually more than ten years. Accelerated weathering tests, designed to simulate natural weather

exposures with the same corrosion mechanisms, are more popular ways to evaluate the corrosion performance, as described in section 1.2.5.

ASTM B117 has been commonly used to evaluate Mg modified Zn protective layers. Red rust resistance showed 10-20 times longer life time for Mg modified Zn protective layers than Zn rcih coatings [21]. With 500 hour of salt spray, Zn-Mg layers maintain its initial corrosion potential (around -1.1V versus saturated calomel electrode (SCE)). In contrast, Zn galvanic layers moved its initial corrosion potential -1.1V vs SCE to a positive direction around -0.8V vs SCE, when the primer lost its cathodic protection [13].

Cyclic corrosion tests including Prohesion™ tests were also very useful especially to simulate the effects of exposure in industrial applications and natural environments. The time to appearance of red rust was 3 times longer for Zn-Mg layers than Zn layers [13], and was much longer in the investigation [19]. Corrosion products were mainly $ZnCl_2 \cdot 4Zn(OH)_2$, and a few ZnO [17].

Immersion tests showed that Zn-Mg layers had rust after 41 days compared with 10 days for Zn rich primer [22]. The corrosion potential showed 10mV more negative than that of Zn rich primer. But the corrosion current was similar [13]. With 5wt% NaCl solution immersion, MgO was formed on the surface instead of powder-like $Mg(OH)_2$, which produced a better barrier property [24]. Other corrosion products were $Zn(OH)_2$, ZnO, and $ZnCl_2 \cdot 4Zn(OH)_2$.

The possible reactions during corrosion tests are listed in Table 6.1. The possible corrosion products would be $Fe(OH)_2$, $FeO \cdot Fe_2O_3$, Fe_2O_3, $Zn(OH)_2$, ZnO, $ZnCl_2 \cdot 4Zn(OH)_2$, $ZnCO_3$, $Zn_4CO_3(OH)_6$, MgO, $Mg(OH)_2$, $MgCO_3$, $Mg_2CO_3(OH)_2$, $Mg_5(CO_3)_4(OH)_2$, and Mg modified Zn based corrosion products [19].

Table 6.1. Possible reactions that may occur during corrosion tests [13, 19, 25]

Categories	Materials	Reactions	Comments
Cathodic Reduction	H^+	$2H^+(aq) + 2e^- \rightarrow H_2(g)$	Acidic environments
	O_2	$H_2O(l) + \frac{1}{2}O_2(aq) + 2e^- \rightarrow 2OH^-(aq)$	Basic environments
Anodic	Fe	$Fe(s) \rightarrow Fe^{2+}(aq) + 2e^-$	Passivation when pH > 10 OCP: -0.7382V vs SCE
		$Fe^{2+}(aq) + 2OH^-(aq) \rightarrow Fe(OH)_2(s)$	Dark greenish
		$6Fe(OH)_2(aq) + O_2(aq) \rightarrow 4H_2O(l) + 2FeO \cdot Fe_2O_3 \cdot H_2O\ (s)$	Green
		$FeO \cdot Fe_2O_3 \cdot H_2O\ (s) \rightarrow H_2O(l) + FeO \cdot Fe_2O_3(s)$	Black
		$2FeO \cdot Fe_2O_3(s) + \frac{1}{2}O_2(aq) + 3H_2O(l) \rightarrow 3Fe_2O_3 \cdot H_2O(s)$	Red-Brown
Anodic	Zn	$Zn(s) \rightarrow Zn^{2+}(aq) + 2e^-$	Passivation when pH between 6 and 10 OCP: -1.05V
		$Zn^{2+}(aq) + 2OH^-(aq) \rightarrow Zn(OH)_2(aq) \rightarrow ZnO(s) + H_2O(l)$ $ZnO(s) + 2OH^-(aq) + H_2O(l) \leftrightarrow Zn(OH)_4^{2-}(aq)$	White ZnO stable for slightly acidic to alkaline conditions
		$5ZnO(s) + 2Cl^-(aq) + 6H_2O(l) \leftrightarrow Zn_5(OH)_8Cl_2 \cdot H_2O(s) + 2OH^-(aq)$	White pH between 5.5 to 11.5
		$4ZnO(s) + 2HCO_3^-(aq) + 3H_2O(l) \leftrightarrow Zn_4CO_3(OH)_6 \cdot H_2O(s) + CO_3^{2-}(aq)$ $Zn_4CO_3(OH)_6 \cdot H_2O(s) + 3CO_3^{2-}(aq) \leftrightarrow 5ZnCO_3(s) + 6OH^-$	Acidic environments with CO_2 incorporated

Table 6.1. Possible reactions that may occur during corrosion tests (continued) [13, 19, 25]

Categories	Materials	Reactions	Comments
Anodic	Mg	$Mg(s) \rightarrow Mg^{2+}(aq) + 2e^-$	Passivation when pH>11 OCP: -1.6V
		$Mg^{2+}(aq) + 2OH^-(aq) \rightarrow Mg(OH)_2(s)$	$Mg(OH)_2$ insoluble when pH>10.27
		$Mg(OH)_2(s) + CO_2(aq) \rightarrow MgCO_3(s) + H_2O(l)$ $2Mg(OH)_2(s) + CO_3^{2-}(aq) + 3H_2O(l) \leftrightarrow Mg_2CO_3(OH)_2 \cdot 3H_2O(s) + 2OH^-(aq)$ $5Mg_2CO_3(OH)_2 \cdot 3H_2O(s) + 3CO_3^{2-}(aq) + 4H_2O(l) \leftrightarrow 2Mg_5(CO_3)_4(OH)_2 \cdot 5H_2O(s) + 6OH^-(aq)$	CO_2 incorporated

With all these corrosion tests, if the environment solution is acidified, magnesium corrosion products would be dissolved and leached out due to unstable and soluble magnesium corrosion products [13]. Salt spray tests yielded rust much earlier than immersion tests [22]. However, different exposure conditions provided different environments, in which corrosion products and corrosion mechanisms would be also different [20].

6.2.3. Zn-Mg Protective Layers Characterizations

The characterizations of Zn-Mg layers were electrochemical characterizations, visual characterizations, and structural characterizations. Scanning electron microscopy was used to check surface morphologies of organic coatings and element compositions of corrosion products [14]. Corrosion products of Zn-Mg protective layers were more densely packed than corrosion products of Zn protective layers [17], shown in Figure 6.1. Optical microscopy was also used to obtain surface morphologies and dendrite structures [15]. Red rust resistance could be an indicator for corrosion resistance ability. Mg inhibited red rust formation [19]. With the higher content of Mg in Zn-Mg protective layers, the resistance against red rust became higher [17].

Mass loss measurements showed that the corrosion rate of Mg-Zn layers had a higher corrosion rate than pure Zn layers, although corrosion potentials were similar [20].

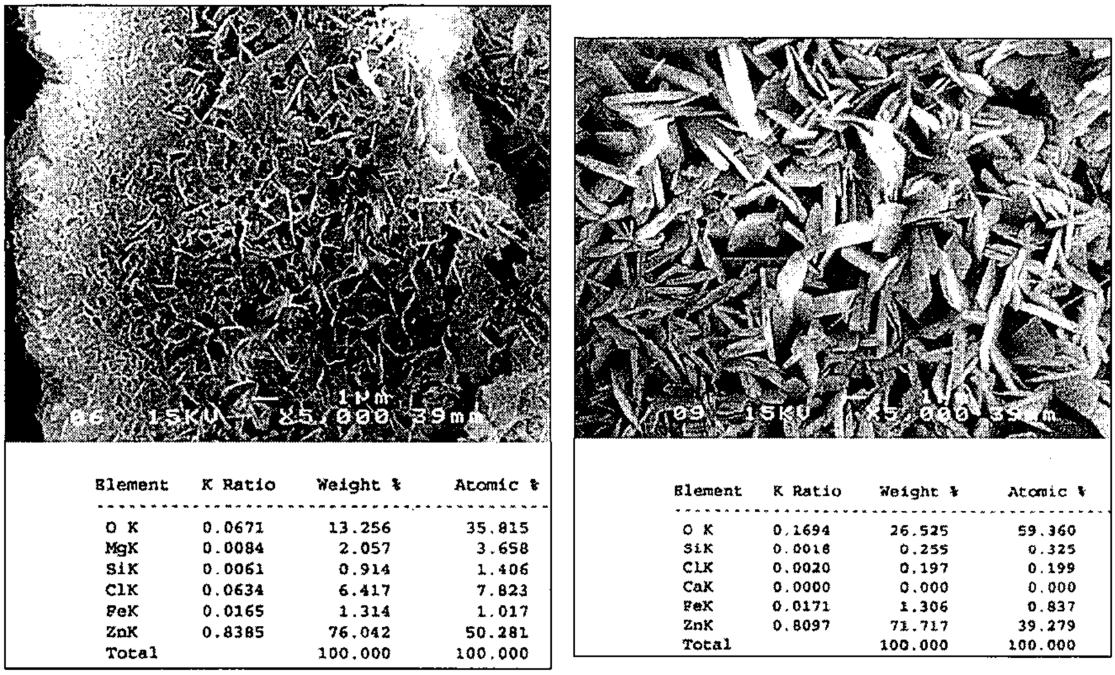

Element	K Ratio	Weight %	Atomic %
O K	0.0671	13.256	35.815
MgK	0.0084	2.057	3.658
SiK	0.0061	0.914	1.406
ClK	0.0634	6.417	7.823
FeK	0.0165	1.314	1.017
ZnK	0.8385	76.042	50.281
Total		100.000	100.000

Zn-0.5%Mg-0.2%Al

Element	K Ratio	Weight %	Atomic %
O K	0.1694	26.525	59.360
SiK	0.0018	0.255	0.325
ClK	0.0020	0.197	0.199
CaK	0.0000	0.000	0.000
FeK	0.0171	1.306	0.837
ZnK	0.8097	71.717	39.279
Total		100.000	100.000

Zn-0.2%Al

Figure 6.1. SEM and EDS of corrosion products for two types of primers. With permission from [17]. Copyright 2000 Nippon Steel & Sumitomo Metal Corporation.

Time lapsed optical microscopy was used to monitor the corrosion phenomena, such as the progression of anodic development and the corrosion product rings [16]. With pH indicator, it was used to monitor pH gradients and their changes. As shown in Figure 6.2, the primary anode initiated and expanded. Then the corrosion product ring emerged and became clear. Chloride penetration occurred and a diffusion region started to form and expand. Then the whole process started to repeat to form a new anodic site, corrosion product ring, and chloride region.

X-ray diffraction was used to characterize corrosion products by its crystallographic structures and chemical compositions [14]. A more stable and dense simonkolleite ($ZnCl_2 \cdot 4Zn(OH)_2$) was formed with Zn-Mg protective layers instead of a porous and unstable

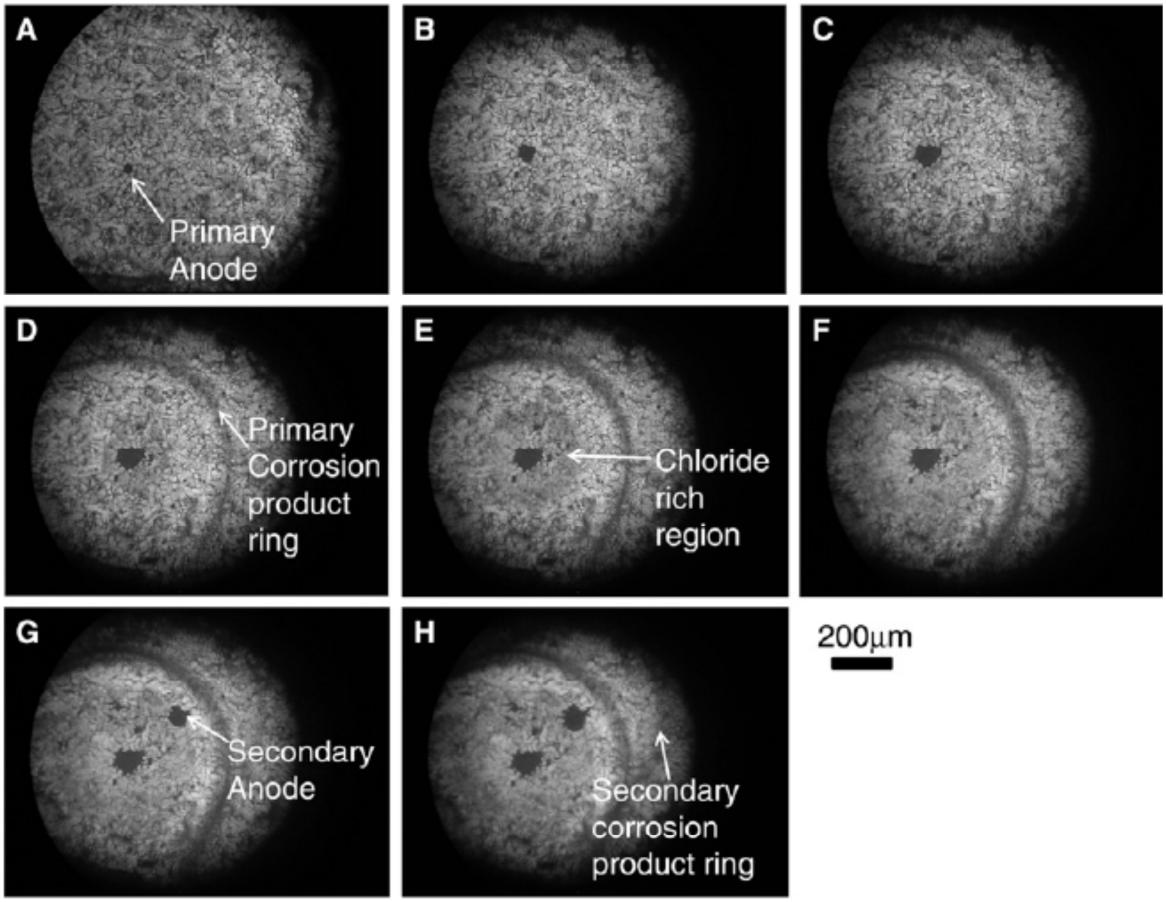

Figure 6.2. Time lapse optical microscopy of the Zn-Mg-Al galvanized alloys with immersion in 0.1% NaCl for a time interval of 10 min. With permission from [16]. Copyright 2011 Elsevier.

zinc oxide (ZnO) with pure Zn protective layers [17], although simonkolleite was also found as the initial corrosion product of Zn protective layers [19]. The rate of Zn consumption was greater for pure Zn protective layers than for Zn-Mg protective layers [17]. X-ray photoelectron spectroscopy (XPS) has also been used to determine the corrosion products not only in crystal form but also in amorphous form [26]. It is more surface sensitive than XRD [13]. Corrosion products were identified within a specific region, for example grey region and white region [26] based on identification of the binding energies of elements. In Figure 6.2, the grey region had

simonkolleite and other zinc corrosion products, while the white region did not have any MgO or $Mg(OH)_2$.

EIS was used to check the life time of the primers and to discover the mechanisms of the corrosion protection behaviors [17]. Corrosion potential was used to evaluate cathodic protection and to predict the life time of the primers. As shown in Figure 6.3, Zn-Mg layers gave longer cathodic protection due to longer periods of negative potential than pure Zn layers. Potentiodynamic scans, as shown in Figure 6.4, indicated that Zn-Mg protective layers had lower cathodic current than Zn layers but had the same anodic current as Zn layers. The reason could be the densely packed corrosion products hindering the cathodic reaction, with Mg areas served as small anodes to increase anodic reaction.

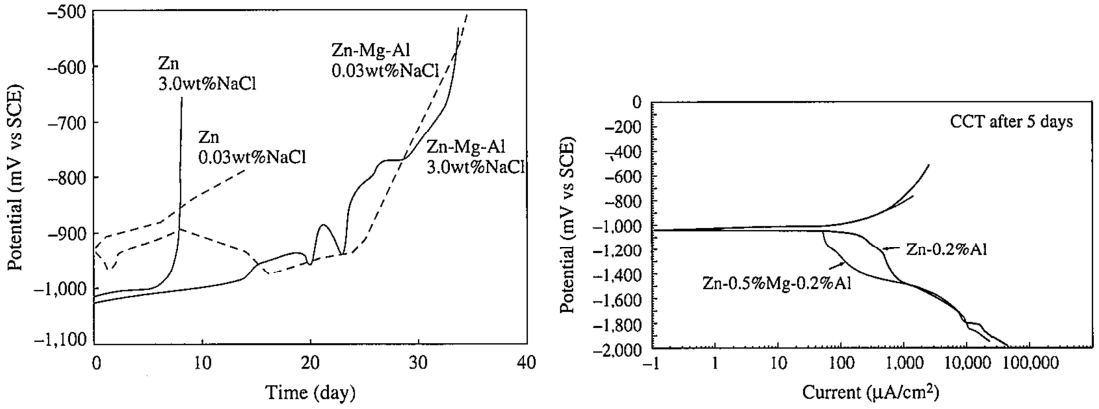

Figure 6.3. The left: Corrosion potential change with time; The right: Potentiodynamic scan of primers. With permission from [17]. Copyright 2000 Nippon Steel & Sumitomo Metal Corporation.

The scanning vibrating electrode technique (SVET) was used to investigate cut edge corrosion [15] in galvanized systems. The anodic and cathodic locations can be detected by SVET as well as local current densities. It was a good way to evaluate local corrosion rates as well as localized corrosion behaviors. As shown in Figure 6.4, with Mg concentration increases from MG00 to MG05, more anodic sites had increased corrosion rates.

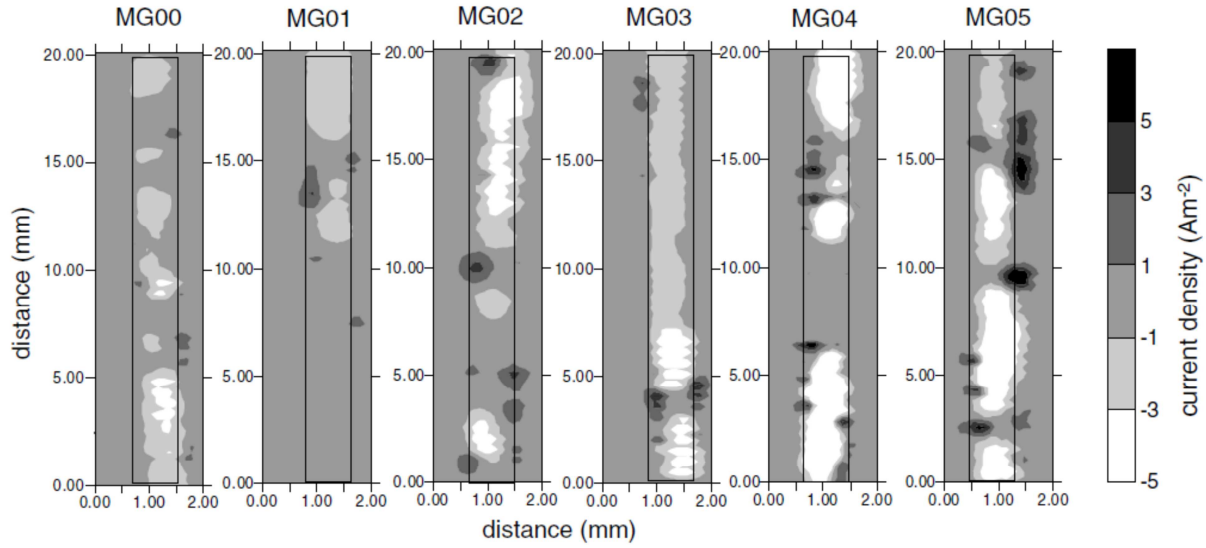

Figure 6.4. SVET plots with the anodic (dark) and cathodic (light) current density distribution with samples after 12 hour immersion in 5% aqueous NaCl. With permission from [15]. Copyright 2008 Elsevier.

6.2.4. Proposed Mechanism of Zn-Mg Protective Layers

Corrosion mechanisms of Zn-Mg protective layers used to protect steel substrates will depend on substrates, primers, and most importantly corrosive environments.

For a pure Mg layer in B117 exposure, a thin and porous magnesium hydroxide layer was formed [27], as well as blisters formed on the coating surfaces. With field and nature exposure, a thick and compact magnesium carbonate layer was formed with good protection from further corrosion [27], without blisters formed on the coatings surfaces. For a pure Zn layer, zinc salts, such as simonkolleite and hydrozincite, were formed as corrosion products on top of the layers and improved the corrosion resistance [28].

For Zn-Mg layers, from Figure 6.5, the corrosion started from the primary anode, which came from the preferred dissolution/oxidation of $MgZn_2$. Corrosion product rings came from the reaction between anodic products and cathodic products. The pH gradients were formed due to the cathodic reactions, which increased pH with the generation of OH^- ions. The Cl^- rich region

was developed due to the anodic reactions, which increased positive charges. All these processes caused galvanized layers phase corrosion.

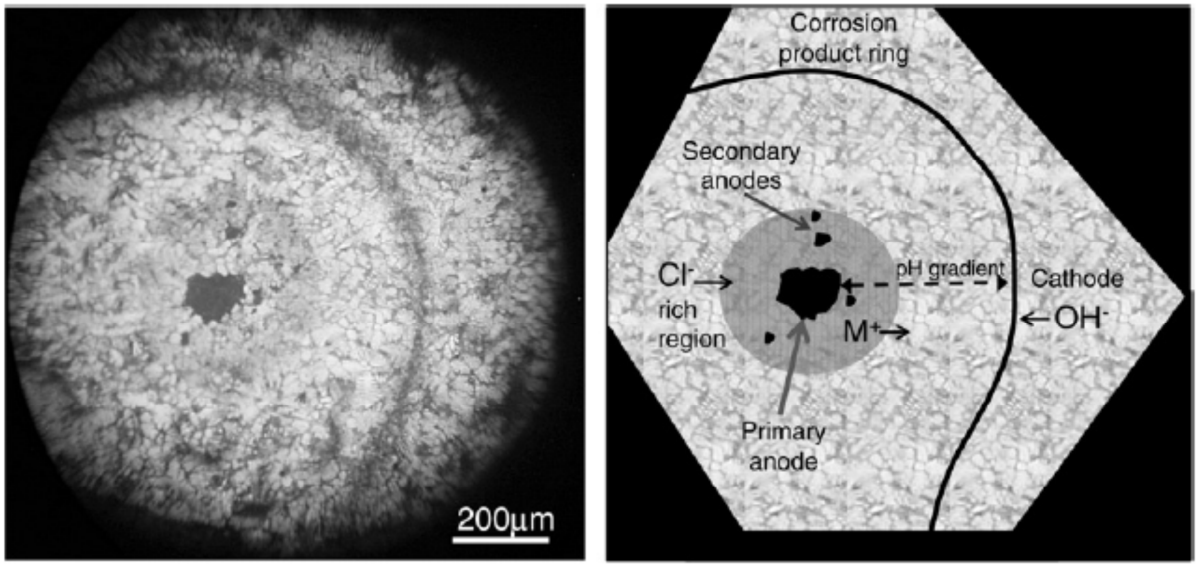

Figure 6.5. The optical microscope image of the corrosion sites and a schematic diagram of the corrosion mechanism. With permission from [16]. Copyright 2011 Elsevier.

However, the previous work did not explain the increasing lifetime of corrosion protection for Zn-Mg layers. Some research showed that the densely packed and stable corrosion products simonkolleite protected the substrates from further corrosion by barrier protection, which increased lifetime of primers [17]. Simonkolleite formation was promoted by Mg presence to alter the corrosion environments. However, simonkolleite was thermal dynamically formed whether there was Mg in present or not, although Mg^{2+} seemed to help stabilize simonkolleite by reacting with carbonate to form $MgCO_3$ [19]. The presence of Mg^{2+} instead of Mg could also decrease the corrosion rate of zinc protective layers [13].

The blister and delamination mechanisms came from chloride penetration resulting in electrochemical reactions [20] with the further dissolution of the passive layer and delamination. Mg incorporated $MgZn_2$ alloy in the galvanizing layers seemed to eliminate the cathodic

delamination due to an adverse potential gradient between defect areas and intact areas. With only low rate of anodic delamination, it might be further improved to be avoided with the selection of the composition of Zn-Mg rich coatings [20].

Although a lot of papers showed that addition of Mg to a galvanized layer increased the corrosion resistance, magnesium additions may increase cut edge corrosion rate, because Mg additions initiated more zinc corrosion sites [15].

From the above statements regarding mechanisms of corrosion resistance improvement, corrosion products should be compact, stable, and electrical inert for longer barrier protection. Simonkolleite was preferably formed in the presence of Mg^{2+} ion [29], although Mg^{2+} did not favor simonkolleite formation when pH was adjusted to 9.2 [30, 31].

6.3. Scope of Investigation

The focus of the investigation was to improve corrosion resistance of current commercial Zn rich primers. With evidence that mixing/alloying Mg with Zn in galvanizing layers increases the corrosion resistance [13, 17], the addition of Mg particles into Zn rich primer was studied for improved corrosion resistance of this class of coatings. The following studies carried out for the development of new Zn-Mg rich primers.

1. Different ratios of Mg incorporated into Zn rich primers were investigated for their impact on corrosion resistance and life time.
2. The effects of different corrosive environments were studied with their corrosion resistance, since the corrosion behaviors of Zn-Mg layers strongly depended on the corrosion conditions and coating formulations [20].
3. Besides the performance of Zn-Mg rich primers, performance of Zn-Mg rich primers with sealing primers was also investigated.

Part of investigation will be focused on the development of Zn-Mg rich primers for industrial applications. It consists of four chapters. Chapter 6 introduces the current research about Zn-Mg layers. Chapter 7 describes corrosion behaviors of Zn-Mg rich primers with different test environments. Chapter 8 evaluates performances of Zn-Mg rich primers with sealing primers on. Finally, chapter 9 makes the conclusions and the recommendations for future research.

6.4. References

1. Berger DM, Applicator's guide to zinc-rich primers, Chemical Engineering, 1977, 84(6), 147-150
2. Chang LM, Zayed T, Dricker JD, Steel bridge protection policy: Evaluation of bridge coating system for INDOT steel bridges, Joint Transportation Research Program Technical Reports, West Lafayette IN, 1999. (accessed http://docs.lib.purdue.edu/cgi/viewcontent.cgi?article=1667&context=jtrp on Oct. 14, 2012)
3. Sorensen PA, Kiil S, Dam-Johansen K et al., Anticorrosive coatings: A review, Journal of Coatings Technology and Research, 2009, 6(2), 135-176.
4. Kalendova A, Effects of particle sizes and shapes of zinc metal on the properties of anticorrosive coatings, Prog. Org. Coat., 2003, 46, 324-332.
5. Panossian Z et al., Steel cathodic protection afforded by zinc, aluminium and zinc/aluminium alloy coatings in the atmosphere, Surface & Coatings Technology, 2005, 190, 244-248.
6. Marchebois H et al., Zinc-rich powder coatings corrosion in sea water: influence of conductive pigments, Prog. Org. Coat., 2002, 45(4), 415-421.

7. Shreepathi S, Bajaj P, Mallik B, Electrochemical impedance spectroscopy investigations of epoxy zinc rich coatings: Role of Zn content on corrosion protection mechanism, Electrochim. Acta, 2010, 55, 5129-5134.

8. Bastos AC, Zheludkevich ML, Ferreira, A SVET investigation on the modification of zinc dust reactivity, Progress in Organic Coatings, 2008, 63, 282-290.

9. Giudice C, Benitez J, and Pereyra A, Influence of extender type of performance of modified lamellar zinc primers. J. Coat. Technol. Res., 2004, 1(4), 291-304.

10. Feliu Jr. S et al., Effect of the Di-iron phosphide conductive extender on the protective mechanisms of Zinc-rich coatings, J. Coat. Technol. Res., 1991, 63(794), 67-72.

11. Simko F and Simpson V, New class of conductive extenders in Zinc-rich coatings, JCT Coatings Tech, 1976, 48(614), 61-66.

12. Marchebois H et al., Characterization of zinc-rich powder coatings by EIS and Raman spectroscopy, Surf. Coat. Technol., 2002, 157(2-3), 151-161.

13. Hosking NC, Strom MA, Shipway PH et al., Corrosion resistance of zinc-magnesium coated steel, Corrosion Science, 2007, 49(9), 3669-3695.

14. Pathak SS, Blanton MD, Mendon SK et al., Carbonation of Mg powder to enhance the corrosion resistance of Mg –rich primers, Corrosion Science, 2010, 52, 3782-3792.

15. Elvins J, Spittle JA, Sullivan JH et al., The effect of magnesium additions on the microstructure and cut edge corrosion resistance of zinc aluminium alloy galvanised steel, Corrosion Science, 2008, 50, 1650-1658.

16. Sullivan J, Mehraban S, Elvins J, In situ monitoring of the microstructural corrosion mechanisms of zinc-magnesium-aluminium alloys using time lapse microscopy, Corrosion Science, 2011, 53, 2208-2215.

17. Nishimura K, Kato K, Shindo H, Highly corrosion-resistant Zn-Mg alloy galvanized steel sheet for building construction materials, Nippon Steel Technical Report N0. 81, January 2000.

18. Schuhmacher B, Schwerdt C, Seyfert U et al., Innovative steel strip coatings by means of PVD in a continuous pilot line: process technology and coating development, Surface and Coatings Technology, 2003, 163-164: 703-709.

19. Volovitch P, Allely C, Ogle K, Understanding corrosion via corrosion product characterization: I. Case study of the role of Mg alloying in Zn-Mg coating on steel, Corrosion Science, 2009, 51, 1251-1262.

20. Hausbrand R, Stratmann M, Rohwerder M, Corrosion of zinc-magnesium coatings: Mechanism of paint delamination, Corrosion Science, 2009, 51, 2107-2114.

21. Kawafuku J, Katoh J, Toyama M et al., Properties of zinc alloy coated steel sheets obtained by continuous vapor deposition pilot-line, SAE Technical Paper, 1991, 912272.

22. Morishita M, Koyama K, Murase M et al., Improvement in the corrosion resistance of zinc plated steel by electrodeposition of magnesium from a molten salt, ISIJ International, 1996, 36(6), 714-719.

23. Bastos AC, Zheludkevich ML, Kluppel I et al., Modification of zinc powder to improve the corrosion resistance of weldable primers, Progress in Organic Coatings, 2010, 69, 184-192.

24. Morishita M, Koyama K, Mori Y, Self-healing ability of zinc plated steel coated with magnesium electrodeposited from a molten salt, Materials Transactions, JIM, 1997, 38(8), 719-723.

25. Sorensen PA, Kiil S, Dam-Johansen K et al., Anticorrosive coatings: a review, J. Coat. Technol. Res., 2009, 6(2), 135-176.

26. Schurz S, Luckeneder GH, Fleischanderl M et al., Chemistry of corrosion products on Zn-Al-Mg alloy coated steel, Corrosion Science, 2010, 52, 3271-3279.

27. Pathak SS, Blanton MD, Mendon SK et al., Investigation on dual corrosion performance of magnesium-rich primer for aluminum alloys under salt spray test (ASTM B117) and natural exposure, Corrosion Science, 2010, 52, 1453-1463.

28. de la Fuente D, Castano JG, Morcillo M, Long term atmospheric corrosion of zinc, Corrosion Science, 2007, 49, 1420

29. Prosek T, Thierry D, Taxen C et al., Effect of cations on corrosion of zinc and carbon steel covered with chloride deposits under atmospheric conditions, Corrosion Science, 2007, 49, 2676-2693.

30. Ishikawa T, Matsumoto K, Yasukawa A et al., Influence of metal ions on the formation of artificial zinc rusts, Corrosion Science, 2004, 46, 329-342.

31. Ishikawa T, Murai M, Kandori K et al., Structure and composition of artificially synthesized rusts of Zn-Fe and Zn-Ti alloys, Corrosion Science, 2006, 48, 3172-3185

7. ZINC-MAGNESIUM RICH PRIMERS IN ACCELERATED TESTS

7.1. Introduction

Mg incorporated into a Zn galvanizing layer has been shown to increase corrosion resistance of galvanized steels as discussed above in Chapter 6. Sometimes this occurs even if the rate of galvanizing layer corrosion is increased [1]. As stated in section 6.2.4, mechanism of the enhanced protection of Zn+Mg rich layer vs. Zn-only layers has not been conclusively identified. Particulate Zn+Mg rich primers have not been here-to-fore been studied to protect ferrous structures. The optimization of Zn-Mg ratio for corrosion resistance in such primers has thus not been investigated.

In this chapter, mechanisms of (Mg+Zn) rich primers in accelerated tests were investigated. Different ratios of Zn to Mg at a fixed pigment volume concentration were prepared to discover the optimum Zn/Mg ratio for corrosion resistance. The ASTM B117 and Prohesion™ accelerated cabinet exposure protocols were used to assess the relative performance of this set of coatings. Immersion tests were performed to monitor pH change in the accelerated corrosion based solutions to help understand the behaviors of these primers in ASTM B117 and Prohesion™ exposure. The cathodic protection provided by these primer films was evaluated by potenotio-dynamic polarization scans (PDS). Koenig hardness testing was used to investigate the mechanical properties of the epoxy binder system. Corrosion products were characterized with X-ray diffraction test (XRD). A possible mechanism of the enhanced protection of steel by Zn+Mg vs. the Zn only metal rich primer was inferred from corrosive environment effects and characterization of corrosion products.

7.2. Experimental Methods

7.2.1. Materials

The materials used in the coating formulation are shown in Table 7.1. It is a two-component coating formulation. Part A was the epoxy binder system + pigments and additives, while part B was the curing system (polyamide + solvents). For the Part A, epoxy was mixed with the pigments and the additives using mechanical stirring for 10 minutes and maintained for another 30 minutes to allow sufficient pigment wetting. The pigmentation of the (Zn + Mg) rich coatings was kept at a total PVC at 53%, but had different volume ratios of Zn and Mg, as shown in Table 7.2. For the Part B, polyamide was mixed with solvents acetone and n-butanol. Then the part B was poured into the part A. The two parts were mixed together with a spatula. Xylene solvent from Sigma-Aldrich with reagent grade was used to adjust the viscosity before spray application. The spray application was finished less than 30 minutes after part A and part B were mixed.

Table 7.1. Materials used for Zn-Mg rich primer

Categories	Materials	Function	Weight/g
Part A	Epon 828	Primary Binder	8.45
	Texaphor 963	Dispersing agent	0.45
	Zinc Dust	Pigment	Varies*
	Mg 3820	Pigment	Varies*
	Cymel	Secondary Binder	1.495
	MIBK	Solvent	1.53
	Acetone	Solvent	1.51
	Aromatic 100	Solvent	10.36
Part B	Epicure 3164	Curing agent	11.04
	Acetone	Solvent	0.99
	n-butanol	Solvent	0.99

* Shown in Table 7.2.

S36 steel panels, purchased from Q-Lab, were used as the substrate in this portion of the study. Ammonia sulfate and sodium chloride, purchased from Sigma-Aldrich with reagent grade,

Table 7.2. Pigments usage for each formulation

Formulation	Name	Zn weight/g	Mg weight/g	Mg volume ratio/%	PVC/%
1	Zn0Mg0	0	0	0	0
2	Zn10Mg0	152.52	0	0	53
3	Zn9Mg1	137.27	3.77	10	53
4	Zn8Mg2	122.02	7.53	20	53
5	Zn7Mg3	106.76	11.30	30	53
6	Zn6Mg4	91.51	15.06	40	53
7	Zn5Mg5	76.26	18.82	50	53
8	Zn4Mg6	61.00	22.60	60	53
9	Zn3Mg7	45.76	26.36	70	53
10	Zn2Mg8	30.50	30.12	80	53
11	Zn1Mg9	15.25	33.88	90	53

were used as dilute Harrison's solution (DHS) and 5wt% sodium chloride solution preparation. Deionized water (DI water) was prepared by Milli-Q Advantage A10 Ultrapure Water Purification System with a resistivity of 18.2MΩ·cm at 25˚C.

The phosphate surface treatment described in section 6.2.1 was used based on the solution described in Table 7.3. Steel panel S36 was immersed in the phosphate solution for 5 minutes. It was taken out of the solution, and rinsed with methanol, purchased from Sigma-Aldrich with reagent grade, three times. Then the panel was left air-dry for 30 minutes before the spray application.

Table 7.3. Phosphate solution preparation

Materials	Source	Function	Volume ratio/%
Phosphate acid	Sigma	Treatment	18
1-propanol	Sigma	Dispersing agent	35
2-propanol	Sigma	Pigment	25
DI water	Milli-Q A10	Pigment	22

7.2.2. Characterizations

A Gamry Potentiostat Reference 600 was used for potentiodynamic polarization test. The electrolytes were dilute Harrison's Solution (DHS), which is comprised of 0.35wt% $(NH_4)_2SO_4$

and 0.05wt% NaCl in distilled water, and 5wt% sodium chloride solution. Potentiodyanmic polarization scans were run from -1.8V vs SCE to 0.8V vs SCE with a scan rate 1mV/s. Pendulum hardness tests were performed using a BYK Gardner Pendulum Hardness Tester following ASTM D4366. The measurements used 3 points for an average. The pH measurements were taken using an Oakton pH 1100 for continuous pH monitoring. The XRD testing was performed using a Philips X'Pert MPD Powder X-ray Diffractometer. The scanning angle was from 20 degrees to 80 degrees with the step size of 0.03 degree and scan step time 2 seconds. The unit generator was setting up with 45kV voltage and 40mA current.

7.2.3. Experimental Set-up

The Zn-Mg rich primers formulated at constant PVC but with various Mg volume ratios were immersed into DHS solution and 5wt% NaCl solution. The pH values of solutions were monitored up to three days to evaluate environmental change during the immersion test. These environmental changes, especially pH value changes, were used to determine corrosion reactions occurred in accelerated corrosion tests.

For accelerated corrosion tests, Zn-Mg rich primers were put into ASTM B117 chamber and Prohension™ chamber with different time periods. The samples were initially visually inspected, and characterized with pendulum hardness test to test the mechanical performance of the epoxy binder. Potentiodynamic polarization scans (PDS) to test the cathodic protection property of zinc rich primer were performed, and then XRD measurement was performed to characterize corrosion products.

7.3. Results and Discussions

7.3.1. Formulation Verification

The chapter describes our examinations of the effect of Mg addition into Zn rich primer on corrosion behaviors. Formulations of coating systems, especially the percentage of Mg addition, were critical for mechanisms of corrosion behaviors. In order to accurately state the performance of Zn-Mg rich primers, formulations of coating systems were verified with initial calculated formulations. XRD test was used to characterize the concentration of Mg particles [2], and with the same principles the ratio of Zn and Mg particles.

The formulation verification was using XRD test to characterize the ratios of Zn and Mg particles and to compare with the ratios of Zn and Mg particles from initial formulations. The XRD calculation was based on semi-quantitative X-ray diffraction reference intensity ratio methods [3]. The result is shown in Figure 7.1. It could be seen r equals to 0.99781, very close to 1.0, which indicates that XRD test results were in agreement with the original formulation.

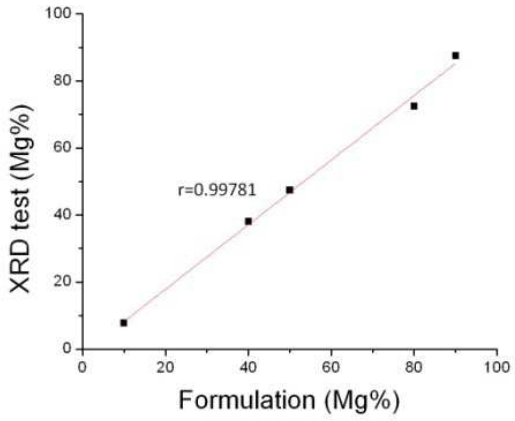

Figure 7.1. Comparison between XRD test and original formulation. The red line was fitted result from the experimental dot points.

In conclusion, XRD could be used to test the volume ratio of Mg particles and Zn particles inside the primer system.

7.3.2. Immersion Corrosion Tests

Immersion corrosion test is used to evaluate the corrosive environment, especially the pH values, which can be used to predict the possible corrosion reactions and the corresponding corrosion products.

With immersion testing, it was determined from Figures 7.2 and 7.3 that pH values of immersing solutions kept increasing with the time of the immersion up to 1800 seconds. The higher concentration of Mg incorporated in the Zn-Mg rich primer, the higher the pH value after 1800 seconds immersion. From Figure 7.2 with the immersion in DHS solution, the highest pH value after the immersion was around 8. However, Zn9Mg1 primer had the similar behavior with Zn10Mg0 and Zn0Mg0, which showed pH around 5.8 after 1800 seconds immersion. For the other Zn-Mg rich primers, all showed a higher pH and a faster pH change with the immersion. From Figure 7.4, it could be seen clearly that pH values for around 30 minute immersions were similar. From Figure 7.3 with the immersion in 5wt% NaCl solution, the highest pH after the immersion was around 10, less than 10.17, the precipitation pH of $Mg(OH)_2$ [4]. It is presumed here all Mg corrosion products, such as MgO and $Mg(OH)_2$ [5], were soluble. The Zn10Mg0 primer had the similar behavior with the negative control Zn0Mg0 primer. Any further Mg incorporated into a Zn-Mg rich primer showed a faster pH value change with the immersion, especially Zn6Mg4 primer. From Figure 7.4B, it could be seen clearly that pH values for around 30 minute immersions were increased with Mg concentration. From Figures 7.2 and 7.3, pH value changes in 5% NaCl solution were faster than pH value changes in DHS solution.

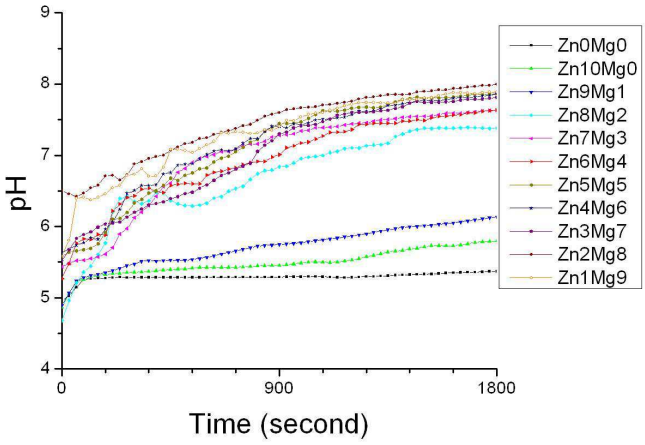

Figure 7.2. The pH change with the immersion time in DHS solution for different formulations.

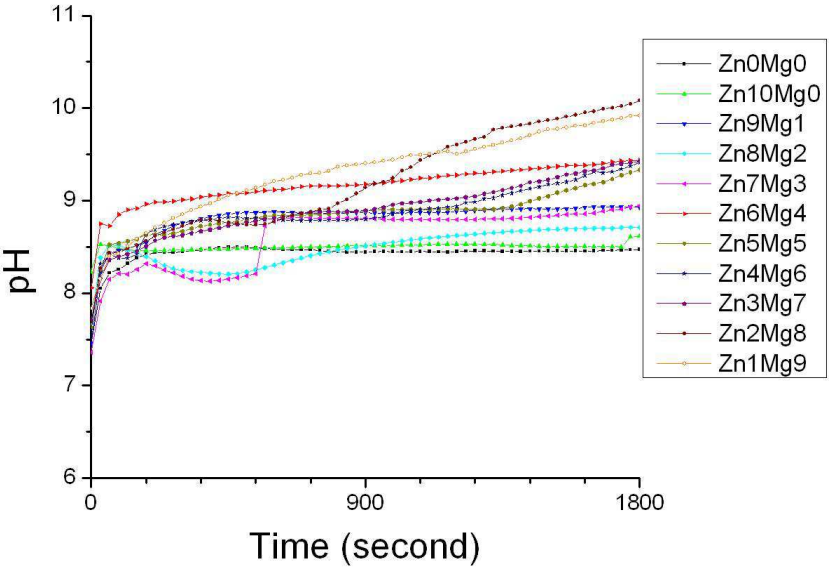

Figure 7.3. The pH change with the immersion time in 5wt% NaCl solution for different formulations.

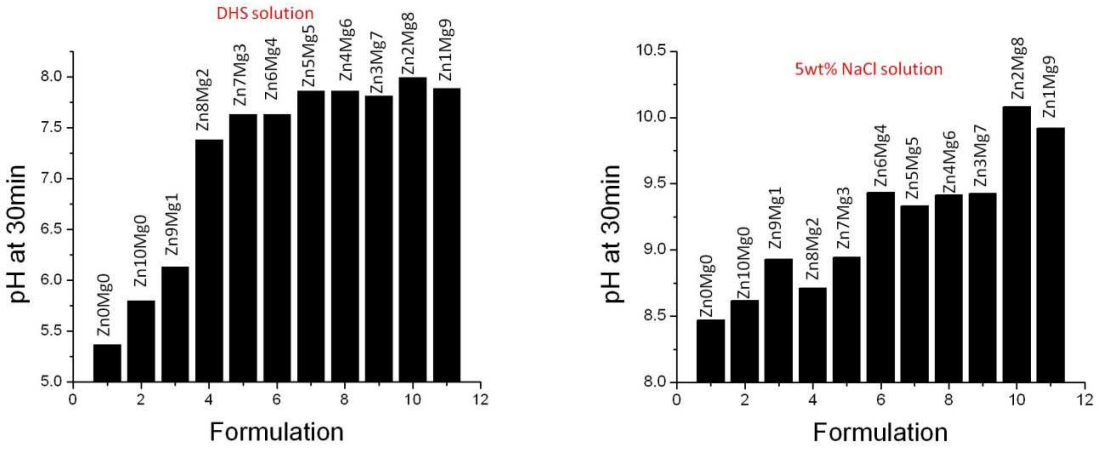

Figure 7.4. The pH value of different formulations immersed in different solutions for half hour.

In the immersion test, Zn0Mg0 and Zn10Mg0 primers had a low reactivity, while Zn-Mg rich primers had a high reactivity due to the existence of Mg particles. For DHS solution, the reaction [6] would be

$$Mg + 2H^+ \rightarrow Mg^{2+} + H_2$$

The reaction depended on the concentration of H^+, once enough Mg particles were exposed to solution. When the volume concentration of Mg in the Zn-Mg rich primer was over 20vt%, the pH value of the immersion solution seemed constant, which indicated that the concentration of H^+ controlled the reaction rate due to enough Mg particles exposure, as indicated in Figures 7.2 and 7.4A. For Zn9Mg1 primer, the barrier property was good enough to resist Mg particles exposure in solution, while with more Mg addition, the barrier properties were poor for the reaction of Mg particles, due to the higher oil absorption of Mg particles than Zn particles [7].

For 5wt% NaCl solution, the reaction [6, 8] would be

$$Mg + 2H_2O \rightarrow Mg^{2+} + 2OH^- + H_2$$

The higher concentration of Mg particles resulted into the higher pH value, as indicated in Figure 7.4B. However, as shown in Figure 7.3, Zn6Mg4 showed the fastest reaction speed, due that the

competition between the dissolution of Mg particles and the inhibition by the corrosion products, such as MgO and $Mg(OH)_2$ [9], and the competition between the dissolution of Mg particles and the galvanic effect between Mg particles and Zn particles. The higher concentration of Mg particles with the temporary formed more $Mg(OH)_2$ which could inhibit Mg from further reactions. Provided the galvanic effect between Zn and Mg particles, the higher volume concentration of Mg particles with the smaller cathodic area had the lower reaction rate [6]. The reaction rate in DHS solution was slower than that in 5wt% NaCl solution due that the penetration effect of Cl^- ion [10].

In conclusion, Zn-Mg rich primers in 5wt% NaCl solution showed a higher reaction rate than that in DHS solution. When Mg particles had a volume concentration higher than 20%, barrier properties became worse. Zn6Mg4 primers showed the fastest initial reaction speed when immersed in 5wt% NaCl solution.

7.3.3. B117 Corrosion Tests

The visual appearance of different formulation primers after exposure under the ASTM B117 protocol are shown in Figure 7.5 with the detailed results in Table 7.4. The primers Zn0Mg0 and Zn10Mg0 exhibited rusts after only 24 hours of exposure. The primer Zn7Mg3 and primers with higher concentration of Mg, similar to Zn4Mg6, also showed red rust after 24 hours of B117 exposure. The primer Zn8Mg2 showed no red rust even after 72 hours of B117 exposure, but showed red rust after 216 hours. The Zn9Mg1 primer did not show any rust in the entire 216 hour B117 corrosion test. The Zn9Mg1 primer increased the protective life time at least 9 times with respect to red rust formation. With the previous immersion study, Zn0Mg0 and Zn10Mg0 had low reaction rates, which would supply low cathodic current density. The primers with higher concentration than 30vt% with poor barrier properties could expose more cathode area

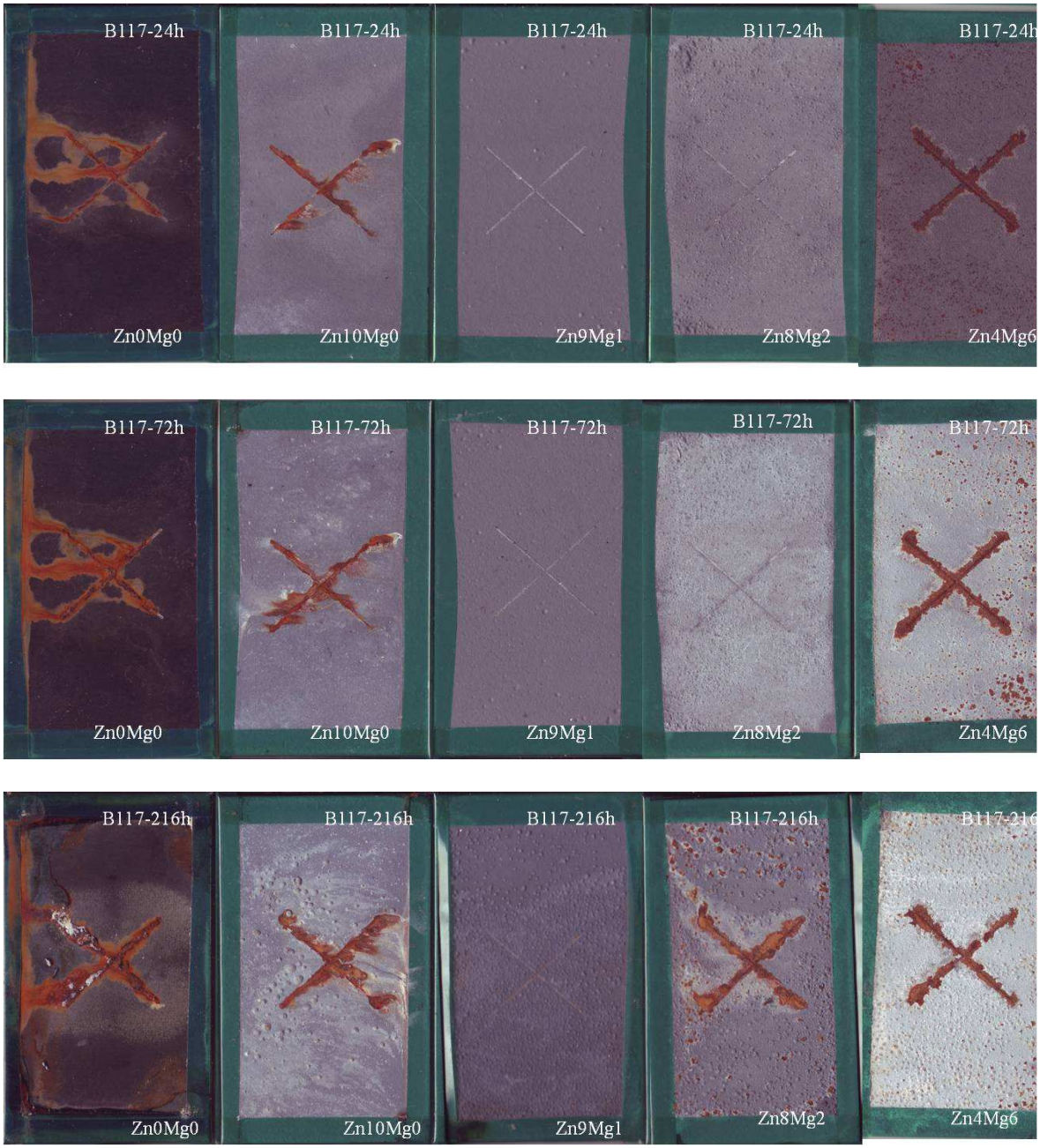

Figure 7.5. Different formulation primers with ASTM B117 corrosion test for different time periods.

than the scribed area only. Under both circumstances, Zn-Mg rich primers would not supply sufficient and/or durable cathodic protection for the scribed area. The Zn9Mg1 primer, not only

potentially supplying enough cathodic current density due to high reactive Mg particles inside, but also holding good barrier property, showed no rust in the investigation period.

Table 7.4. Visual results of the first appearance of corrosion products in primers of varying Mg content in ASTM B117 exposure.

Formulation	Rust/hour	Blister/hour	White corrosion products/hour
Zn0Mg0	24	No	No
Zn10Mg0	24	72	24
Zn9Mg1	No	24	24
Zn8Mg2	216	24	24
Zn7Mg3	24	24	24
Zn6Mg4	24	24	24
Zn5Mg5	24	24	24
Zn4Mg6	24	24	72
Zn3Mg7	24	24	72
Zn2Mg8	24	24	72
Zn1Mg9	24	24	72

No blisters were found on the surface of the primer Zn0Mg0. The blisters started to form on the surface of Zn10Mg0 primer after 72 hour B117 test. All other Zn-Mg rich primers had blisters after only 24 hours of B117 exposure. With the high reactivity of Mg particles and the penetration of Cl^-, the hydrogen evolution caused blisters at the earlier stages for Zn-Mg primers than Zn10Mg0 primer [11]. Without active metals, Zn0Mg0 did not form any blister any all.

White corrosion products started to form on the surfaces of Zn-Mg rich primers with Mg volume concentration less than 60vt% for 24 hours, and on the surfaces of Zn-Mg rich primers with Mg volume concentration higher than 60vt% for 72 hours. The white corrosion products formed rapidly in the Zn rich primer and Zn-Mg rich primers when Mg volume concentrations were less than 60vt%. Zn-Mg rich primer with Mg more than 60vt% possibly might have Mg corrosion products initially and then produced Zn white corrosion products later, which did not shown any white corrosion precipitates. White corrosion products were mainly Zn corrosion products, because it was discussed in the immersion test, Mg corrosion products was not stable at

the low pH condition. The primers with lower concentration of Mg particles had a higher concentration of Zn particles and had Zn corrosion products earlier. In galvanic series, Mg is more electronegative than Zn. The primers with higher concentration of Mg particles could have Zn particles protected by Mg particles and delayed zinc corrosion products, which were white corrosion precipitates stated here.

Pendulum hardness test results are shown in Figure 7.6. The primer Zn0Mg0 showed increasing hardness with B117 corrosion test. Zn10Mg0 primer did not have a significant change of hardness with B117 corrosion test. Zn-Mg rich primers showed decreasing hardness with B117 corrosion test. For Zn-Mg rich primers with less than 80vt% Mg incorporated, hardness kept decreasing with the time of corrosion test. Zn2Mg8 and Zn1Mg9 rich primers decreased the hardness but maintained with further corrosion test.

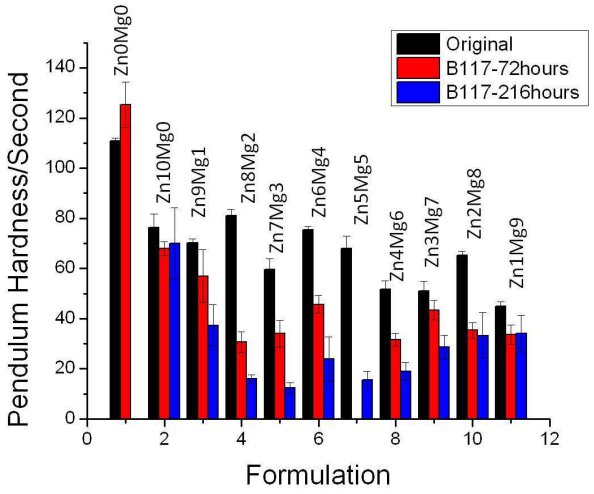

Figure 7.6. Pendulum hardness of different formulations with different periods of ASTM B117 test.

Pendulum hardness increased for Zn0Mg0 primer due to the aging and/or degradation of epoxy binders [12, 13]. With blister formation to provide porous structure for Zn-Mg rich primer, pendulum hardness decreased due to the porous structure, while for Zn10Mg0 primer, pendulum

hardness maintained with no blister formation. For the primers of Zn2Mg8 and Zn1Mg9 with the most Mg particles inside, the stable porous structures were the earliest to be formed due to the higher reactivity of Mg particles than Zn particles. So after 72 hours B117 exposure, the Zn2Mg8 and Zn1Mg9 primers started to maintain their pendulum hardness.

Potentiodyanmic polarization tests are shown in Figure 7.7. For Zn10Mg0 and Zn9Mg1, the open circuit potential moved into a negative direction, because the primers started to break down when the active metals Zn and Mg were exposed to electrolytes. With the consumption of

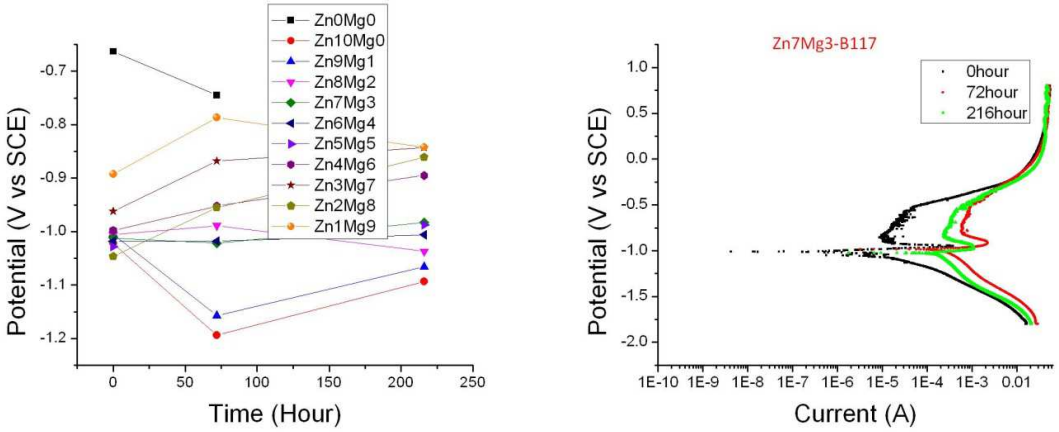

Figure 7.7. Open Circuit Potential of primers (Left) and Potentiodynamic polarization of Zn7Mg3 primer (Right) with different time of B117 tests.

the active metals Zn and Mg, the open circuit potential started to move into a positive direction. For the primers with Mg volume concentration higher than 50vt%, the open circuit potential moved into a positive direction with the accelerated test. There were two reasons. The first one was that Mg was more active than Zn [6], or Zn was protected by Mg [14]. During the corrosion test, Mg would react faster than Zn, and consumed faster. With no precipitation accumulated by Mg corrosion products, discussed in the section 7.3.2, porous structures formed. The second one was that the conductivity as well as the corrosion current might be higher with higher volume concentration of Mg particles in Zn-Mg rich primers, because Mg has larger oil absorption value

than Zn [7], which might result into less packing density [15], and Mg is more conductive than Zn. Both reasons consumed active metals and moved the open circuit potential into positive direction. For the primers with Mg volume concentration lower than 50vt% and higher than 10vt%, the open circuit potential maintained, which was around -1.02V vs SCE, which also are seen in potentiodyanmic polarization in Figure 7.7 that the corrosion potential did not change significantly for Zn7Mg3 primer. However, the corrosion current increased with the periods of B117 tests, and decreased a little bit with a longer periods of B117 tests. The reason might be better barrier properties with the porous structure sealed by the corrosion products with a longer time of B117 corrosion tests and/or the alkaline environment by Mg particles [16].

XRD results are shown in Table 7.5. It could be found out Zn10Mg0 primer, zinc oxide was formed. For the Zn-Mg rich primers, simonkolleite was formed without zinc oxide possible due to the alkaline environment [16]. For Zn9Mg1 primer, when Mg particles were consumed after 72hour B117 test, zinc oxide started to form. However, for Zn6Mg4 primer, even when Mg particles were consumed earlier than 72 hour B117 test, zinc oxide still did not appear due to the fact that the Mg^{2+} ion did affect the corrosion products and facilitated simonkolleite formation [17], and/or the remaining alkaline environment.

Table 7.5. XRD results of the primers within B117 test.

Formulation	Original	B117-72 hours		B117-216 hours	
	Mg%	Mg%	Corrosion products	Mg%	Corrosion Products
Zn10Mg0	0	0	Simonkolleite, ZnO	0	Simonkolleite, ZnO
Zn9Mg1	7.73	7.73	Simonkolleite	0	Simonkolleite, ZnO
Zn6Mg4	38.00	0	Simonkolleite	0	Simonkolleite

7.3.4. Prohesion™ Corrosion Tests

The visual appearances of primers of different formulation after Prohesion™ exposure are shown in Figure 7.8 with the detailed results in Table 7.6. All the primers showed red rust

Figure 7.8. Different formulation primers with Prohesion™ corrosion test for different time periods.

after only 24 hours of exposure. However, the primers Zn10Mg0 and Zn9Mg1 had the trace amount of red rust. The amount of rust that could be visually observed increased with exposure time. White corrosion products were formed after 144 hour Prohesion™ exposure for the

Zn10Mg0 primer, and became predominant around 288 hour Prohesion™ test for all primers. Blisters started to form on Zn9Mg1 primer after 288 hour Prohesion™ test. However, no blisters were founded for other primer systems. As discussed in Section 7.3.2, the primers in DHS solution showed slow reaction rate, and as well low cathodic current density. With the slow reaction rate, white corrosion products appeared in a long time period. With the low cathodic current density, red rust appeared in a short time period. The low concentration of Cl^- limited penetration of corrosive environments into the primers [11], so the blisters were seldom formed.

Table 7.6. Visual results of different formulation primers with Prohesion™ exposure – the time values are the time it took to observe the corrosion product

Formulation	Rust/hour	Blister/hour	White corrosion products/hour
Zn0Mg0	24	No	No
Zn10Mg0	24	No	144
Zn9Mg1	24	288	144
Zn8Mg2	24	No	288
Zn7Mg3	24	No	288
Zn6Mg4	24	No	288
Zn5Mg5	24	No	288
Zn4Mg6	24	No	288
Zn3Mg7	24	No	288
Zn2Mg8	24	No	288
Zn1Mg9	24	No	288

In Figure 7.9, the pendulum hardness values of of Zn0Mg0, Zn10Mg0, and Zn-Mg rich primers with Mg concentration higher than 50vt% did not change significantly or increased with a long time exposure up to 288 hours. Zn-Mg rich primers with Mg concentration lower than 50vt% had decreasing pendulum hardness with the time of the exposure.

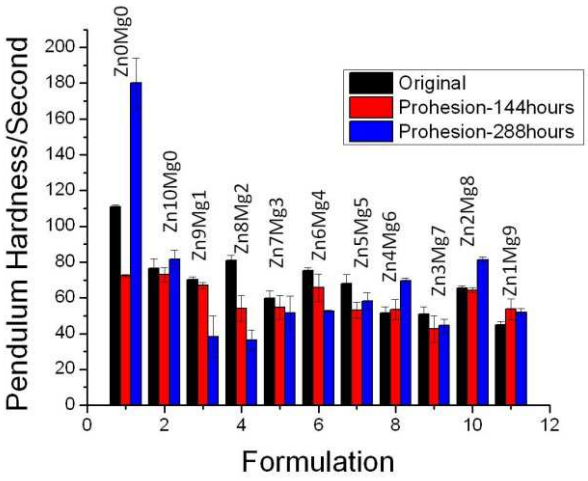

Figure 7.9. Pendulum hardness of different formulations with different periods of Prohesion™ test.

For Zn0Mg0 primer, the pendulum hardness increased after 288 hour Prohesion™ test due to the aging of the primer [12, 13]. For Zn10Mg0 primer, the pendulum hardness maintained due to the good barrier property to maintain the integrity of the primer. For Zn-Mg rich primers with Mg concentration higher than 50vt%, the pendulum hardness increased possibly due to the corrosion products precipitation within the local alkali environment by the high concentration of Mg particles. For Zn-Mg rich primer with Mg concentration lower than 50vt%, the pendulum hardness decreased with Prohesion™ exposure possibly due to the leaching out of active metals, especially the dissolution of Mg particles.

Potentiodyanmic polarization tests are shown in Figure 7.10. For Zn10Mg0, Zn9Mg1, Zn8Mg2, and Zn7Mg3, the open circuit potential moved into the negative direction initially, because initially barrier property of the primers started to break down and then the active metals started to be effective, and then started to move into the positive direction due to the consumption of the active metals. For the primers with Mg volume concentration higher than 30vt%, the open circuit potential moved into a positive direction, because Mg reacted faster than

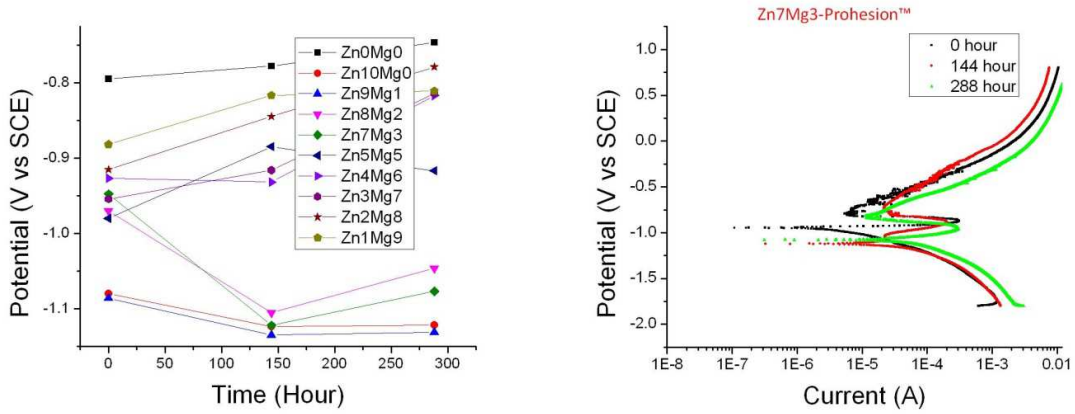

Figure 7.10. Open Circuit Potential of primers (Left) and Potentiodynamic polarization of Zn7Mg3 primer (Right) with different time of Prohesion™ tests.

Zn and was consumed faster to form porous structures. From the potentiodyanmic polarization of Zn7Mg3 primer shown in Figure 7.10, the corrosion potential moved into the negative direction, while the corrosion current did not change significantly. The reason was that without the penetration effect of Cl^- ions, the corrosion behaviors happened mostly on the surface.

XRD results were shown in Table 7.7. It could be found that no zinc oxide as the corrosion products was formed on the primer surface. The only corrosion product was simonkolleite no matter Mg particles existed or not. The reason might be the transformation of zinc oxide to simonkolleite [18] even at the temperature as low as 6˚C, due to the thermodynamic stabilization of simonkolleite. However, if the concentration of $ZnCl_2$ was higher than 0.5M, ZnO was completely transformed. With the dry cycle increasing the concentration of salts, such as $ZnCl_2$, all ZnO were transformed into simonkolleite. Another observation was that Mg particles were not observed from XRD characterization after 144 hour Prohesion™ test.

Table 7.7. XRD results of the primers within Prohesion™ test

Formulation	Original	Prohesion™- 144 hours		Prohesion™-288 hours	
	Mg%	Mg%	Corrosion products	Mg%	Corrosion Products
Zn10Mg0	0	0	Simonkolleite	0	Simonkolleite
Zn9Mg1	7.73	0	Simonkolleite	0	Simonkolleite
Zn6Mg4	38.00	0	Simonkolleite	0	Simonkolleite

7.3.5. Discussion of B117 Tests and Prohesion™ Tests

7.3.5.1. Blister Formation

From corrosion tests, it could be found that blisters were formed quickly for B117 exposure. In contrast, there were no significant blisters in Prohesion™ exposure. Blisters are caused by two reasons. One is hydrogen evolution [19]. The other one is water penetration due to osmotic effects [20]. For our situation, all the formulations were kept at the same PVC. If Mg concentration was high, hydrogen evolution would be high due to the high reactivity of Mg particles. However, with the depletion of Mg, porous structures were formed [2]. The hydrogen gas could be easily diffuse through the coating without the blister formation. If Mg concentration was low or none, Zn corrosion products could be formed on the surface to block the surface. The pores caused by the active metal dissolution on the surface would have the osmotic effects to cause the blister formation.

For B117 corrosion test, with high concentration of Cl^- ion, the reaction of Mg particle would be significantly high [10], which could generate more hydrogen faster than Prohesion™ corrosion test. Another reason was that with B117 a continuous spray exposure and Prohesion™ a cyclic spray exposure, B117 is more prone to wash away corrosion products and to leave voids behind, since the dry cycle in Prohesion™ corrosion test not only decreases the corrosion rate of active metals [10], but also helps stabilize corrosion products and precipitate corrosion products. These voids not only could damage adhesion of the coatings, but also could serve the osmatic

cells, which helps blister formation [21]. In fact, for B117 corrosion test, Zn-Mg primers with Mg particles inside had blisters around 24 hours, due to high reactivity of Mg and high concentration of Cl^- ion, while Zn10Mg0 had blisters around 72 hours. For Prohesion™ corrosion test, Zn-Mg primers did not have any blister formation except Zn9Mg1 primer. A little bit of Mg particles inside would cause voids, which were quickly covered and severed as the osmatic cells.

In conclusion, faster blister formation and more blisters occur in B117 corrosion test.

7.3.5.2. Composition Change

From the previous results, it could be found that Mg particles consumed much faster in Prohesion™ corrosion test, at least on the surface within the XRD detection depth, than in B117 corrosion test, although Cl^- ions had a high penetration ability and B117 always had a higher corrosion temperature as well as longer spray periods. There was also evidence that corrosion current in B117 corrosion test was higher than Prohesion™ corrosion test. The reason why Mg still consumed faster in Prohesion™ corrosion test was that Mg had a more negative potential in DHS solution than Mg in 5wt% NaCl solution. In contrary, Zn (Fe) had a more positive potential in DHS solution than Zn in 5wt% NaCl solution. With the larger potential gap between Mg and Zn(Fe) in DHS solution than in 5wt% NaCl solution, Mg would have a faster reaction speed in DHS solution due to galvanic corrosion. It would cause Mg consumption faster in DHS solution at least at the surface area.

7.3.5.3. Corrosion Products

Although there was no quantitative results for corrosion products, hardness value of primers with Prohesion™ exposure were larger than hardness values of primers with B117 exposure. Corrosion current with Prohesion™ corrosion test maintained, while corrosion current

with B117 corrosion test increased. These evidences indicated barrier property of primers with Prohesion™ corrosion test was better than that with B117 corrosion test. The reason was attributed to the corrosion product formation. The inorganic corrosion precipitates not only helped maintained the hardness of primers, but also helped protection of corrosive environments as the barrier protection.

Another phenomenon of corrosion product formation was that zinc oxide was formed for Zn rich primer, and Zn9Mg1 primer after Mg particle was consumed for B117 corrosion test. However, zinc oxide was not formed for Zn-Mg rich primer with higher concentration of Mg particles even after Mg particle was consumed. The reason might be due to higher pH value caused by Mg consumption which helped the transformation of zinc oxide to simonkolleite. For Prohesion™ corrosion test, only simonkolleite was formed for all tested primers. The reason might be due to the dry cycle of corrosion test, which transformed zinc oxide to the stable simonkolleite due to thermodynamic force. The stable simonkolleite formed on the surface might help maintain the good barrier property of primers with Prohesion™ corrosion tests.

7.3.5.4. Mechanism of Corrosion Protection

From the previous results, it was clear to see that Zn9Mg1 primer showed better corrosion protection than Zn10Mg0 primer for the protection of steel substrate for B117 corrosion tests. For Prohesion™ corrosion test, Zn9Mg1 was comparable with, if not better than, Zn10Mg0 primer for the corrosion mitigation ability.

For the corrosion tests of Zn rich primer and Zn-Mg rich primers, there were two corrosion mitigation methods, cathodic protection and barrier protection. Cathodic protection was exhausted quickly for Zn-Mg rich primer with Mg concentration higher than 60%, and with Mg concentration higher than 40% in B117 corrosion test and in Prohesion™ corrosion test,

respectively. The reason might be the higher consumption rate of active metal particles with higher concentration of Mg particles and with Prohesion™ corrosion test. Barrier protection was good for Prohesion™ corrosion test based on corrosion current of potentiodynamic polarization test. Stable and dense corrosion product simonkolleite would help the barrier protection. However, the Mg particle consumption with void left possibly offset the barrier protection with simonkolleite formation. It was why there was no significant improvement of barrier protection of Zn-Mg rich primers compared with Zn rich primer.

With the previous statements, Zn-Mg rich primers did not shown a significant improvement of barrier protection compared with Zn rich primer, and showed no better cathodic protection using open circuit potential criteria than Zn rich primer. However, Zn-Mg rich primers showed a longer corrosion protection than Zn rich primer. The reason might be the combination of the basic environment and the voids created in the coatings by the corrosion of Mg particles, shown in Figure 7.11. In Figure 7.11, zinc is corroded with the volume expansion and protected by its corrosion products. Magnesium is corroded with the volume decreased even if any corrosion products precipitate and leaves voids at the sites. The reason was due to the density change shown in Table 7.8.

With the higher concentration of Mg particles, the higher pH of the environments helped transform zinc corrosion products to the stabilized simonkolleite. However, the higher concentration of Mg particles, the more voids left in the coatings decreased the barrier properties of coatings, and in contrary increased the conductivity of coatings when the electrolytes were filled into the voids. The optimization of the concentration of Mg particles produced a good corrosion mitigation method to protect steel substrates.

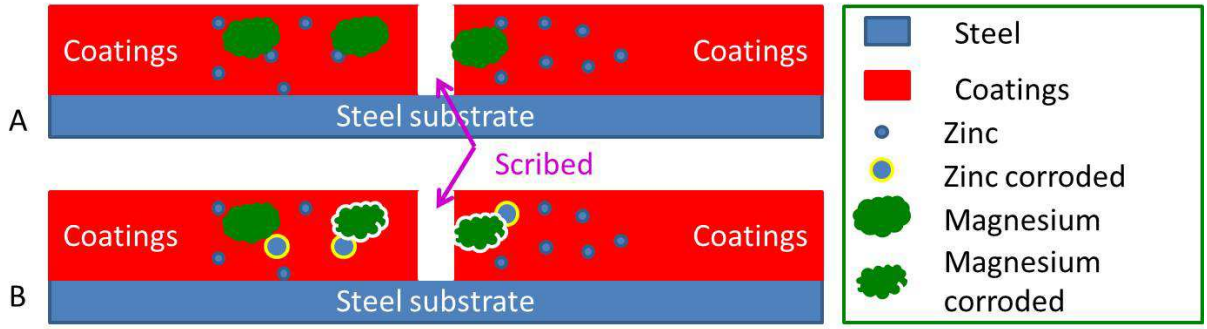

Figure 7.11. Schematic of mechanisms of Zn-Mg rich primer to protect steel substrates.

Table 7.8. Density of Zn-Mg related materials

Materials	Density/(g/cm^3)
Zinc	7.14
Zinc oxide	5.61
Simonkolleite	3.30
Magnesium	1.74
Magnesium oxide	3.58
Magnesium hydroxide	2.34

In conclusion, the mechanism of Zn-Mg rich primers for the corrosion mitigation improvement is that the addition of magnesium particles to supply a basic environment for the transformation of simonkolleite, and void spaces with the balance of conductivity and the barrier property of coatings.

7.4. Conclusions

Zn rich primer and Zn-Mg rich primers with different concentration of Mg particles were tested by B117 corrosion tests and Prohesion™ corrosion tests. Zn9Mg1 primer showed a significant corrosion protection improvement in B117 corrosion tests, and showed a comparable corrosion protection improvement in Prohesion™ corrosion tests with Zn10Mg0 primer.

Blister formation was one of the main fail characteristics due to the hydrogen gas evolution and the osmotic cell formation. Corrosion products were mainly simonkolleite for Zn-Mg rich primers for B117 corrosion test. For Zn rich primer additional zinc oxide corrosion

products were also formed. For Prohesion™ corrosion test, only simonkolleite was formed for all primers. Mg consumed faster in Prohesion™ corrosion test than in B117 corrosion test due to the more acidic environment.

To improve the corrosion mitigation of Zn rich primer, Mg particles should be optimized to supply a basic environment for the corrosion behaviors and to increase the conductivity of the coatings with the sacrifice of the barrier property of coatings.

7.5. References

1. Elvins J, Spittle JA, Sullivan JH et al., The effect of magnesium additions on the microstructure and cut edge corrosion resistance of zinc aluminium alloy galvanised steel, Corrosion Science, 2008, 50, 1650-1658.
2. King AD, Scully JR, Sacrificial anode-based galvanic and barrier corrosion protection of 2024-T351 by a Mg-rich primer and development of test methods for remaining life assessment, Corrosion, 2011, 67, 055004-1-22.
3. Connolly JR, Introduction quantitative X-ray diffraction methods, April 18, 2012. (http://epswww.unm.edu/xrd/xrdclass/09-Quant-intro.pdf, accessed on November 9, 2012)
4. Lu XY, Zuo Y, Zhao XH et al., The study of a Mg-rich epoxy primer for protection of AZ91D magnesium alloy, Corrosion Science, 2011, 53, 153-160.
5. Schurz S, Luckeneder GH, Fleischanderl M et al., Chemistry of corrosion products on Zn-Al-Mg alloy coated steel, Corrosion Science, 2010, 52, 3271-3279.
6. Revie RW, Uhlig HH, Corrosion and corrosion control: An introduction to corrosion science and engineering, John Wiley & Sons Inc, 2008, Hoboken, New Jersey.
7. Nie J, Improvements in the use of Mg pigments in corrosion protective coatings, Ph. D. Dissertation, North Dakota State University, Fargo, ND, 2010.

8. Song GL, A dipping E-coating for Mg alloys, Progress in Organic Coatings, 2011, 70, 252-258.

9. Hosking NC, Strom MA, Shipway PH et al., Corrosion resistance of zinc-magnesium coated steel, Corrosion Science, 2007, 49, 3669-3695.

10. Song G, Atrens A, St John D et al., The anodic dissolution of magnesium in chloride and sulphate solutions, Corrosion Science, 1997, 39(10-11), 1981-2004.

11. Panagopoulos CN, Georgiou EP, Gavras AG, Composite zinc-fly ash coating on mild steel, Surface and Coatings Technology, 2009, 204(1-2), 37-41.

12. Kouloumbi N, Ghivalos LG, Pantazopoulou, Determination of the performance of epoxy coatings containing feldspars filler, Pigment and Resin Technology, 2005, 34/3, 148-153.

13. Odegard GM, Bandyopadhyay, Physical aging of epoxy polymers and their composites, Journal of Polymer Science Part B: Polymer Physics, 2011, 49(24): 1695-1716.

14. Song GL, Atrens A, Corrosion mechanisms of magnesium alloys, Advanced Engineering Materials, 1999, 1(1), 11-33.

15. Xu H, Magnesium alloy particulates used as pigments in metal-rich primer system for AA2024 T3 corrosion protection, Ph. D. Dissertation, North Dakota State University, Fargo, ND, 2011.

16. Cabot PL, Cortes M, Centellas FA et al., Cathodic reduction of the annodically formed species as a contribution to the study of the potentiodynamic passivation of zinc in alkaline media, Electrochimica Acta, 1987, 32(9), 1321-1329.

17. Volovitch P, Vu TN, Allely C et al., Understanding corrosion via corrosion product characterization: II. Role of alloying elements in improving the corrosion resistance of Zn-Al-Mg coatings on steel, Corrosion Science, 2011, 53, 2437-2445.

18. Tanaka H, Fujioka A, Futoyu A et al., Synthesis and characterization of layered zinc hydroxychlorides, Journal of Solid State Chemistry, 2007, 180, 2061-2066.

19. Lu XY, Zuo Y, Zhao XH et al., The study of a Mg-rich epoxy primer for protection of AZ91D magnesium alloy, Corrosion Science, 2011, 53(1), 153-160.

20. http://www.corrosionservices.com/newsletters/blistered_epoxy_coating.html, accessed on April 16, 2013.

21. Hansen CM, New developments in corrosion and blister formation in coatings, Progress in Organic Coatings, 1995, 26(2-4), 113-120.

8. PERFORMANCE OF ZINC-MAGNESIUM RICH PRIMERS

8.1. Introduction

Although it was described in Chapter 7 that Zn-Mg rich primers could increase the corrosion protection lifetime vs. similar Zn-rich primers over steel substrates in accelerated tests, the standard procedure for complete testing of this type of corrosion protection coating systems for steel substrates is to examine their performance in the top coated systems. The topcoat would not only improve barrier property, but also prevent metal pigment self-corrosion [1]. In the standard procedure, the Zn-Mg rich primers were not exposed to the test environment directly, but would be top coated. The use of topcoats on Zn-Mg rich primers and Zn rich primer can possibly change the details of their performance in exposure. In this chapter, an epoxy sealing primer was coated on top of all of the primes to emulate the barrier protection that is provided by most topcoats. The whole coating systems with the sealing primer on top of the metal rich primers were tested in accelerated corrosion tests and the details of their performance was evaluated by visual inspection, thickness measurements, and electrochemical characterizations.

8.2. Experimental Methods

8.2.1. Materials

A Zn rich primer and Zn-Mg rich primers were prepared as shown in Tables 7.1 and 7.2. MIL-DTL-53022 D Type II primer, bought from Sherwin Williams, was used as the sealing primer. The sealing primer was sprayed over a week room temperature cured films of Zn-rich primer and Zn-Mg rich primers, and cured for another week at the room temperature.

8.2.2. Characterization Studies

An Elcometer 345 FS was used to measure the thickness of organic coatings on steel S36 substrate. A Gamry Potentiostat Reference 600 was used for potentiodynamic polarization test

and electrochemical impedance measurement. The electrolyte was DHS, which comprised of 0.35wt% $(NH_4)_2SO_4$ and 0.05wt% NaCl in distilled water. Potentiodyanmic polarization was performed starting at -1.8V vs SCE and ending 0.8V vs SCE with scan rate 1mV/s. EIS data was collected over a 0.01Hz to 100kHz frequency range with a 10mV rms amplitude at 10points/dec.

8.2.3. Experimental Set-up

The experimental set-up was the same as the experimental set-up described in section 7.2.3. The topcoat/primer systems with the sealing primer on top of the metal rich primers was put into the accelerated corrosion test chambers and characterized with visual inspection, thickness measurements, and electrochemical characterizations.

8.3. Results and Discussions

8.3.1. B117 Corrosion Performance

Visual pictures of different primer systems after exposure to the ASTM B117 corrosion test environment are shown in Figure 8.1. The primer system Zn1Mg9 had adhesion failure after 24 hours of ASTM B117 test exposure, with the coating peeled off from the substrate. The Zn5Mg5 primer system had adhesion failure after 72 hours ASTM B117 exposure, with blisters formed on the surface. After 120 hours of ASTM B117 exposure, both the primer system Zn10Mg0 and the primer system Zn9Mg1 showed the adhesion failure with blisters formed on the surface. The blisters grew bigger with 120 hour ASTM B117 corrosion test for Zn5Mg5 primer system and with 432 hour ASTM B117 corrosion test for both Zn10Mg0 and Zn9Mg1 primer systems. From Table 8.1, it could be found that Zn-rich primer had rust a little earlier than Zn-Mg rich primers with Mg volume concentration less than 50% and showed blisters at the same with Zn-Mg rich primers with Mg volume concentration less than 30%. The blisters

formed earlier with more Mg particles inside, due to the high reactivity of Mg particles in B117 corrosion test [2]. To compare with bare primers in Chapter 7, the top-coated primer systems had earlier rust formation for some Zn-Mg rich primers, such as Zn10Mg0 primer and Zn9Mg1 primer. The others had blister formation later than similarly exposed primer only systems.

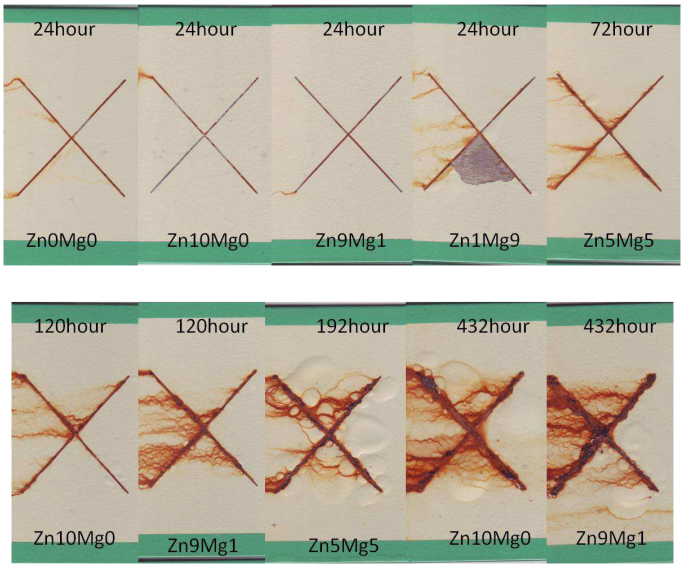

Figure 8.1. Different primer systems with ASTM B117 corrosion test for different time periods.

Table 8.1. Visual results of different primer systems with ASTM B117 corrosion test

Formulation	Rust/hour	Blister/hour
Zn0Mg0	24	192
Zn10Mg0	24	192
Zn9Mg1	72	192
Zn8Mg2	72	192
Zn7Mg3	72	192
Zn6Mg4	72	120
Zn5Mg5	72	120
Zn4Mg6	24	72
Zn3Mg7	24	72
Zn2Mg8	24	72
Zn1Mg9	24	24

Electrochemical tests were shown in Figures 8.2 and 8.3. From Figure 8.2, it could be found that the impedance decreased with the B117 exposure time. This can be attributed to the

barrier property failures, since the sealing primer epoxy could not resist water penetration during B117 corrosion test [3]. Zn-Mg rich primers with higher volume concentration of Mg particles failed in barrier properties faster than Zn-Mg rich primer with lower volume concentration of Mg particles. The reason might be due to the blister formation, as shown in Table 8.1 with the higher concentration of Mg particles resulted into the earlier blister formation, which discussed in Chapter 7 may be attributed to the high reactivity of Mg particles. Potentiodynamic polarization tests showed no significant change in total current vs potential results with exposure. However, the open circuit potential moved into a positive direction faster vs. exposure time for Zn-Mg rich primers with the higher volume concentration of Mg particles than 60vt%, which may indicate a quicker cathodic protection failure, due to higher consumption rate of Mg particles, as discussed in Chapter 7. The primers had the similar behaviors with the bare primers in Chapter 7 in a longer period.

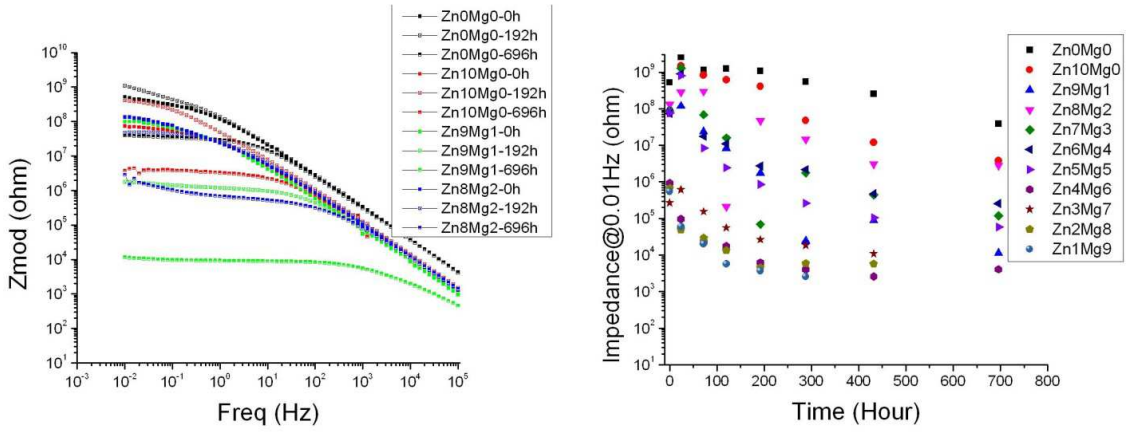

Figure 8.2. Electrochemical impedance measurements of different primer systems with different periods of ASTM B117 corrosion tests (A) and the impedance at 0.01 Hz for different primer systems with different periods of ASTM B117 corrosion tests (B).

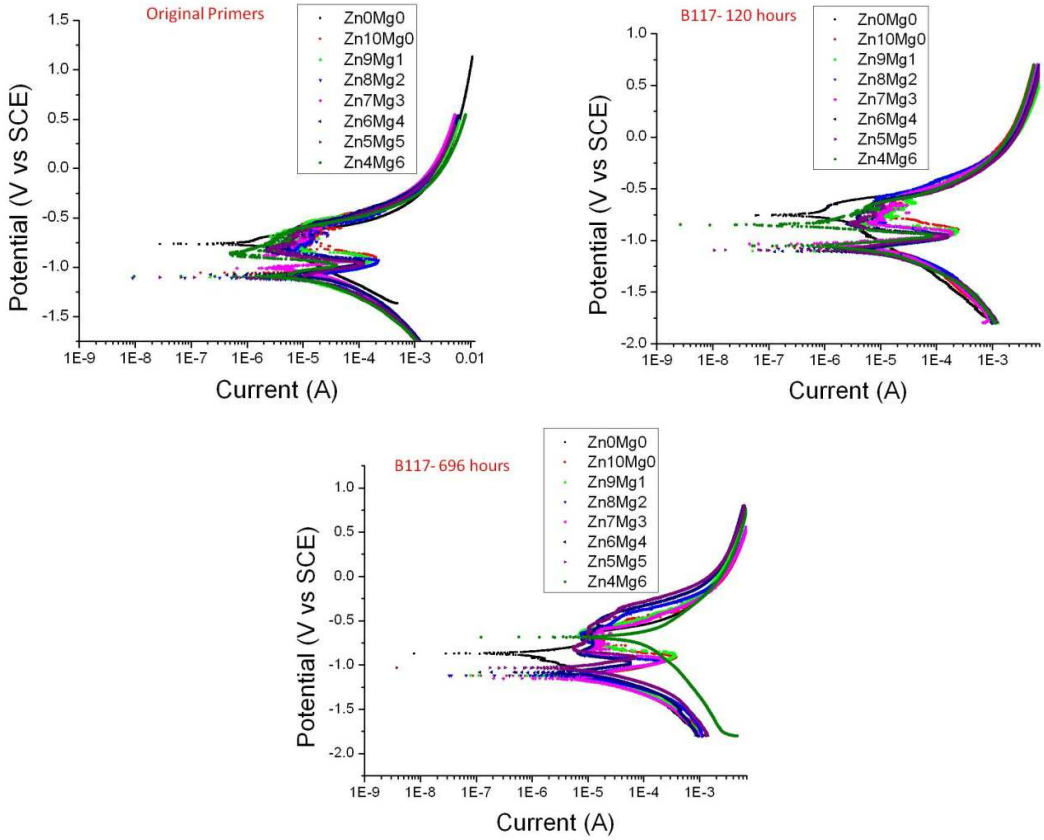

Figure 8.3. Potentiodynamic polarization scans of different primer systems with different periods of ASTM B117 corrosion tests.

In conclusion, for ASTM B117 corrosion test, the sealing primer served as a barrier protection to aid the corrosion mitigation to increase the lifetime, since the rust formation and blister formation appeared later than those of bare primer systems. However, without enough resistance, the corrosion behaviors were similar with those of bare primers in the exposure to ASTM B117 corrosion test.

8.3.2. Prohesion™ Corrosion Performance

Visual pictures of different primer systems exposed under the Prohesion™ corrosion test protocol are shown in Figure 8.4. All the primer systems did not have any significant adhesion failure until 336 hours of Prohesion™ test exposure. With 899 hours of Prohesion™ exposure,

the Zn-rich primer and Zn9Mg1 primer systems showed edge delamination. In contrast, Zn8Mg2, Zn7Mg3, Zn6Mg4, and Zn5Mg5 primer systems still showed good adhesion to the substrates without any blisters or edge delamination.

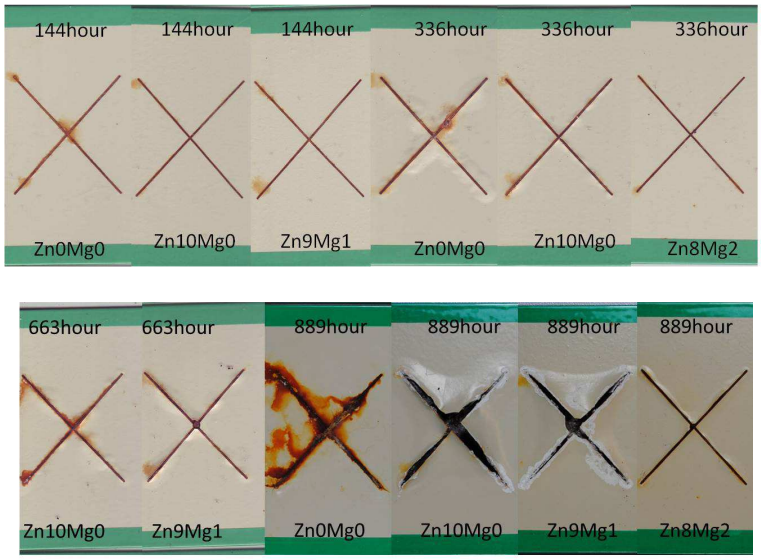

Figure 8.4. Different primer systems with Prohesion™ corrosion test for different time periods.

Table 8.2. Visual results of different primer systems with ASTM B117 corrosion test

Formulation	Rust/hour	Edge delamination/hour
Zn0Mg0	72	889
Zn10Mg0	144	889
Zn9Mg1	144	889
Zn8Mg2	144	
Zn7Mg3	144	
Zn6Mg4	144	
Zn5Mg5	144	
Zn4Mg6	144	889
Zn3Mg7	144	889
Zn2Mg8	144	889
Zn1Mg9	144	889

Electrochemical test results are shown in Figures 8.5 and 8.6. From Figure 8.5, it can be seen that the impedance increased initially with the Prohesion™ exposure time and then stayed relatively constant. This may be attributed to the coating system barrier properties. With the

cyclic corrosion test, sealing primers still showed good barrier properties in the test period for all primer systems. Potentiodynamic polarization tests showed no significant change in current. The corrosion potential did not change significantly either. All these indicated a continuing cathodic protection of the steel by the primers during Prohesion™ exposure. With both electrochemical impedance test and potentiodynamic polarization test, it could be seen that barrier properties stayed well and cathodic protections were still in effect in the test periods.

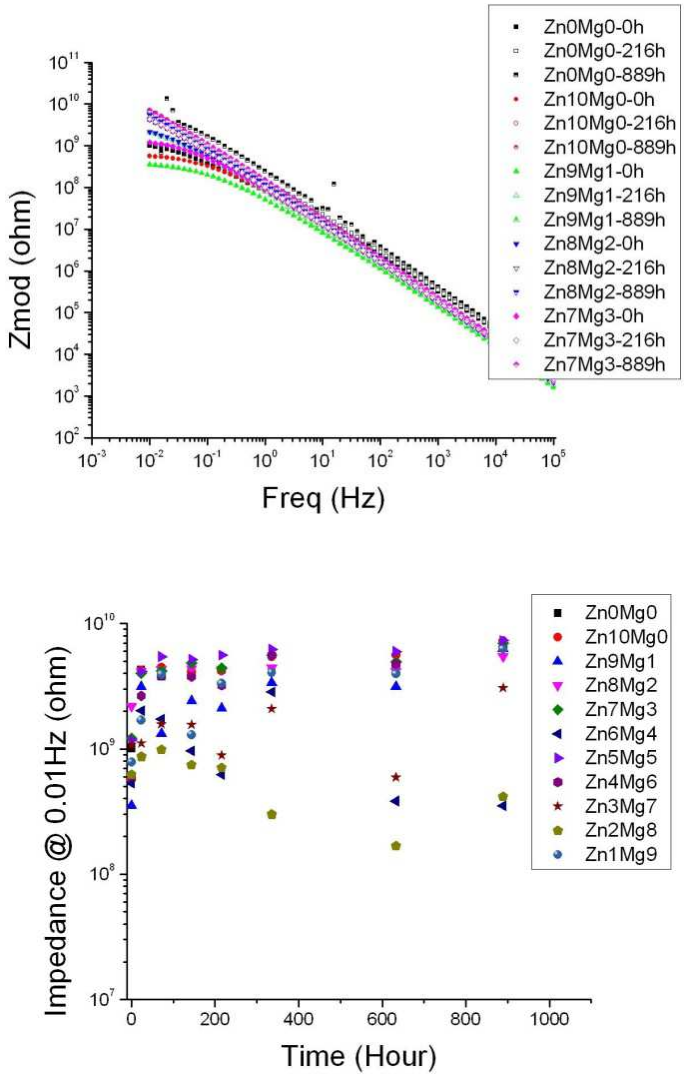

Figure 8.5. Electrochemical impedance measurements of different primer systems with different periods of Prohesion™ corrosion tests (A) and the impedance at 0.01 Hz for different primer systems with different periods of Prohesion™ corrosion tests (B).

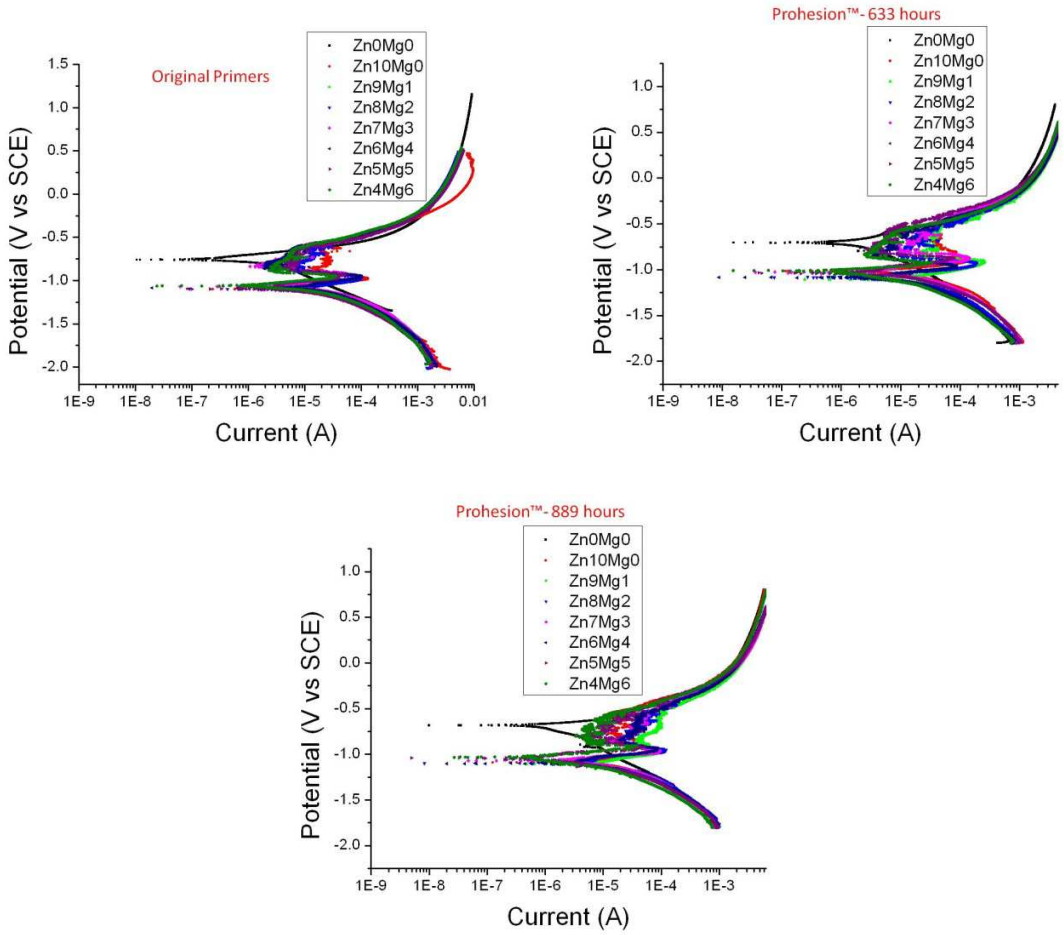

Figure 8.6. Potentiodynamic polarization scans of different primer systems with different periods of Prohesion™ corrosion tests.

In conclusion, for Prohesion™ corrosion test, the sealing primer served as barrier protections to aid the corrosion mitigation to increase the lifetime. The barrier protection maintained well during the test periods. The rust formation and the white corrosion products appeared later than that of bare primer systems. In the meantime, it also increased the cathodic protection periods for all the primer systems. However, edge delamination at the scribe area was the main failure of the coating system.

8.3.3. Discussion of ASTM B117 and Prohesion™ Corrosion Performance

In the previous investigations, sealing primers increased the coating lifetime and cathodic protection than the coating systems without sealing primers, described in Chapter 7. Sealing primers severed as barrier protections for both B117 corrosion test and Prohesion™ corrosion test. Unlike the coating systems without sealing primers with failure modes of rust and blister on the surface of coatings, the coating systems with sealing primers on the top had two failure modes for ASTM B117 corrosion test and for Prohesion™ corrosion test respectively. For ASTM B117 corrosion test, rusts and blisters on the surface were the main failures regardless there were active metal particles inside. The blisters were mainly caused by cathodic delamination due to the easy oxygen penetration through the conductive channels by Cl^- ion [4, 5], since rust could be seen underneath the blisters when the blisters were broken. However, primers with higher concentration of Mg particles had blisters earlier than primers with lower concentration of Mg particles, which indicated hydrogen evolution and osmotic effect might take part into the blister formation, as discussed in Chapter 7. For Prohesion™ corrosion test, edge delaminations on the scribe were the main failures, possible due to the corrosion products built up [6] with the evidence of the high impedance and the white corrosion products on the surface, and the thermal stress caused by the cyclic behaviors [7] with the different thermal conductivity of metal rich primers and sealing primers. The corrosion products of Mg particles had a higher density than Mg particles, while the corrosion products of Zn particles had a lower density than Zn particles. Mg corrosion products would cause internal compression stress, while Zn corrosion products would cause internal tension stress. With the internal tension stress possibly causing delamination [8], primers with higher concentration of Zn particles would fail faster by edge

delamination. However, porous Mg corrosion product [6] would possibly give poor interfacial adhesion, resulting into delamination. So primers with higher concentration of Mg particles would be quicker for edge delamination. With the combined behaviors, Zn8Mg2 and Zn7Mg3 primers showed better edge delamination resistance than other primers. For both of failures appeared around the scribe area, it confirmed that the sealing primers served as barrier protection.

8.4. Conclusions

The sealing primer served as barrier protection for both ASTM B117 corrosion test and Prohesion™ corrosion test with a durable period for cathodic protection, compared with the bare primers in Chapter 7. The different behaviors in ASTM B117 corrosion test and in Prohesion™ corrosion test are listed in the followings.

1. Primers exposed to ASTM B117 corrosion test showed blisters with further delamination as the main failure, while primes exposed to Prohesion™ corrosion test showed edge delamination at the scribed area as the main failure.
2. Impedance of coatings maintained for Prohesion™ corrosion test, while decreased for ASTM B117 corrosion test. It may be due that corrosion products could be built up for Prohesion™ corrosion test, while could not stay for ASTM B117 corrosion test.
3. It showed a quicker coating failure in ASTM B117 corrosion test than Prohesion™ corrosion test. The higher concentration of Cl^- ion in ASTM B117 corrosion test than in Prohesion™ corrosion test resulted into more and more rapid blister formation.

8.5. References

1. King AD, Scully JR, Sacrificial anode-based galvanic and barrier corrosion protection of 2024-T351 by a Mg-rich primer and development of test methods for remaining life assessment, Corrosion, 2011, 67, 055004-1-22.

2. Pathak SS, Blanton MD, Mendon SK et al., Investigation on dual corrosion performance of magnesium-rich primer for aluminum alloys under salt spray test (ASTM B117) and natural exposure, Corrosion Science, 2010, 1453-1463.
3. Bagherzadeh MR, Mahdavi F, Preparation of epoxy-clay nanocomposite and investigation on its anti-corrosive behavior in epoxy coating, Progress in Organic Coatings, 2007, 60(2), 117-120.
4. Schneider O, Kelly RG, Localized coating failure of epoxy-coated aluminium alloy 2024-T3 in 0.5M NaCl solutions: Correlation between coating degradation, blister formation and local chemistry within blisters, Corrosion Science, 2007, 49, 594-619.
5. Chuang TJ, Nguyen T, A non-osmotic blister growth model in coating systems, Damage and Failure of Interfaces, Rossmanith, 1997, Balkema, Rotterdam, ISBN 9054108991.
6. Battocchi D, Simoes AM, Tallman DE et al., Electrochemical behavior of a Mg-rich primer in the protection of Al alloys, Corrosion Science, 206, 48, 1292-1306.
7. http://www.qstolpaint.com/pc/PdfFiles/performance_testing_anticorrosive_coatings_DAC.pdf, accessed on April 16, 2013.
8. Carlson RL, Kardomateas GA, Craig JI, Mechanics of Failure Mechanisms in Structures, Springer, 2012, New York, NY.

9. CONCLUSIONS AND FUTURE RECOMMENDATIONS

9.1. Conclusions

In these studies, active metal rich primers, pigmented with mixtures of (Zn + Mg) pigments and Zn-rich primer with sealing primer on the top were exposed under two accelerated test environments, ASTM B117 and Prohesion™ exposure protocols. The mechanism of Zn-Mg rich primer which gives distinct improvement of this pigmentation vs Zn pigment only was proposed to be the stabilized simonkollete corrosion products caused by the basic environment with the reaction of Mg particles, and to be the complementary volume effect between Mg and Zn corrosion behaviors. The performance of Zn-Mg rich primer with the sealing primer on the top improved considerably compared with bare Zn-Mg rich primer. The improvement was not only by the appearance integrity but also by the duration of the cathodic protection, due to the barrier protection of the sealing primer. Zn-Mg rich primer with sealing primer on the top still showed the significant improvement vs Zn rich primer with sealing primer on the top in Prohesion™ corrosion test. However, it was not better than Zn rich primer with sealing primer on the top in B117 corrosion test. This is consistent with the exposure behavior of Mg-rich systems over Al in which the B117 exposure seemed to cause blister problems which could be stopped by exposure to CO_2 [1,2].

During the project, different coating systems and various exposure conditions have been investigated. Following conclusions can be proposed.

1. To improve the corrosion mitigation of coating systems, optimized Mg concentration should be included to supply a basic environment and to avoid too many voids left by the reaction of Mg particles.
2. Sealing primer increased the durability of coating failure by its barrier protection.

3. For bare metal primer system, the main failure was blister formation and rust formation in both ASTM B117 corrosion test and Prohesion™ corrosion test. The main failure for metal rich primer with sealing primer on in ASTM B117 corrosion test was still blister formation. However, the main failure for metal rich primer with sealing primer on in Prohesion™ corrosion test was edge delamination.

9.2. Recommendations for Future Research

In order to further improve Zn rich primer with the incorporation of Mg particles, suggestions on experiments are as followings.

1. Field test is very important to evaluate organic coatings performance, especially when carbon dioxide could not only decrease hydrogen product rate of Mg particles but also form good barriers with the reaction to Mg particles [2].
2. More characterization should be done to verify our proposed conclusions, especially with SEM. SEM with EDS technique could not investigate the morphology of coatings to check the porosity of coatings, but also characterize corrosion products especially underneath coatings to explain the corrosion process reasonably.
3. Electrochemical mapping techniques should also be applied to explain the complicated three metal systems, for example the initiation of the corrosion sites, the anodic area, and the cathodic area as well as the corrosion current. The mapping techniques would help define the role of each metal and its reaction rate in the corrosion system, and may clarify the mechanism of Zn-Mg rich primer for the protection of steel.
4. Possible addition of $MgCO_3$ to the (Zn + Mg) rich primer formulae could alleviate early blistering problems as has been seen with Mg-rich coatings [1].

9.3. References

1. Pathak SS, Blanton MD, Mendon SK et al., Carbonation of Mg powder to enhance the corrosion resistance of Mg –rich primers, Corrosion Science, 2010, 52, 3782-3792.
2. Pathak SS, Blanton MD, Mendon SK et al., Investigation on dual corrosion performance of magnesium-rich primer for aluminum alloys under salt spray test (ASTM B117) and natural exposure, Corrosion Science, 2010, 52, 1453-1463.